FACULTY OF MECHANICAL ENGINEERING TUL

Dissertation Thesis

Experimental Investigation of Two-Phase Flow Boiling Heat Transfer in Small Diameter Tubes

Study programme: P0715D270002 Machines and Equipment Design
Author: **Ernest Gyan Bediako**
Thesis Supervisor: prof. Ing. Tomáš Vít, Ph.D.
Department of Power Engineering Equipment

Liberec 2023

Declaration

I hereby certify, I, myself, have written my dissertation as an original and primary work using the literature listed below and consulting it with my thesis supervisor and my thesis counsellor.

I acknowledge that my dissertation is fully governed by Act No. 121/2000 Coll., the Copyright Act, in particular Article 60 – School Work.

I acknowledge that the Technical University of Liberec does not infringe my copyrights by using my dissertation for internal purposes of the Technical University of Liberec.

I am aware of my obligation to inform the Technical University of Liberec on having used or granted license to use the results of my dissertation; in such a case the Technical University of Liberec may require reimbursement of the costs incurred for creating the result up to their actual amount.

At the same time, I honestly declare that the text of the printed version of my dissertation is identical with the text of the electronic version uploaded into the IS/STAG.

I acknowledge that the Technical University of Liberec will make my dissertation public in accordance with paragraph 47b of Act No. 111/1998 Coll., on Higher Education Institutions and on Amendment to Other Acts (the Higher Education Act), as amended.

I am aware of the consequences which may under the Higher Education Act result from a breach of this declaration.

September 25, 2023 Ernest Gyan Bediako

Dedication

This thesis is dedicated to my wonderful and supportive family in Ghana especially my mum, Vida Pokuaa who on any day will be my hero. She believed in me and supported me from day one even in her most difficult moments. She went against all odds to make sure her children have the best of education possible. For this, I highly appreciate her. I also dedicate this thesis to my beautiful wife, Kasia, who makes life so easy going for me. She was patient with me during the entire studies and when distance made me miss some important family occasions, she understood and made light of it. She is the one I wish to live, enjoy and learn everything in life with. I finally dedicate this thesis to all my friends who have been there for me both in the good times and in the bad times as well.

Abstract

In recent years, there has been growing interest in exploring two-phase flow boiling heat transfer characteristics in in small diameter tubes, as they offer potential improvement in heat transfer performance and design of compact systems. Despite extensive research in this area, the heat transfer processes and the dominant mechanisms controlling the heat transfer still remain unclear.

This research therefore aims to experimentally investigate two-phase flow boiling heat transfer phenomenon in small diameter tubes, with a focus on understanding the underlying mechanisms, identifying critical parameters and testing predictive models for improved thermal performance.

An experimental setup from the Thermal Two-Phase Lab in Norwegian University of Science and Technology was modified to investigate the heat transfer characteristics under varying operating conditions, including but not limited to mass flux, heat flux, and saturation conditions. The study was performed in a horizontal 5 mm internal diameter and 8 mm external diameter smooth stainless-steel tube with 1,1,1,2-tetrafluoroethane (R134a) as the working fluid.

The main findings reveal that at low and moderate flow boiling conditions, distinct phenomena were observed. A notable peak of heat transfer coefficient near vapor quality of zero, a local minimum and heat transfer deterioration were observed in the low vapor quality region. These distinct observations were sensitive to heat flux but mildly sensitive to mass flux.

The main flow patterns recorded with high speed camera were bubble, slug and intermittent flow in the low vapor quality region, annular, dry-out and mist flow in the high vapor quality region. Similar flow patterns were predicted by well-known flow pattern maps in literature. Varying saturation pressure varies the vapor quality at which the flow pattern transitions from intermittent flow to annular flow.

Generally, mass flux and vapor quality favor convective boiling heat transfer whiles heat flux and saturation conditions favor nucleate boiling heat transfer. However, their interplay is very significant for clear observation. Pressure drop is observed to decrease with increasing saturation pressure.

Overall, this research contributes to the fundamental understanding of two-phase flow boiling heat transfer in small diameter tubes. The insights gained from this study provide valuable guidelines for designing and improving heat exchangers and other thermal system design.

Keywords: Two-phase flow boiling, heat transfer coefficient, pressure drop, small diameter tubes, heat transfer, refrigerants, experimental investigation, compact designs.

Acknowledgement

First and foremost, I would like to use this opportunity to thank God for His grace and mercies over the years and the opportunity to experience life in many different ways.

Next I would like to thank the Czech government through the Ministry of Education, Youth and Sports for granting me scholarship funding throughout my entire research study.

I would also like to thank my wonderful supervisor, prof. Ing. Tomáš Vít for supporting me in many ways I could not even imagine. He created many opportunities for my growth and development during all the periods of my studies for which I very much appreciate. I would not have made it through this Ph.D. journey without his support and guidance.

I would like to thank the head of department of Power Engineering Equipment (KEZ) who also happens to be my co-supervisor, doc. Petra Dancova. She was very supportive and available to help anytime I needed her assistance.

I would also like to acknowledge and appreciate Prof. Carlos Alberto Dorao and Maria Fernandino of the Thermal Two-Phase Flow laboratory of Energy and Process Engineering department in Norwegian University of Science and Technology (NTNU). They welcomed me to their lab during my research internship where most of my experiments were performed. They taught me how to build and run an experimental facility and get things working in a lab. I was exposed to many research tools and software through their supervision.

I am extremely grateful to Mgr. Radka Dvořáková and Ing. Dana Semotjuková of the study department for their unwavering assistance and guidance during my studies. Not leaving out Ing. Marcela Válková of the internal office for her support during the numerous internships abroad that I embarked on.

Lastly, I would like to extend my profound gratitude to all my colleagues in the universities and labs that I visited for their support and encouragement. Certainly, I collaborated more closely with certain individuals than with others, but this interaction played a pivotal role in ensuring the success of this study.

Nomenclature

Abbreviations and acronyms

ATC	Applied Thermal Control
A	Annular
CHF	Critical Heat Flux
DNB	Deviation from Nucleate Boiling
DP	Differential Pressure
FPS	Frame Per Second
HTC	Heat Transfer Coefficient
I	Intermittent
LHV	Latent Heat of Vaporization
MAE	Mean Average Error
MRE	Mean Relative Error
M	Mist
MW	Molecular Weight
NBP	Normal Boiling Point
ONB	Onset of Nucleate Boiling
RMS	Root Mean Square
RSS	Root Sum Square
S	Stratified
SW	Stratified Wavy

Symbols

a	Thermal diffusivity (m^2/s)
A	Cross sectional area (m^2)
c	Specific heat capacity (J/(kg K))
C_{sf}	Constant in the nucleate pool boiling correlation of Rohsenow (1)
d	Bubble diameter (m)
d	Tube diameter (m)
D	Channel diameter (m)
f	Frequency (Hz)
G	Mass flux ($kg/(m^2 s)$)
h	Enthalpy (J/kg)

F	Enhancement factor (1)
h	Heat transfer coefficient (W/(m K))
k	Thermal conductivity (W/(m K))
K	Flow coefficient (valve) (kg/s)
l	Length (m)
L	Heated length (m)
$\dot{m}$	Mass flow rate (kg/s)
M	Molecular mass (kg/kmol)
P	Pressure (Pa)
q''	Heat flux (W/m^2)
q'''	Volumetric heat flux (W/m^3)
r	radius (m)
R	radius (m)
S	Suppression factor (1)
t	Time (s)
T	Temperature (°C)
x	Vapor quality (1)
U	Voltage (V)
ρ	Density (kg/m^3)
μ	Dynamic viscosity (Pa s)
σ	Surface Tension (N/m)
g	Acceleration due to gravity (m/s^2)
λ_L	Laplace length scale (capillary length) (1)

Non-dimensional Parameters

Bd	Bond number
Bo	Boiling number
Co	Confinement number
Cv	Convective number
f	Frictional factor
Fa	Fang number
Fr	Froude number
La	Laplace constant

Nu	Nusselt number
Pr	Prandtl number
Re	Reynolds number
We	Weber number

Subscript

Bd	bubble diameter
cb	convective boiling
crit	critical
elect	electric
€	inner
nb	nucleate boiling
o	outer
s	surface
sat	saturation
sp	single phase
sub	subcooled
w	wall

Superscript

m	dimensional constant
n	dimensional constant, Chen's generalized exponential component

Table of Contents

Dedication iii

Abstract iv

Acknowledgement v

Nomenclature vi

Table of Contents ix

List of Figures xii

1 Introduction 1

1.1 Aim and Objectives 4

1.2 Organization of Thesis 4

2 Background and Literature Review 6

2.1 Pool boiling 7

2.2 Flow Boiling 11

2.3 Flow Boiling Heat Transfer 13

2.4 Two Phase Flow patterns 14

2.4.1 Flow patterns in a vertical channel 15

2.4.2 Flow patterns in a horizontal channel 16

2.5 Flow pattern maps 17

2.6 Qualitative description of heat transfer 21

2.7 Experimental investigation on flow boiling heat transfer 26

2.8 Chapter Conclusion 35

3 Description of Experimental Methods 36

3.1 Experimental Setup 36

3.1.1 Reservoir 38

3.1.2 Pre-Conditioner 38

3.1.3 Heat Source 39

3.1.4 Valves 39

3.1.5 Condenser 39

3.1.6 Conditioner 39

3.1.7 Test Section 39

3.1.8 Visualization Section 40

3.1.9 Chillers and Heat exchangers 41

3.1.10 Pump 41

3.2 Measurements and Accuracy of Measurements 41

3.3 Measurements 42
3.3.1 Mass Flux 43
3.3.2 Temperature 43
3.3.3 Heat Flux 43
3.3.4 Pressure 44
3.4 Measurement Accuracy 45
3.4.1 Measurement Uncertainties 46
3.4.2 Experimental Conditions for the facility 46
3.4.3 User Interface of Software 46
3.5 Experimental procedure and Data Reduction 48
3.5.1 Operational steps for the experimental facility 48
3.5.2 Experimental Procedure 48
3.5.3 Data Reduction 50
3.5.4 Heat transfer coefficient 50
3.5.5 The inner wall temperature 50
3.5.6 Vapor Quality 51
3.5.7 Heat Flux 51
3.6 Concluding Remarks 52
4 Results and Discussion 53
4.1 Experimental Validation 54
4.1.1 Heat Transfer Validation of the Test Section 54
4.1.2 Comparison of Results with Similar Work from Literature 55
4.1.3 Test of Repeatability 56
4.1.4 Pressure Drop Validation (Single phase) 57
4.2 Heat Transfer Coefficient from Subcooled Liquid Region through Saturation Region to Superheated Vapor Region 58
4.2.1 Subcooled Region 58
4.2.2 Two-Phase Region (Saturated Region) 62
4.2.3 Dry-Out Incipience and CHF 66
4.2.4 Superheated Region 66
4.2.5 Temperature Profile 67
4.2.6 Pressure Drop 70
4.3 Effect of Saturation Pressure on heat transfer 72
4.3.1 Flow Boiling Heat Transfer Coefficient 72
4.3.2 Flow Patterns 76
4.3.3 Frictional Pressure Drop 82
4.3.4 Comparison of Experimental Results with Correlations of Heat Transfer Coefficient Developed Based on Different Theories 83
4.4 Flow boiling Heat Transfer Characteristics at Varying Heat Fluxes 92

5 Conclusion 96

5.1 Recap 96

5.2 Final Remarks and recommendation 98

Publications 100

References 101

List of Figures

Figure 1.1: a. Air-conditioning units mounted on flats in Singapore b. industrial refrigeration for food storage in a shopping center.....2

Figure 1.2: Schematic and working principle of refrigeration system 3

Figure 2.1: Boiling regimes of the flow boiling curve [13] 8

Figure 2.2: Classical boiling curve with accompanying heat transfer mechanism during pool boiling process [14] 9

Figure 2.3: Representation of two-phase flow and boiling regimes in a vertically oriented channel at moderate but uniform heat flux [13] 12

Figure 2.4: Flow regimes and heat transfer regimes at moderate heat flux in a uniformly heated horizontal oriented channel [13] 13

Figure 2.5: Flow patterns for upward vertical flow in channels [20] 15

Figure 2.6: Flow patterns for horizontal flow in channels [20] 17

Figure 2.7: Flow pattern map of Baker for flow in a horizontal tube [27] 18

Figure 2.8: Flow pattern map of Mandhane for flow in a horizontal tube [30] 19

Figure 2.9: Flow pattern map of Kattan et al. in solid blue lines for flow in a horizontal tube (refrigerant = R410A, T_{sat} = 5°C and 13.84 mm internal diameter) [34].....20

Figure 2.10: Flow pattern map of Wojtan et al. for flow in a horizontal tube (refrigerant = R22, G = 100 kg/m^{2}s, q" = 2.1 kW/m^2, Tsat = 5 °C and 13.84 mm internal diameter) [38].....21

Figure 2.11: Heat transfer coefficient behavior as a function of quality and heat flux from Collier and Thome [56] 23

Figure 2.12: Heat transfer coefficient behavior as a function of quality according to Kandlikar [58]. 24

Figure 2.13: schematic flow regimes and variation of heat transfer coefficient for nucleate boiling by Kim and Mudawar [67] 25

Figure 2.14: schematic flow regimes and variation of heat transfer coefficient for convective boiling by Kim and Mudawar [67]. 26

Figure 3.1: Picture of the experimental facility 37

Figure 3.2: Simplified schematic of the experimental flow loop 38

Figure 3.3: Schematic representation of the test section 40

Figure 3.4: Visualization section 40

Figure 3.5a: LabVIEW software interface (Main control screen) 47

Figure 3.6: LabVIEW software interface (monitoring screen) 47

Figure 3.7: Picture of monitor for monitoring steady state condition to observe the time averaged changes in the experimental conditions 49

Figure 3.8: Picture of the steady state condition to observe the time averaged changes in the experimental conditions 49

Figure 4.1: Comparison of single-phase liquid and vapor heat transfer coefficient results with prediction by Dittus–Boelter correlation 54

Figure 4.2: Comparison of two-phase flow heat transfer coefficient from this case with a similar case from the literature [84] 55

Figure 4.3: Comparison of the two-phase flow heat transfer coefficient from this case with a similar case from the literature [99] 56

Figure 4.4: Test of repeatability for the heat transfer coefficient results 57

Figure 4.5: Validation of single-phase pressure drop 58

Figure 4.6: Variation in measured heat transfer coefficient for fixed mass flux of 200 kg/(m^2 s), constant pressure of 460 kPa and varying heat flux of 4.6 kW/m^2 and 8.5 kW/m^2 as a function of vapor quality. The ranges of the different boiling modes, as presented in Figure 13a–e, are indicated in the graph 59

Figure 4.7: Variation in measured heat transfer coefficient for fixed mass flux of 300 kg/(m^2 s), constant pressure of 460 kPa and varying heat flux of 4.6 kW/m^2 and 8.5 kW/m^2 as a function of vapor quality. 60

Figure 4.8: Variation in measured heat transfer coefficient for fixed heat flux of 4.6 kW/m^2, constant pressure of 460 kPa and varying mass flux of 200 kg/(m^2 s) and 300 kg/(m^2 s) as a function of vapor quality. The ranges of the different boiling modes, as presented in Figure 14a–e, are indicated in the graph 60

Figure 4.9:Variation in measured heat transfer coefficient for fixed heat flux of 8.5 kW/m^2, constant pressure of 460 kPa and varying mass flux of 200 kg/(m^2 s) and 300 kg/(m^2 s) as a function of vapor quality. 61

Figure 4.10: Slug flow pattern (x < 0.1); (**b**). Slug intermittent flow pattern ($x \approx 0.1$); (**c**). Intermittent flow pattern (x = 0.15-0.4); (**d**). Annular flow pattern (x > 0.4);). Dry-out–mist flow pattern (x > 0.9) of (G = 200 kg/(m^2 s), q" = 4.6 kW/m^2, P_{sat} = 460 kPa), (G = 200 kg/(m^2 s), q" = 8.5 kW/m^2, P_{sat} = 460 kPa) and (G = 300 kg/(m^2 s), q" = 8.5 kW/m^2, P_{sat} = 460 kPa. 62

Figure 4.11: a) Slug flow pattern (x < 0.10); (b) Intermittent flow pattern (0.1 < x < 0.4); (c) Intermittent–annular flow pattern ($x \approx 0.42$); (d) Annular flow pattern (x > 0.4); (e) Dry-out–mist flow pattern (x > 0.9); Flow pattern for G = 300 kg/(m^2 s), q" = 4.6 kW/m^2, P_{sat} = 460 kPa.... 65

Figure 4.12: Variation in measured wall, fluid and calculated saturation temperatures as a function of vapor quality for G = 200 kg/(m^2 s) and q" = 4.6 kW/m^2 at a constant saturation pressure of 460 kPa 67

Figure 4.13: Variation in measured wall, fluid and calculated saturation temperatures as a function of vapor quality for G = 200 kg/(m^2 s) and q" = 8.5 kW/m^2 at a constant saturation pressure of 460 kPa 68

Figure 4.14: Variation in measured wall, fluid and calculated saturation temperatures as a function of vapor quality for G = 300 kg/(m^2 s) and q" = 4.6 kW/m^2 at a constant saturation pressure of 460 kPa 68

Figure 4.15: Variation in measured wall, fluid and calculated saturation temperatures as a function of vapor quality for G = 300 kg/(m^2 s) and q" = 8.5 kW/m^2 at a constant saturation pressure of 460 kPa 69

Figure 4.16: Variation in pressure drop as a function of vapor quality for a varied mass flux, fixed heat flux and constant saturation pressure. 70

Figure 4.17: Variation in pressure drop as a function of vapor quality for a varied mass flux, fixed heat flux and constant saturation pressure. 70

Figure 4.18: Variation in pressure drop as a function of vapor quality for a varied heat flux, fixed mass flux and constant saturation pressure. 71

Figure 4.19: Variation in pressure drop as a function of vapor quality for a varied heat flux, fixed mass flux and constant saturation pressure. 71

Figure 4.20: Effect of saturation pressure on heat transfer coefficient for mass flux 150 kg/(m^{2}s) and heat flux of 8.26 kW/m^2. 74

Figure 4.21: Effect of saturation pressure on heat transfer coefficient for mass flux of 150 kg/(m^{2}s) and heat flux of 23.3 kW/m^2 75

Figure 4.22: Effect of saturation pressure on heat transfer coefficient for mass flux of 300 kg/(m^2 s) and heat flux of 8.26 kW/m^2 75

Figure 4.23: Effect of saturation pressure on heat transfer coefficient for mass flux of 300 kg/(m^2 s) and heat flux of 23.3 kW/m^2. 76

Figure 4.24: Flow pattern predictions by Wojtan et al. for increasing saturation pressures from 460 kPa to 660 kPa at G = 150 kg/(m^{2}s), q"8.26 kW/m^2 **(a-c)**, G = 150 kg/(m^{2}s), q" = 23.3 kW/m^2 **(d-f)**, G = 300 kg/(m^{2}s), q" = 8.26 kW/m^2 **(g-i)** and G = 300 kg/(m^{2}s), q" = 23.3 kW/m^2 **(j-l)**. 79

Figure 4.25: Flow pattern evolution with increasing vapor quality for G = 150 kg/(m^{2}s), q" = 8.26 kW/m^2, P_{sat} = 560 kPa 80

Figure 4.26: Flow pattern evolution with increasing vapor quality for G = 300 kg/(m^2 s), q" = 8.26 kW/m^2, P_{sat} = 560 kPa 81

Figure 4.27: Effect of saturation pressure on adiabatic frictional pressure drop at **(a)** G = 150 kg/(m^{2}s), q" = 8.26kW/m^2, **(b)** G = 150 kg/(m^{2}s), q" = 23.3 kW/m^2, **(c)** G 300 kg/(m^{2}s), q" = 8.26 kW/m^2 and **(d)** G = 300 kg/(m^{2}s), q" = 23.3 kW/m^2 83

Figure 4.28: (a–l) Comparison between each experimental result measured at conditions of G = 150-300 kg/(m^{2}s), q" = 8.26-23.3 kW/m^2, P_{sat} 460-660 kPa and the calculated heat transfer coefficient developed based on different theoretical assumptions by Cooper [19], Tran et al. [31], Berstch et al. [32], Warrier et al. [33], Wattelet et al. [110], Liu and Winterton [111] and Kandlikar [112] 87

Figure 4.29: (a–l) Comparison of how predictive models of Cooper [19], Tran et al. [31], Berstch et al. [32], Warrier et al. [33], Wattelet et al. [110], Liu and Winterton [111] and Kandlikar [112] are able to capture experimental trend over vapor quality for conditions of G = 150-300 kg/(m^2 s), q" = 8.26-23.3 kW/m^2, P_{sat} = 460-660 kPa. 89

Figure 4.36: Heat transfer coefficient of R134a for mass flux of 300 kg/(m^{2}s), saturation pressure of 460 kPa and heat fluxes from 7.2 to 14.3 kW/m^2 (convective boiling case) 93

Figure 4.37: Heat transfer coefficient of R134a for mass flux of 300 kg/(m^2s), saturation pressure of 460 kPa and heat fluxes from 28.1 to 47.4 kW/m^2 (Nucleate boiling case 93

Figure 4.38a & b: Wall, fluid, saturation temperature, heat transfer coefficient and corresponding flow pattern evolution for both convective and nucleate boiling cases. 95

Chapter 1

1 Introduction

With the continuous rise in demand for air-conditioning and refrigeration in both industrial and domestic applications, the world is confronted with an impending and potentially catastrophic "cold crunch" which threatens to undermine global warming targets and emission control by policy makers. The projected increase in global air conditioning and refrigeration usage due to rising incomes in developing countries and urbanization is anticipated to cause a 33-fold surge in power consumption by 2100. Currently, the United States consumes an equivalent amount of electricity for cooling buildings as the entire continent of Africa uses for all purposes. China and India are rapidly approaching similar levels of consumption. The demand for cooling is already substantial, expanding rapidly, and currently being addressed using methods that have remained largely unchanged for many years. However, the importance of cooling in energy discussions is often overlooked. Failing to transform our approach to removing heat will result in significant and impactful consequences. People now have the expectation of air conditioning to ensure comfort in homes, offices, and vehicles, enabling habitable conditions in numerous cities. In the developed world, the majority of food is refrigerated or frozen, and refrigeration is vital for storing medicines, including vaccines [1], [2].Figure 1.1 is an image of air-conditioning units mounted on flats in Singapore demonstrating how cooling has become part of us in recent times [3], [4].

Also, due to rapid technological advancements and the demand for compact yet powerful devices, there have been significant concerns with finding solution to meet the current heat loads posed by these advancements. Traditional methods like air cooling and single-phase heat transfer face challenges in addressing the increasing heat flux requirements posed by these technological

advancements. Various industrial and domestic sectors are seeking an efficient heat removal technique that can effectively handle high heat flux demands. By utilizing the advantages offered by latent heat transfer instead of sensible heat transfer, two-phase flow boiling technique demonstrates the potential to greatly enhance heat transfer with a high heat transfer coefficient, surpassing the capabilities of conventional single-phase processes [5].

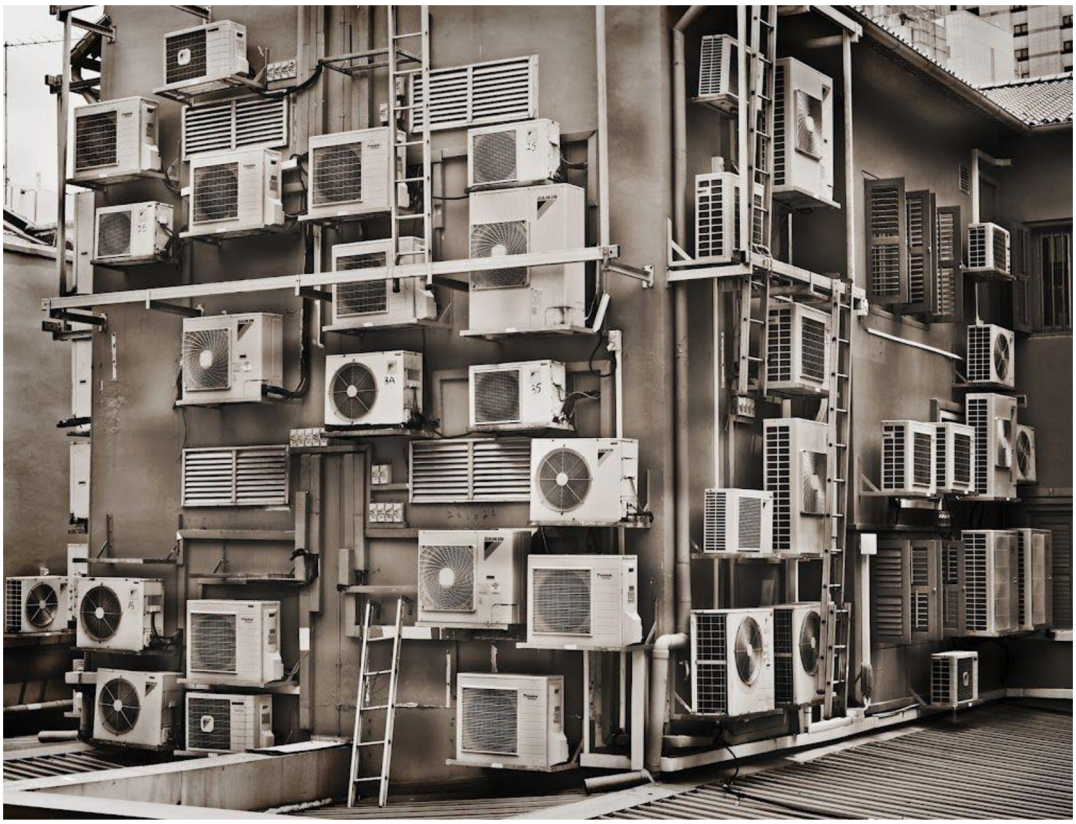

Figure 1.1: Air-conditioning units mounted on flats in Singapore

In air-conditioning, refrigeration and many other cooling applications described above, evaporator; which is a two-phase component is an essential component for removing or exchanging heat with the goal of providing cooling. Since two-phase flow boiling is encountered in the evaporator, a better understanding of the two-phase flow boiling process and related mechanisms is thus significant for better sizing and design of the evaporator and subsequently cooling systems. Figure 1.2 below shows the schematic of a refrigeration system with evaporator serving as a significant component.

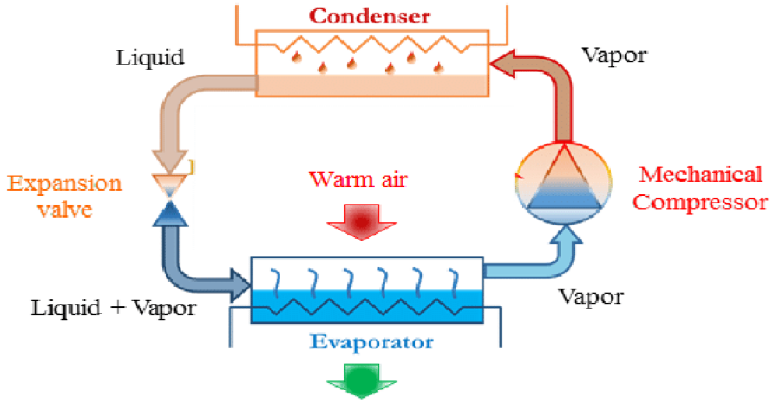

Figure 1.2: Schematic and working principle of refrigeration system

When it comes to two phase flow boiling heat transfer, for the past few years, research in this field has gained an increasing popularity for unravelling the dominant mechanism responsible for controlling heat transfer and identifying a parametric trend for understanding the characteristics of flow boiling heat transfer. This has led to several assumptions and models for predicting heat transfer during flow boiling without any known generalized mechanism. This popularity regarding research in the area of flow boiling heat transfer is because flow boiling heat transfer has been identified as an efficient technique for dissipating heat from small diameter tubes [6]. For flow boiling heat transfer, two mechanisms, namely nucleate boiling and convective boiling, are assumed to control the heat transfer which then relates to the heat transfer coefficient and flow patterns significantly. Nucleate boiling is said to dominate the heat transfer when bubbles generated, grow and coalesce at the walls of the tube are responsible for controlling the heat transfer. Convective boiling on the other hand is assumed to dominate the heat transfer when conduction and convection processes occurring at the thin liquid layer near the wall and liquid–vapor interface, respectively, control the heat transfer. These heat transfer mechanisms are highly affected and controlled by flow parameters such as working fluid, the geometry of the tube, saturation conditions (temperature and pressure), mass flux, heat flux, and vapor quality. For the effect of flow parameters on heat transfer coefficient, when saturation conditions and heat flux affect the heat transfer coefficient significantly, nucleate boiling is considered to dominate and control the heat transfer. When mass flux and vapor quality significantly affect the heat transfer coefficient, convective boiling is considered to dominate and control the heat transfer. Both mechanisms can co-occur over a wide range of vapor quality where the heat transfer coefficient is affected by mass flux, heat flux, and saturation conditions along certain regions of vapor quality [7], [8].

Despite extensive studies on flow boiling heat transfer, the general characteristics and dominant mechanism responsible for controlling the heat transfer remain enigmatic with many contradicting results for seemingly similar experimental conditions reported in the literature. Although several studies have been performed to understand the effect of flow parameters on heat transfer characteristics there is still a lack of consensus on how these flow parameters and their interrelations affect heat transfer behavior during flow boiling with many contradicting results and complex trends of heat transfer coefficient along a range of vapor quality. An accurate prediction and understanding of the heat transfer mechanisms involved in flow boiling offers numerous advantages which include; improved heat transfer coefficient, small thermal resistance between heat transfer devices and their coolant, proper sizing of heat transfer devices and relatively low cost involved in designing heat transfer devices [9]–[11].

1.1 Aim and Objectives

This research thus aims to contribute to better understanding of the mechanism that controls heat transfer during two-phase flow boiling of refrigerants in small diameter tubes. To understand these mechanisms, this study seeks to investigate the effect of flow boiling parameters such as mass flux, heat flux, vapor quality and saturation conditions on flow boiling heat transfer. Achieving these significant aims will help to understand the dominant mechanisms responsible for controlling heat transfer in small diameter tubes identify the parametric trend for flow boiling heat transfer and analyze the obtained findings with available models and correlations in literature.
This aim can be achieved by accomplishing the objectives below:

- Investigate the effect of flow conditions (mass flux, heat flux, vapor quality and saturation conditions) on heat transfer coefficient, pressure drop and flow patterns from subcooled liquid region to superheated vapor region.
- Identify the mechanisms that dominate flow boiling over a wide range but small increment of vapor quality for the flow boiling conditions investigated.
- Analyze flow boiling correlations and models for predicting flow boiling heat transfer developed based on different theories.

1.2 Organization of Thesis

This thesis is organized into five (5) chapters. The first chapter (chapter 1) provides introduction of the study which leads to the development of the main aim and objectives of the thesis. The second chapter (chapter 2) is dedicated to state-of-the-art and up to date review of the work

done in this field. This is to recognize the trends and gaps in literature that motivates the focus area and objectives of this study. In the third chapter (chapter 3), the experimental facility and methodology is described. The test section geometry, the visualization section and all other components involved in setting up the test rig is discussed here with uncertainty analysis clearly discussed. The data reduction process is also elaborated in this chapter. The fourth chapter (chapter 4) is reserved for results and discussion. Here, the main outcomes of the thesis with the achieved objectives will be discussed. This will be based on the effect of flow parameters on heat transfer, pressure drop, flow pattern visualization and comparison of the findings with predictive models in literature. The last chapter (chapter 5) concludes the study with key findings with relation to the aims and objectives of this study and recommendations for future research related to this topic.

Chapter 2

2 Background and Literature Review

Two phase flow can simply be described as two unique phases, having a common interface flowing in a channel. Each of these phases represents a mass or volume of matter. These two phases can be solid-liquid phase, solid-gas phase or liquid-gas phase. For two phase flow within an internal channel, there is the simultaneous motion of both vapor and liquid within the channel. Compared to single phase flow, two phase flow is complex phenomenon that is widely encountered in applications such as refrigeration and air condition applications. For these applications, both liquid and vapor coexist in the evaporator and condensers of the system. This makes understanding two phases flow an important area of research since adequate knowledge helps in the prediction of heat transfer characteristics and pressure drop based on the flow rate, channel size and operating conditions of the flow. It also helps in the proper design of systems that employ two phase flow without oversizing or under-sizing [12].

Boiling is a phase change process in which when a liquid encounters a surface that has surface temperature (T_s) sufficiently higher than the saturation temperature (T_{sat}) of the liquid. Boiling can be categorized into two processes namely:

- Pool boiling
- Flow boiling

This thesis focuses on internal flow boiling heat transfer during two phase flow.

2.1 Pool boiling

With the categories of boiling, firstly, pool boiling refers to the process of boiling that occurs on a heated surface submerged in a pool or body of motionless liquid. It involves the formation and growth of vapor bubbles on the heated surface due to the transfer of heat from the surface to the liquid. To begin exploring pool boiling, it is essential to reference the pool boiling curve as described by Nukiyama's experiment [13]. Nukiyama's experiment, conducted by Japanese scientist Yutaka Nukiyama in 1934, played a significant role in understanding the phenomenon of boiling heat transfer. The experiment was aimed to investigate the relationship between heat flux and wall superheat during pool boiling. In Nukiyama's experiment, an electrically heated wire was submerged in a pool of saturated liquid, typically water. The wire's temperature was measured, and the heat flux at the wire's surface was calculated based on the supplied electric power. The wall superheat, ΔT_w (the temperature difference between the wire's surface temperature, T_w, and the saturation temperature of the liquid, T_{sat}), was also determined. By systematically varying the heat flux and measuring the corresponding wall superheat, Nukiyama obtained data points that formed a characteristic curve known as the "boiling curve" or "Nukiyama curve". This curve represented the relationship between the applied heat flux and the resulting wall superheat during pool boiling. The boiling curve provided insights into the different boiling regimes observed during the experiment. It typically exhibited three distinct regions as shown in Figure 2.1 below:

1. Nucleate Boiling: At low heat fluxes, the curve showed a gradual increase in heat transfer with a relatively small wall superheat. This region represented the dominance of nucleate boiling, where small vapor bubbles formed on the heated surface.
2. Transition Boiling: As the heat flux increased, the curve exhibited a steep rise in heat transfer with a significant increase in wall superheat. This region indicated the transition from nucleate boiling to film boiling, where a continuous vapor film started to form on the heated surface.
3. Film Boiling: At high heat fluxes, the curve showed a relatively constant heat transfer rate with a further increase in wall superheat. This region represented the dominance of film boiling, where a vapor film completely separated the heated surface from the liquid, significantly reducing heat transfer.

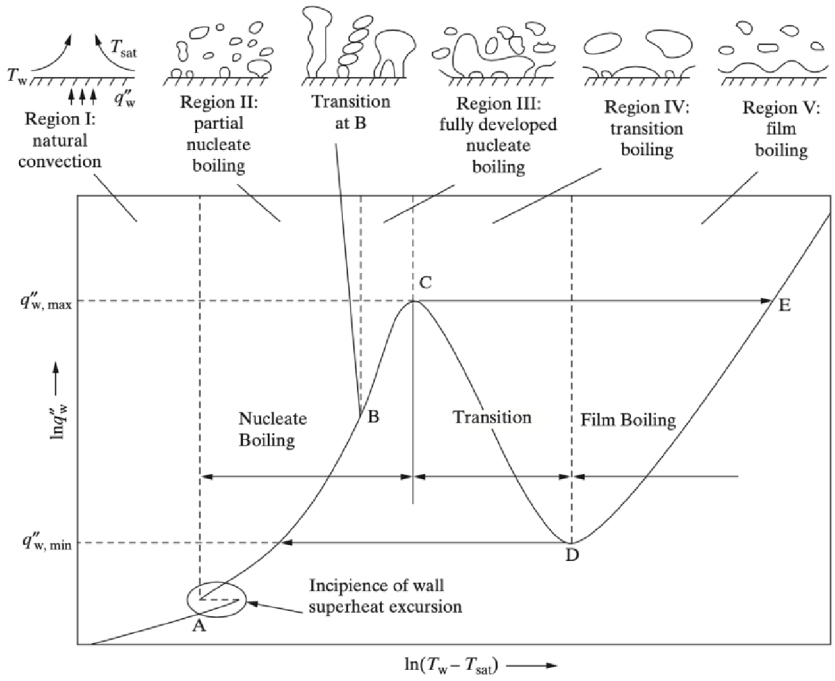

Figure 2.1: Boiling regimes of the flow boiling curve [14]

Nukiyaama's experiment and the boiling curve provided valuable insights into the heat transfer characteristics of pool boiling. The findings have since been instrumental in the development of heat transfer correlations and the understanding of boiling heat transfer phenomena in various applications and engineering designs. Figure 2.2 depicts boiling curve with heat transfer mechanisms that are developed during the boiling process. Initially (O-A), as the rate of heating the surface is increased there's no bubble formation and heat is transferred by natural convection between the hot surface and the liquid vapor interfaces. At a certain value of wall superheat (A) bubble nucleation is initiated on cavities present on the heated surface. This condition is called onset of nucleate boiling (ONB). For liquids that are capable of wetting the surface well, the onset of nucleation may be delayed (A'); for these liquids a sudden activation of a large number of cavities at an increased wall superheat causes a reduction in the surface temperature while the heat flux remains constant (A'-.A"). After inception, the slope of the curve increases dramatically. At first, discrete bubbles are released from randomly located active sites (A-B). At higher heat flux the density of active sites and the frequency of bubble release increase. Transition from isolated bubbles to fully developed nucleate boiling (B-C) occurs when bubbles at a given site begin to merge in the vertical direction and with bubbles from the neighboring sites. Further increasing the heat flux, intense evaporation near the bubble base leads to periodic dry patches on the surfaces that are rewetted by the surrounding liquid (C-D). This results in a reduction in the slope of the curve.

Eventually, liquid is unable to rewet the heating surface and a large area becomes covered by a vapor blanket, causing a large temperature excursion on the heating surface (F). The heat flux corresponding to this condition (D) is known as the critical heat flux (CHF), and represents the upper limit of fully developed nucleate boiling or safe operation of equipment. If the temperature at F exceeds the melting temperature of the heating material, the heater will fail (burn out). The curve E-F represents the stable film boiling–the surface is totally covered with vapor film and the liquid does not contact the solid- and the system can be made to follow this curve by reducing the heat flux. With a reduction in heat flux in film boiling, a condition is reached when the vapor film can no longer be sustained and collapses. The heat flux corresponding to this condition (E) is called the minimum heat flux. The region falling between nucleate and film boiling (D-E) is known as the transition boiling region. Transition boiling is very unstable and essentially inaccessible with constant heat flux boundary condition.

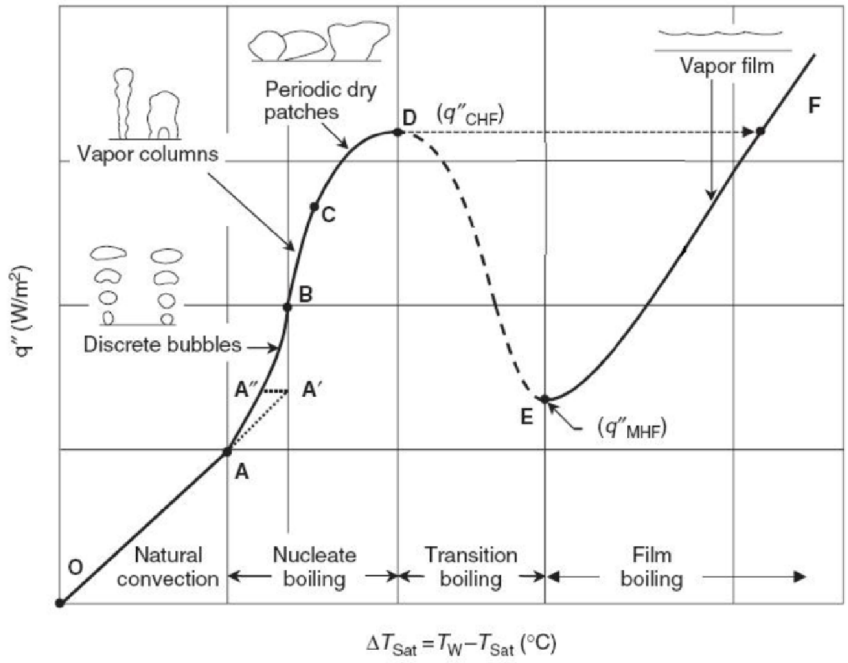

Figure 2.2: Classical boiling curve with accompanying heat transfer mechanism during pool boiling process [15]

The nature of the pool boiling curve is significantly influenced by certain parametric effects. Increased surface wettability, which leads to a decrease in the contact angle between the surface and the liquid, causes a shift of the nucleate boiling line towards the right. This means that for the same temperature difference between the wall and saturation temperature ($T_w - T_{sat}$), lower nucleate

boiling heat transfer coefficients are observed with increased surface wettability. Additionally, increased surface wettability also results in higher maximum heat flux values [16]. On the other hand, increased surface roughness has the effect of shifting the nucleate and transition lines towards the left, indicating an improvement in the nucleate boiling heat transfer characteristics. Surface contamination, such as deposition and oxidation, as well as improved surface wettability, has similar effects to surface roughness. Liquid pool subcooling enhances heat transfer in all boiling regimes, except for the fully developed nucleate boiling region, where its impact is minimal. Furthermore, the orientation of the surface with respect to gravity significantly affects partial boiling and film boiling, but has little influence on fully developed nucleate boiling [14].

Many empirical correlations have been reported in literature for predicting heat transfer during nucleate boiling. These nucleate boiling correlations mostly express the heat transfer coefficient as a function of heat flux, fluid properties, and fluid pressure. Among the widely reported correlations in literature is Rohsenow's correlation [17]. Rohsenow's correlation is one of the early correlations proposed for predicting heat transfer during pool boiling. It is based on the bubble agitation mechanism in nucleate boiling. It is given as:

$$Nu = \frac{h\lambda_L}{k_f} = \frac{1}{C_{sf}} Re^{1-n} Pr_f^m. \qquad 2.1$$

Although it looks simple, it is able to predict the heat transfer fairly well. According to Dhir [18], the use of C_{sf} (fluid-surface pair) to account for the effect of surface characteristics and wettability may be the reason for the correlation's ability to predict heat transfer fairly well. Stephen et al. [19] utilized a statistical multiple regression technique to analyze a large dataset, mostly for horizontal tubes. They divided the data into four fluid categories: water, organics, refrigerants, and cryogens. This correlation is expressed as:

$$Nu = \frac{hd_{Bd}}{k_f}. \qquad 2.2$$

It has been identified to have fairly good accuracy for predicting heat transfer during pool boiling. Cooper's [20] correlation is one of the famous correlations recommended for predicting heat transfer during nucleate boiling. It has also been used by some authors to represent the nucleate boiling contribution to forced convection flow boiling. Cooper conducted an extensive study incorporating approximately 6,000 pool boiling data points from published sources and over 100 experiments. He developed a more accurate pool boiling correlation based on reduced pressure. The correlation takes into account the heat flux, reduced pressure, surface roughness of the boiling surface, and molecular weight of the fluid. It can be expressed as follows:

$$h_{nb} = 55P_R^{0.12}(-log_{10}P_R)^{-0.55}M^{-0.5}q''^{0.67}, \quad 2.3$$

where P_R is the reduced pressure, M is the molecular mass of the fluid and q'' is the heat flux.

Because pool boiling has different regimes which are different from each other, different heat transfer correlations are used for each regime. For example, for natural convection boiling regimes, correlations of natural convection govern the heat transfer rate. In the nucleate boiling regime, nucleation is responsible for the rate of heat transfer. This is where the number of active nucleation sites, rate of bubble formation and many others control the heat transfer. However, these make it extra difficult to develop heat transfer correlations based on theories. For this reason, most correlations for nucleate boiling regime are based on experiment.

2.2 Flow Boiling

Compared to pool boiling, flow boiling is a complex phenomenon due to the hydrodynamic effects and boiling heat transfer process that occur in flow boiling. During flow boiling process, there is a continuous development of heat transfer and flow boiling regimes as vapor quality increases along the flow direction. For most industrial two-phase applications, the flow geometry orientation is either vertical or horizontal. This is why most studies in two phase flow boiling are focused on these two geometrical orientations [14]

For flow boiling in a vertically oriented channel Figure 2.3 shows the heat transfer mechanisms, flow regimes and corresponding temperature profile for a constant flow rate and moderate but uniform heat flux condition. For this condition, the working fluid is assumed to enter the channel as a subcooled liquid. At the entrance of the inlet, where the subcooling of the liquid is sufficiently high to allow bubble formation, the flow regime here consists of single-phase liquid, and the heat transfer occurs through forced convection. In the bubbly and slug flow regimes, nucleate boiling dominates, while annular flow predominates in the forced convective evaporation regime. The latter is particularly efficient for heat transfer as it involves a thin liquid film covering the heated wall. The liquid film cools through evaporation at its surface, preventing significant superheating required for bubble formation. Dispersed droplet flow can occur if the vapor flow rate is sufficiently high, leading to entrainment of droplets. Moving downstream, the liquid film may completely evaporate, resulting in dryout. In the dryout region, there is no sustained contact between the heated surface and the liquid, although occasional droplet deposition may occur. As the entrained droplets continue downstream, they eventually evaporate entirely, leading to a single-phase vapor flow. The heat transfer coefficient in the dryout region is significantly lower compared

to the nucleate boiling or forced convective evaporation regimes. Consequently, dryout is accompanied by a notable wall temperature increase at the heated surface. The occurrence of dryout is similar to the critical heat flux phenomenon observed in pool boiling.

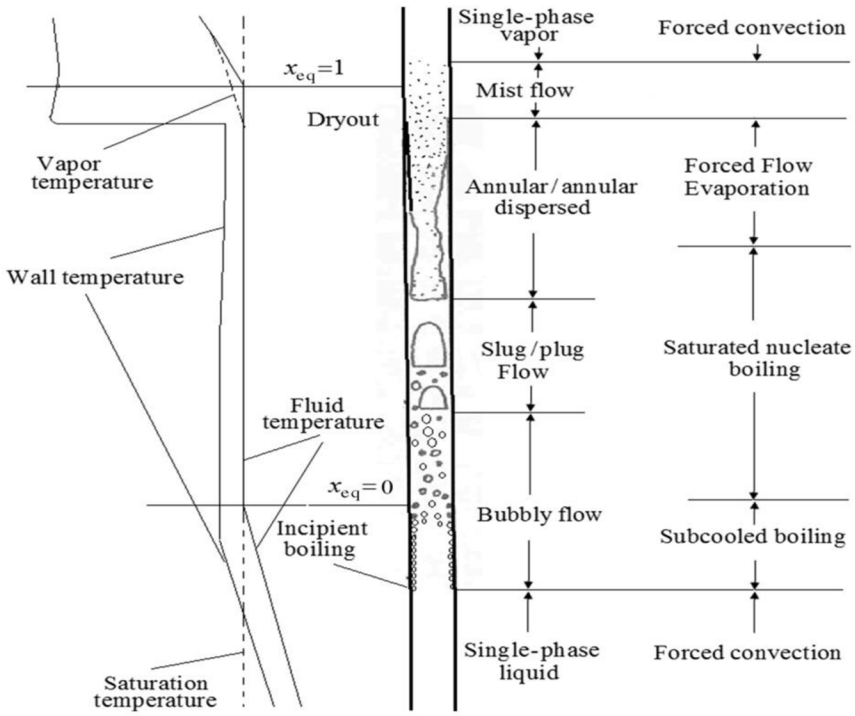

Figure 2.3: Representation of two-phase flow and boiling regimes in a vertically oriented channel at moderate but uniform heat flux [14]

In the case of a uniformly heated horizontally oriented channel (which is the case of this dissertation) as indicated in Figure 2.4, we discuss the conditions for moderate mass and heat flux. How the heat transfer mechanism changes along the channel is also elaborated here. For very high mass flux conditions, the heat transfer and flow patterns are not highly influenced by the channel orientation. While the primary flow and heat transfer regimes resemble those in the vertically oriented channel, the influence of buoyancy can play a significant role. Buoyancy tends to encourage phase stratification, especially when the annular-dispersed flow regime (associated with forced-convective evaporation) is reached. In this scenario, the liquid film tends to drain downward, often leading to partial dryout, where the liquid film breaks down near the top of the heated channel while persisting in the lower regions of the channel perimeter. Due to partial dryout, the critical

heat flux (CHF) conditions in horizontal channels are typically achieved at lower vapor quality region compared to vertical upflow channels.

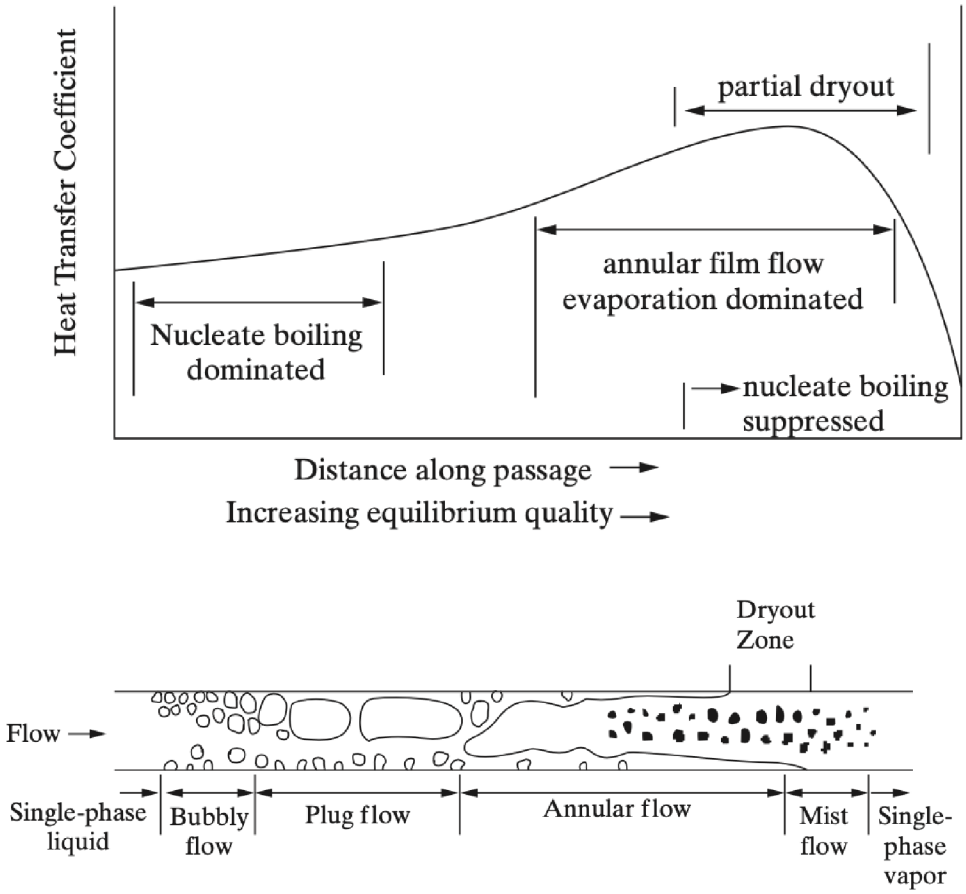

Figure 2.4: Flow regimes and heat transfer regimes at moderate heat flux in a uniformly heated horizontal oriented channel [14]

2.3 Flow Boiling Heat Transfer

With respect to flow boiling involving heat transfer, two distinct mechanisms are assumed to control flow boiling heat transfer in small diameter tubes. These mechanisms are

i) Nucleate boiling and

ii) Convective boiling

In the case of nucleate boiling, formation, growth and detachment of bubbles at the walls of the tube is assumed to control the heat transfer whereas conduction and convection through thin liquid film, evaporation at the liquid-vapor interface and flow velocity are assumed largely to control convective boiling. These two mechanisms can coexist over wide range of vapor qualities. These mechanisms are related to heat transfer coefficient. Because of this, most of the predictive models

and correlations for predicting heat transfer coefficient during flow boiling in literature are developed on the basis of the superposition of these two mechanisms [21]. In 1961, Kutateladze [22] proposed an equation whose approach has been by adopted by Chen [23] by employing a unitary asymptotic exponent for estimating the heat transfer coefficient behavior during flow boiling in a channel given as:

$$h = \sqrt[n]{(S_{nb}.\, h_{nb})^n + (F_{sp}.\, h_{sp})^n} \quad . \qquad 2.4$$

Chen's approach generalizes the exponential component "n" in Kutateladze equation as a unitary component one (1). Here, h_{nb} is the pool boiling heat transfer coefficient contribution and h_c is the single phase forced convection contribution, S_{nb} represents the suppression of the nucleate boiling contribution and F_c is the enhancement factor for convection contribution with increasing vapor quality. Based on the predictive model being employed, the asymptotic exponent n is usually 1 or 2. Generally, nucleate boiling suppression factor is usually between zero and one. However, increasing effect of inertia force has a decreasing effect on this factor. The enhancement factor for convection is usually greater than one (1) and it increases with increasing inertial forces [21]. When the heat transfer coefficient is not affected by mass flux and vapor quality but highly affected by heat flux and saturation pressure, nucleate boiling is assumed to be the predominant mechanism controlling the heat transfer. When the heat transfer coefficient is not affected by heat flux but highly influenced by mass flux and vapor quality, then convective boiling is assumed to be the dominant mechanism controlling heat transfer [24]. These mechanisms are responsible for heat transfer during flow boiling is highly related to flow patterns.

2.4 Two Phase Flow patterns

The study of two-phase flow patterns involves describing how liquid phase and vapor phase are distributed during the flow boiling process. The distribution of the two phases exhibit commonly observed flow structures that have particular identifiable characteristics. Flow patterns are closely related to heat transfer and pressure drop. Because of this, accurately predicting the flow patterns is relevant for understanding the thermodynamics, fluid mechanics and heat transfer characteristics of the flowing fluid and how they are connected with each other [25]. These flow patterns or structures are classified based on the direction of flow, mainly:

- Flow patterns in vertical channels
- Flow patterns in horizontal channels

2.4.1 Flow patterns in a vertical channel

In a vertical upward flow, different flow patterns are observed as described in Figure 2.5. These flow patterns are categorized based visual observations. Flow patterns are generated as a result of buoyancy force causing a slip between the two phases in which the vapor phase flows with a higher velocity compared to the liquid phase. A flow pattern is identified as bubbly flow when small and discrete bubbles begin to form near the walls of the heated channel during the upward flow of the boiling process. These bubbles move in a continuous liquid phase. The small bubbles detach from the heated wall and spread to the bulk liquid flow. As these small bubbles increase in number, they begin to grow and coalesce with each other to form a bullet-shaped Taylor bubble with increased length. Slug flow is close to the diameter of the channel with thin liquid film separating it from the heated wall. This type of flow pattern with elongated bubble is called slug flow. When these slugs become unstable and break into large pieces, churn flow pattern occurs. As vapor quality increases, flow velocity also increases. This then causes a thin liquid film to form near the heated channels with vapor flowing within the core center of the channel. This then leads to a type of flow pattern called annular flow. As vapor quality further increases, the thin liquid film formed near the walls of the channel begin to dryout leaving small droplets flowing in the vapor phase. This flow pattern with increased droplets is thus called wispy annular. Finally, when the entire thin liquid film dries out as a result of increased flow velocity and the entire phase become single phase superheated gas, wispy flow pattern is identified to occur.

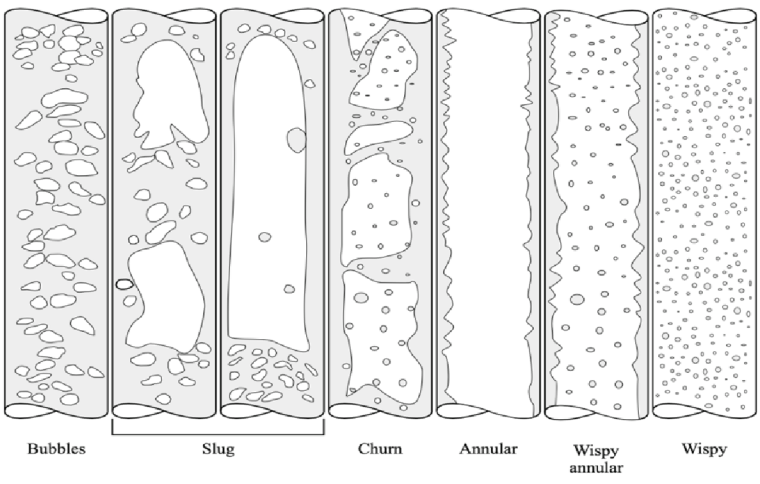

Figure 2.5: Flow patterns for upward vertical flow in channels [21]

2.4.2 Flow patterns in a horizontal channel

In the case of horizontal channel, buoyancy force causes the vapor phase to flow over the liquid phase. The flow patterns observed during horizontal channel flow are bubble flow, stratified flow, stratified wavy flow, plug flow, slug flow, annular flow and mist flow as depicted in Figure 2.6. Like in the case of vertical flow, for bubble flow pattern, small bubbles begin to form near the walls of the heated channel, these bubbles detach from the heated walls and form a continuous phase with the liquid phase. For stratified flow, the effect of gravitational force causes the vapor phase to flow over the liquid phase whereby these two phases are separated by a smooth interface. This flow pattern is usually observed under less velocity flow. When the vapor phase velocity increases, the smooth interface of the stratified flow becomes wavy with observable amplitudes leading to stratified wavy flow. Plug flow is an intermittent type flow pattern with larger bubble size that looks like bubble plugs. They usually flow on top of the liquid phase due to the effect of buoyancy. Slug flow pattern, which is also an intermittent type of flow pattern where the flow is characterized by large vapor bubbles in the shape of bullet called elongated bubbles. A thin liquid film at the upper part of the channel separates the slug from the upper part of the channel. Small discrete bubbles may also be observed in between the slug flows. At high vapor phase velocity, a thin film of liquid forms near the heated channel with vapor flowing at the core center of the channel. The thin liquid film forms around the entire perimeter of the tube with a thicker film in the bottom region of the channel. This flow pattern is known as the annular flow. Mist flow pattern occurs at high flow rates and high vapor quality. As the flow velocity increases, the liquid film near the heated wall becomes thinner and unstable. Eventually, the liquid film dries up with the vapor phase entraining liquid droplets at the core. This leads to a high temperature wall [21], [26].

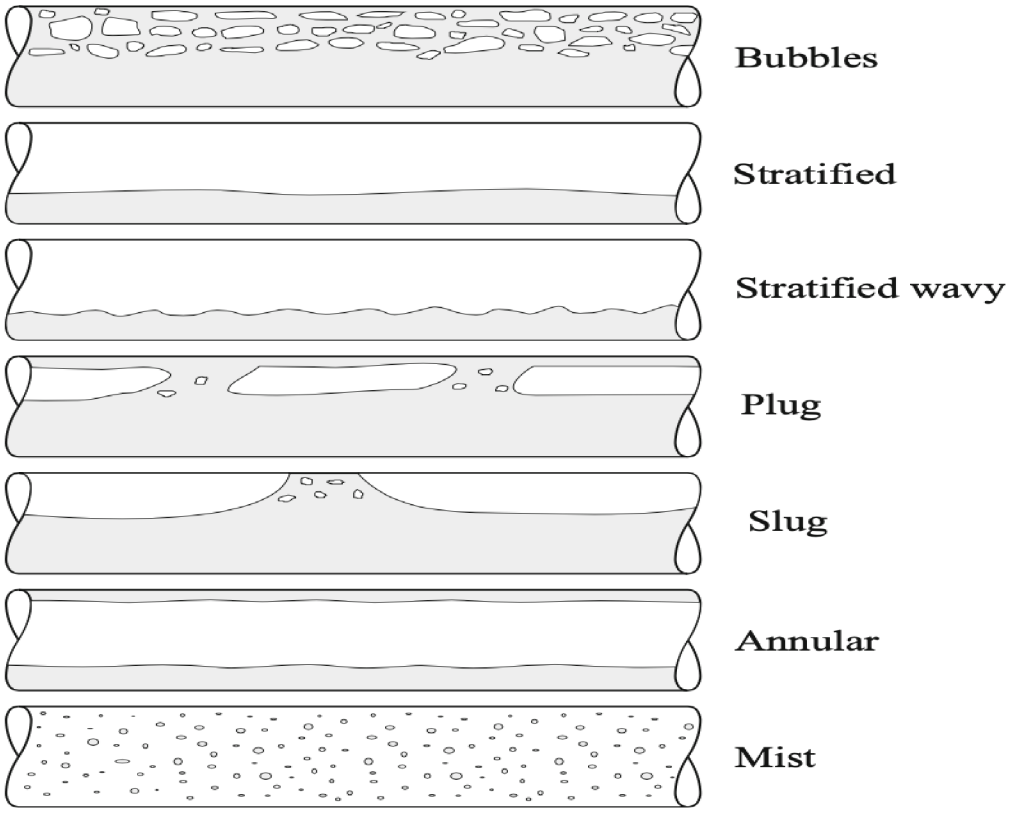

Figure 2.6: Flow patterns for horizontal flow in channels [21]

2.5 Flow pattern maps

Because flow patterns are closely related to heat transfer and pressure drop, different useful tools have been proposed to describe and predict these flow patterns in order to understand how they are related to the two-phase flow phenomenon. These tools are referred to as flow pattern maps. Early flow pattern maps were developed for adiabatic conditions. Data from the adiabatic conditions were then extrapolated to diabatic conditions. However, this situation sometimes resulted in unreliable conclusions [27]. Flow pattern maps typically include axes representing key parameters, such as vapor quality (x-axis) and mass flux or liquid velocity (y-axis). These parameters help locate the specific flow regime that occurs under given operating conditions. They also display boundaries or transition lines that separate different flow regimes. These boundaries are often determined empirically through experiments or derived from theoretical models. They may also include information about the heat transfer characteristics associated with each flow regime. Different flow patterns exhibit varying levels of heat transfer performance, and this information is crucial for system design. Some of these well-known flow pattern maps are briefly described below.

Baker's [28] adiabatic flow pattern map in 1954 was one of the early flow pattern maps developed for horizontal channels. This map was proposed for an adiabatic oil and gas flow in channels. This flow pattern map is presented in Figure 2.7 below.

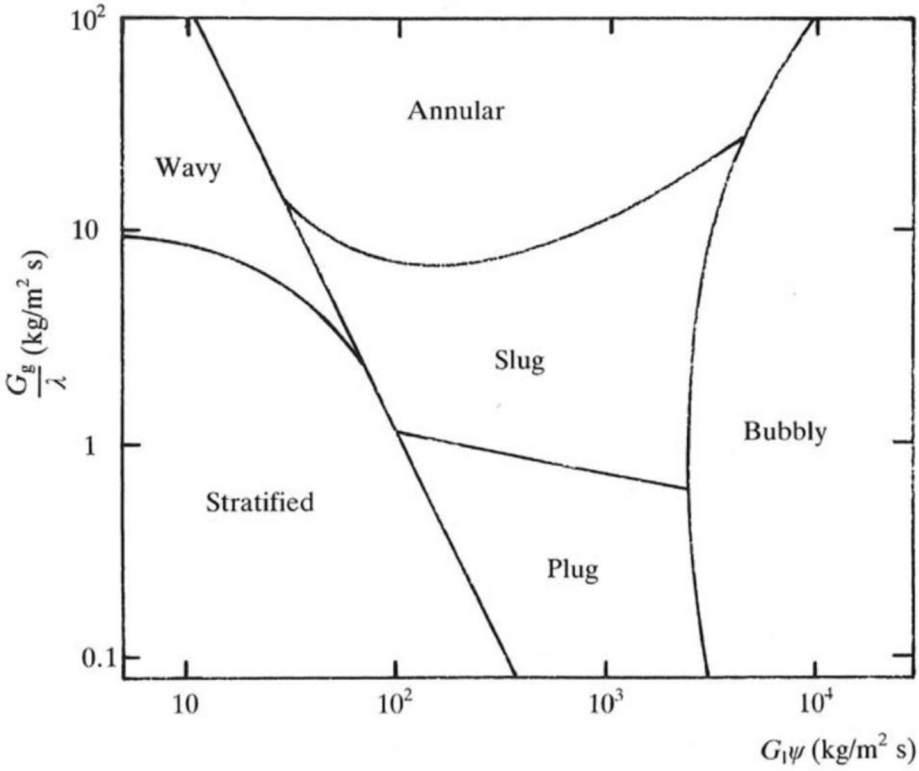

Figure 2.7: Flow pattern map of Baker for flow in a horizontal tube [27]

Hewitt and Robert [29] in 1969 also proposed an adiabatic flow pattern map for vertical channel upflow which has widely been adopted in literature. For diabatic conditions, Sato et al [30] in 1971 proposed a flow pattern map for flow boiling heat transfer in a horizontal channel based on the flow rate and vapor quality. The flow pattern of Mandhane [31] in 1974 as shown in Figure 2.8 has been relevant for many years. Although it was proposed for air – water system, it is capable for representing other flow conditions and also represents the transitions between adjacent flow patterns as wide bands of lines.

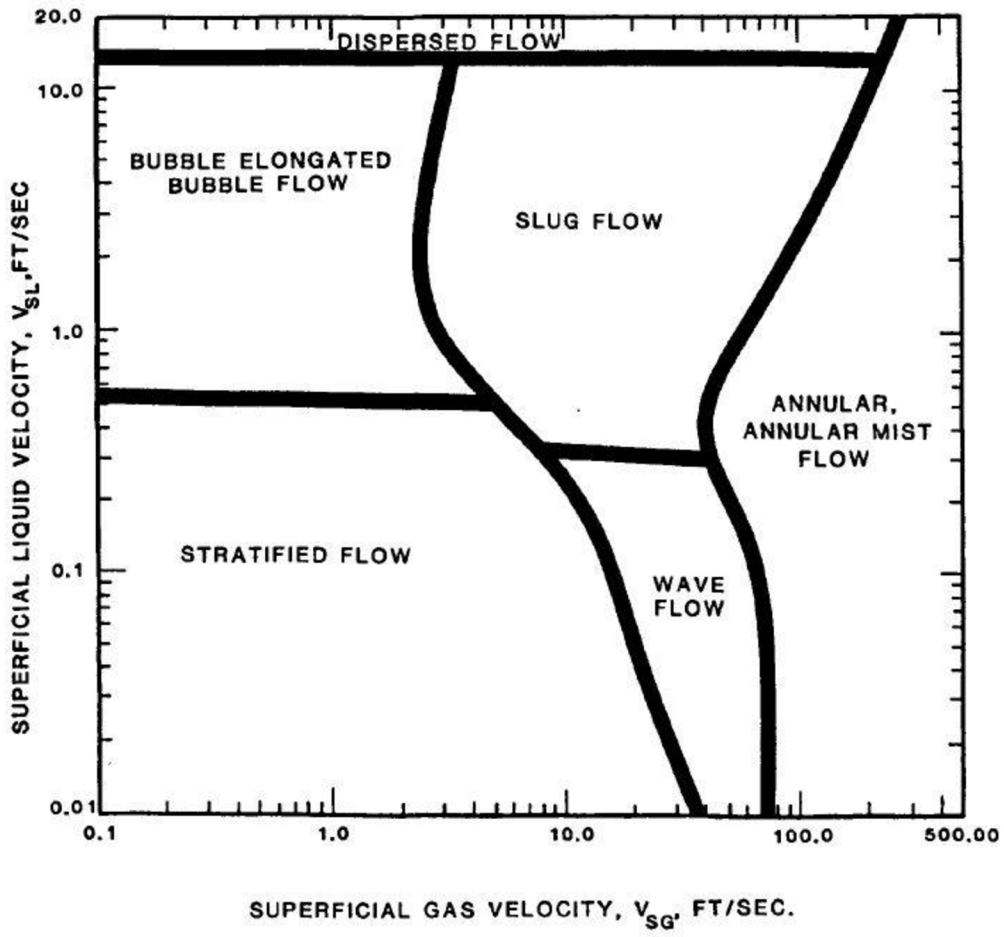

Figure 2.8: Flow pattern map of Mandhane for flow in a horizontal tube [31]

Ishii [32] in 1975 also developed a very useful flow pattern for separated flow, dispersed and mixed flows. The flow pattern map of Taitel and Dukler [33] in 1976 is one of the most cited flow pattern maps. It is capable of predicting transitions between flow regimes for adiabatic flows in horizontal channels. Many other flow pattern maps were developed from this. For example, Steiner [34] in 1993 developed flow pattern map which was a modified version of Taitel and Dukler. Based on Steiner's modified flow pattern map, Kattan et al. [35] in 1998 also developed a flow pattern map for heat exchangers and is capable of predicting dryout inception in an evaporating annular flow as presented in Figure 2.9.

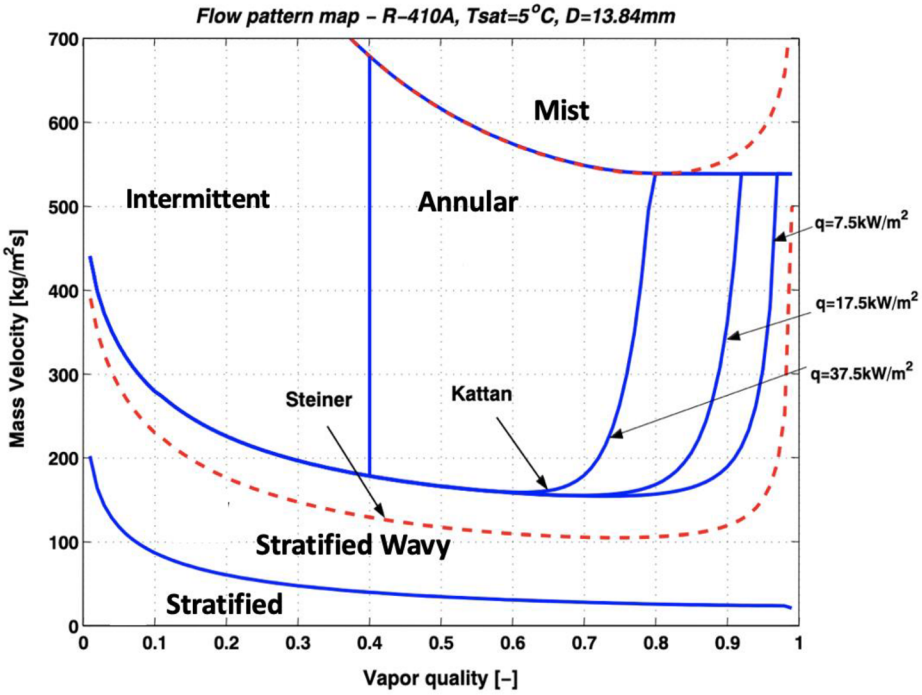

Figure 2.9: Flow pattern map of Kattan et al. in solid blue lines for flow in a horizontal tube (refrigerant = R410A, T_{sat} = 5 °C and 13.84 mm internal diameter) [35]

Thome et al. [36] improved this flow pattern with an extensive database. El Hajal et al [37] 2003 also introduced vapor void fraction calculation method using Rohani-Axelson model. Zurcher et al [38] modified the transition between annular and intermittent to stratified flow of Kattan et al. [35] flow pattern map. Another widely quoted flow pattern map is the flow pattern map of Wojtan et al. [39] in 2005 which is a modification of Kattan et al's flow pattern map as presented in Figure 2.10. Their flow pattern map divided the stratified wavy region into three (3) subdivisions namely slug, slug/stratified–wavy and stratified wavy. They added transition lines for annular to dryout and dryout to mist flows and how heat flux influences these transition lines.

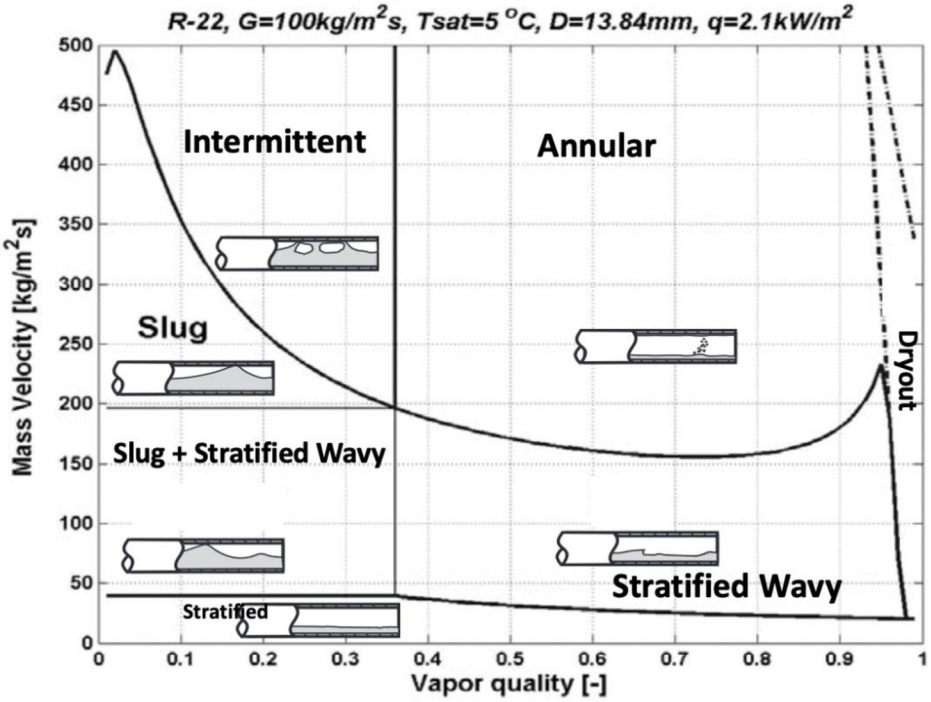

Figure 2.10: Flow pattern map of Wojtan et al. for flow in a horizontal tube (refrigerant = R22, G = 100 kg/(m² s), q'' = 2.1 kW/m², T_{sat} = 5 °C and 13.84 mm internal diameter) [39]

Barbieri et al. [40] in 2008 further modified the intermittent to annular transition line of Kattan et al. flow pattern. Cheng et al [41] in 2008 also developed a specific flow pattern map for CO_2 flow in horizontal channels. Although this flow pattern was developed for CO_2, it is widely adopted for other flow conditions. Flow pattern map of Mastrullo et al [42] 2012 is another flow pattern map for describing convective flow boiling of R410a and CO_2 flow in horizontal channels, focusing on the effect of reduced pressure on the flow. Generally, flow pattern maps help to understand and predict the behavior of fluid as it undergoes phase change (from liquid to vapor) and the heat transfer within the system. They also play critical role in optimizing design performance of two- phase systems.

2.6 Qualitative description of heat transfer

Research in the area of flow boiling spans over many decades. This is because, flow boiling heat transfer has been identified as an efficient technique for dissipating heat from small diameter tubes which finds its application in air conditioners, refrigeration systems and many more applications as in previous sections above [43]–[45][6], [46]. In most of these applications, the flowing refrigerant enters the evaporator usually as a subcooled single-phase liquid, goes through saturation phase and exits as a superheated single phase vapor. In this process, three stages of phases are

encountered (subcooled phase, saturation phase and superheated vapor phase). Although there have been many studies on flow boiling [11], there have been limited studies in literature that have considered heat transfer characteristics from subcooled liquid phase through two-phase to superheated vapor phase in a single experiment [47]. Enormous number of these studies have focused on heat transfer coefficient within vapor quality range of zero (0) and one (1) representing two phase process [48]–[53]. Few of these studies have tried to study this behavior below vapor quality of zero (0) representing subcooled liquid region or above vapor quality of one (1) representing superheated vapor region [54]–[56].

Several qualitative descriptions of flow regimes for heat transfer coefficient spanning from subcooled liquid region to superheated vapor region have been proposed by different authors. Popular among these descriptive maps include Collier and Thome and Kandlikar [57]–[59]. However, due to the complexity involved in the experimental determination of heat transfer coefficient [60] over wide range of vapor quality, not adequate experimental study has been performed to investigate this parameter from subcooled region through two-phase to superheated vapor with the goal of validating the proposed qualitative descriptions for heat transfer coefficient and the mechanisms controlling this parameter. According to Hewitt [61] as cited by Barbosa [54], these descriptive schemes have been the basis for design calculation and formulation of various flow boiling correlation for many years. Heat transfer coefficient measures how effective heat is being transferred from the walls of a tube to the bulk fluid flowing through the tube during flow boiling. It is the ratio of heat flux to temperature difference between the flowing surface and bulk fluid flow [62], [63]. Because of the relevance of this parameter, various flow regimes and transition schemes have been suggested by different authors to represent the characteristics of this parameter during flow boiling. These suggested qualitative descriptions and maps of flow boiling have been employed in the development of predictive tools and for the understanding of heat transfer phenomena as fluid flows within a heated tube. According to Kandlikar [59], qualitative descriptions of flow boiling provide an important guide to represent the complex interrelations among variables that control heat transfer in different regions.

Collier and Thome [57] developed a qualitative description of flow boiling for a single value of mass flux which was relatively specific to water at low pressures. It represented approximate trend in different regions as shown in Figure 2.11. This represents schematic description of flow boiling as described by Collier and Thome [57] which qualitatively describes how heat transfer coefficient varies along a heated tube for a fixed heat flux over the heated tube length. It illustrates the variation of heat transfer coefficient as a function of quality as heat flux increases with regimes

and transitions of flow boiling which qualitatively describes how heat transfer coefficient varies along a heated tube.

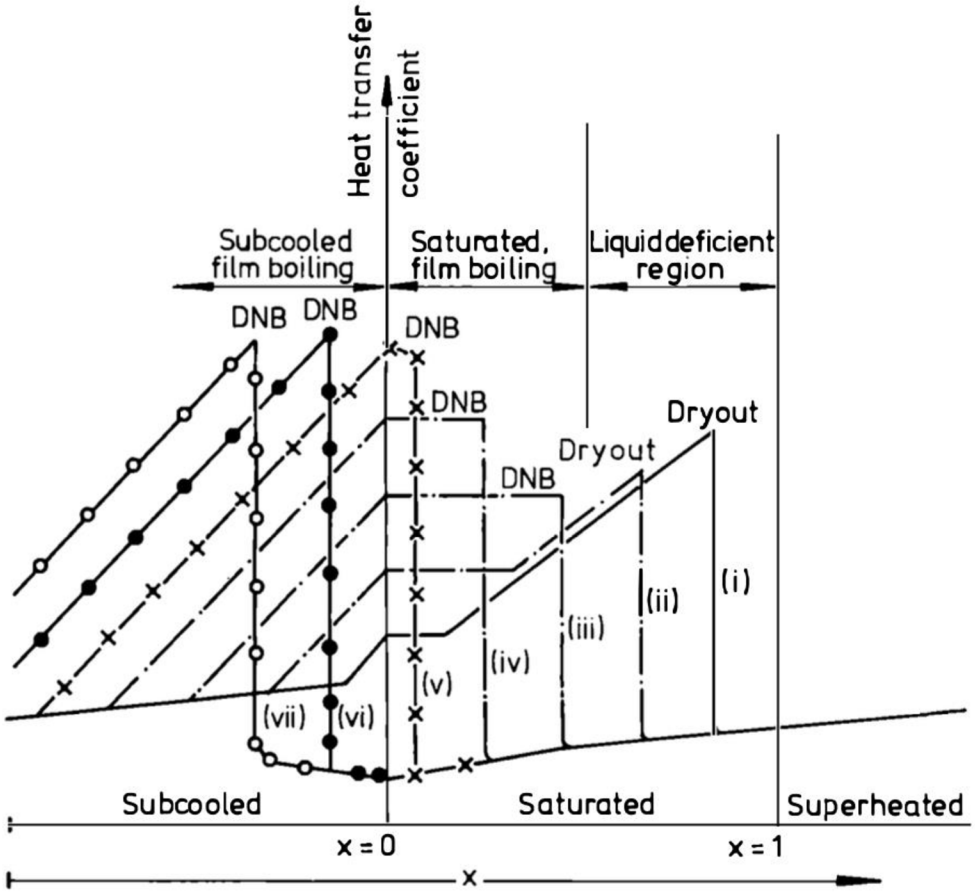

Figure 2.11: Heat transfer coefficient behavior as a function of quality and heat flux from Collier and Thome [57]

For variation of heat transfer coefficient at increasing heat flux from (i) to (vii), curve (i and ii) are low heat flux conditions which are typical operating conditions for evaporators. At this low vapor heat flux regions, subcooling begins with an increasing heat transfer coefficient until saturation begins. When saturation begins, the heat transfer coefficient remains constant and independent of vapor quality for low vapor quality regime. Nucleate boiling is deemed to be the dominant mechanism for the heat transfer. As vapor quality increases, force convection dominates and heat transfer coefficient increases with vapor quality until dryout is encountered due to critical heat flux (CHF). At low heat flux, there is a consumption of liquid near the wall region which takes place at a relatively high vapor quality resulting in the occurrence of liquid film dryout. However, at low vapor quality, this occurrence is known as departure from nucleate boiling (DNB). At high heat fluxes, saturated film boiling is encountered by the process of going through the departure from nucleate boiling which is critical heat flux in this situation [54].

Kandlikar [59] indicated that, the qualitative description of heat transfer coefficient by Collier and Thome [57] is not accurately represented in that, according Collier and Thome [57], heat transfer coefficient in vapor quality below zero (0) region is assumed to be a linear increase. According to Kandlikar [59], the linear increase is not an accurate representation of heat transfer coefficient in the negative quality region. He also indicated that Collier and Thome's schematic representation of heat transfer coefficient from vapor quality of zero (0) to one (1). He observed that, the trend of constant heat transfer coefficient in the nucleate boiling regime and an ever-increasing heat transfer coefficient with vapor quality for convective boiling is not entirely accurate. Kandlikar [59] developed a flow boiling schematic description and map from negative quality to vapor quality of 0.8. His work considered varying parameters such as heat flux and mass flux which was not the case of Collier and Thome [57] where only the effect of heat flux was considered. However, the schematic description of heat transfer coefficient by Kandlikar [59] does not consider the effect of critical heat flux and dryout conditions. It also does not consider the entire range from single phase all liquid through two-phase to single phase all vapor. Figure 2.12 illustrates flow boiling map as described by Kandlikar [59].

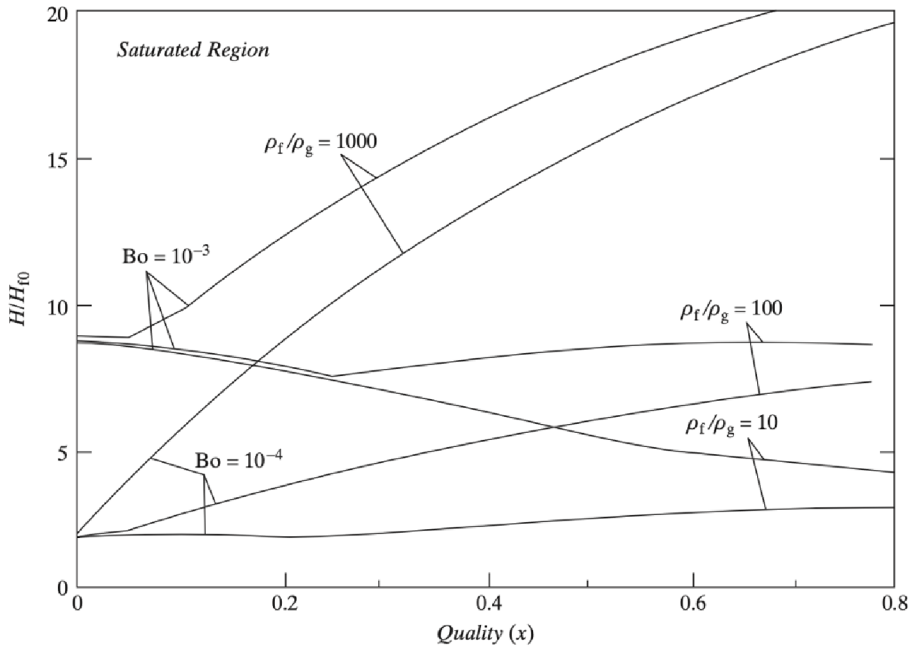

Figure 2.12: Heat transfer coefficient behavior as a function of quality according to Kandlikar [59].

At the transition between negative vapor quality and the positive vapor quality, experimental study by Kandlbinder, Urso et al., Kattan et al., and Thome [4] [18]–[21] observed a sudden rise in heat transfer coefficient which was not described in the classical schematic description of Collier and Thome, and Kandlikar. According to Hewitt [61], heat transfer coefficient description

by Kandlikar and Collier and Thome has been the basis of design calculation and formulation of various flow boiling correlation for many years.

Kim and Mudawar [68] also provided a schematic description of the variation of heat transfer coefficient along an axial direction in a mini/micro-channel which has been adopted by many authors for flow boiling studies. Figure 2.13 and Figure 2.14 describe flow regimes for heat transfer during flow boiling based on the dominant mechanism as the flow approaches dryout regime. Figure 2.13 depict a regime that is dominated by nucleate boiling heat transfer where bubble and slug flow occupy majority of the tube length. According to this description, heat transfer coefficient decreases along the tube length due to suppression of nucleate boiling. Figure 2.14 illustrates a regime that is dominated by convective heat transfer. For this regime, greater portion of the channel is annular and heat transfer coefficient increases along the channel as a result of gradual thinning of the annular liquid film. In both convective and nucleate boiling dominated region, heat transfer coefficient decreases at the onset of dryout or partial dryout which he considered to occur before vapour quality of one (1) for flow boiling. However, an experimental study by [50], [69], [70] showed a different behavior of dryout incipience for both convective and nucleate boiling under different experimental conditions which does not entirely reflect the descriptive scheme by Kim and Mudawar for flow boiling. The position and characteristics of dryout incipience as de-

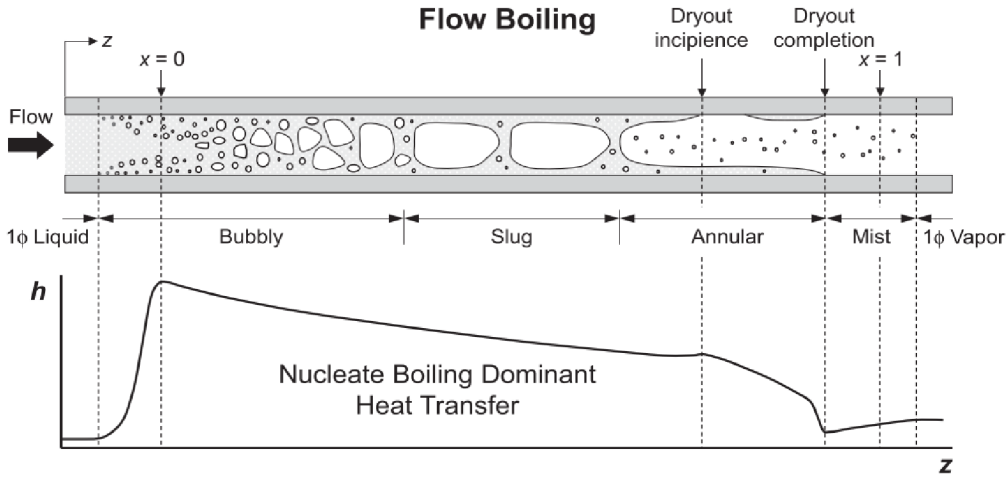

Figure 2.13: schematic flow regimes and variation of heat transfer coefficient for nucleate boiling by Kim and Mudawar [68]

scribed by Kim and Mudawar [68] is more complicated than depicted by their flow boiling scheme [71]. Their schematic description of flow boiling did not also consider departure from nucleate boiling as described by Collier and Thome (1994). Barbosa [54] reports that, these descriptive

schemes do not represent heat transfer coefficient within certain regimes of flow boiling correctly. Their experimental work studied heat transfer coefficient from subcooled region to low vapor quality region, where this observation was made.

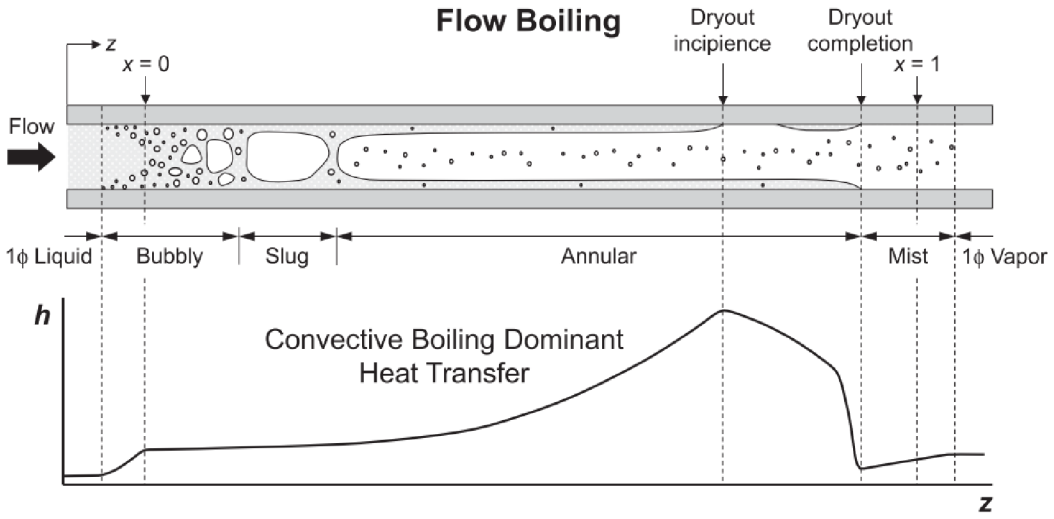

Figure 2.14: schematic flow regimes and variation of heat transfer coefficient for convective boiling by Kim and Mudawar [68].

Although several authors have adopted these descriptive flow boiling schemes and mostly within vapor quality of zero and one, not adequate experimental studies have been reported for heat transfer coefficient from subcooled region through two-phase to superheated vapor region, with the goal of validating qualitative descriptions and maps of flow boiling as described above upon which several theories and predictions have been developed.

2.7 Experimental investigation on flow boiling heat transfer

With respect to experimental investigations, many researchers in the field of air conditioners and refrigeration application have become much interested in flow boiling heat transfer using small diameter tubes over the past few years. These experimental investigations usually focus on the accurate determination and prediction of heat transfer coefficient, pressure drop, flow patterns and understanding of the dominant mechanism controlling the heat transfer This is because, understanding flow boiling heat transfer plays a significant role in the optimal design of evaporators for heat exchangers in air conditioners and refrigeration systems as discussed in the sections above [68], [72]–[74], [75].

For the effect of flow parameters on heat transfer coefficient, when saturation conditions and heat flux affect the heat transfer coefficient significantly, nucleate boiling is considered to dominate and control the heat transfer. When mass flux and vapor quality significantly affect the heat transfer coefficient, convective boiling is considered to dominate and control the heat transfer [69], [76]. Both mechanisms can co-occur over a wide range of vapor quality where the heat transfer coefficient is affected by mass flux, heat flux and saturation conditions along certain regions of vapor quality [75], [77]. Despite extensive studies on flow boiling heat transfer, the general characteristics and dominant mechanism responsible for controlling the heat transfer remain enigmatic with many contradicting results for seemingly similar experimental conditions reported in literature [9], [10]. According to [11], although several studies have been performed to understand the effect of flow parameters on heat transfer characteristics there is still lack of consensus on how these flow parameters and their interrelations affect heat transfer behavior during flow boiling with many contradicting results and complex trends of heat transfer coefficient along a range of vapor quality.

Also, saturation conditions such as saturation pressure and temperature have significant influence on the boiling properties of heat transfer, however according to [78], less attention has been given to their direct influence on heat transfer characteristics during flow boiling in small diameter tubes. Much of concern is about how saturation conditions influence heat transfer mechanism and the trend evolution of heat transfer coefficient with varying vapor quality, heat flux and mass fluxes. To identify the gaps in literature in relation to the objectives of this thesis, an extensive literature review has been conducted.

For example, some studies report an increasing effect of saturation conditions on heat transfer coefficient [79]–[82]. Greco and Vanoli [79] investigated the flow boiling heat transfer characteristics of R134a in a smooth horizontal tube of 6 mm internal diameter. They considered saturation pressures of 300 - 1200 kPa, mass flux of 360 kg/(m^2s) and heat fluxes of 11-21 kW/m^2. Their study reported that heat transfer coefficient increased with increasing saturation pressure. With the trend of heat transfer coefficient versus vapor quality, they reported that, heat transfer coefficient decreased to a minimum in the low-quality region and increased at high vapor quality region, signifying the dominance of nucleate boiling in low quality region and convective boiling in the high vapor quality annular region. They further concluded that, at high heat fluxes and saturation pressures, nucleate boiling dominated the heat transfer. However, at low heat flux and saturation pressure, convective boiling was the dominant mechanism controlling the heat transfer. Celen and Dalkilic [80] also evaluated the effect of operating parameters such as saturation pressure, mass flux, heat flux and vapor quality on heat transfer coefficient of R134a working fluid for a horizontal tube of 8.62 mm internal diameter. They evaluated the effect of saturation pressures

of 490 - 600 kPa, mass flux of 290 - 381 kg/(m^{2}s) and heat flux of 10 - 15 kW/m^2. They concluded that, increasing saturation pressure resulted in increasing heat transfer coefficient. With the trend of heat transfer coefficient with vapor quality, their study indicated an increasing trend of heat transfer coefficient over the entire vapor quality range.

Another study by Eckels and Pate [81] investigated the heat transfer characteristics of R134a in an 8 mm internal diameter tube. The flow boiling study was performed for saturation pressure range of 248 - 390 kPa for a mass flux of 125 - 400 kg/(m^{2}s) and heat flux of 12 kW/m^2. Their study reported that, heat transfer coefficient increased significantly with increasing saturation pressure. Xu et al. [82] experimentally evaluated the effect of mass fluxes of 185 - 935 kg/(m^{2}s), heat fluxes of 18.0 - 35.5 kW/m^2 and saturation pressures of 578 - 820 kPa on flow boiling heat transfer characteristics of R134a in a 4.065 mm internal diameter tube. Their study concluded that, heat transfer coefficient increased significantly with increasing saturation pressure. They reported an almost linear trend of heat transfer coefficient over the entire range of vapor qualities until dryout was reached.

Some experimental studies also report a negligible effect of saturation conditions on heat transfer coefficient [51], [83], [84]. For example, Grauso et al. [84] presented an experimental investigation in a 6 mm internal diameter smooth stainless-steel tube for saturation pressure of 264 - 450 kPa, mass flux of 146 - 520 kg/(m^{2}s) and heat fluxes of 5 - 20.4 kW/m^2. The working fluid was R134a. They investigated the effect of these conditions on heat transfer coefficient and reported that increasing saturation pressure did not have any significant effect on heat transfer coefficient. However, it was observed that, with the trend of heat transfer coefficient with vapor quality, heat transfer coefficient decreased slightly to a minimum at around vapor quality of 0.5 before increasing over the entire vapor quality range until dryout is reached. They reported that this observation indicated the dominance of nucleate boiling in the low vapor quality region and convective boiling in the high vapor quality region. Guo et al. [83] also investigated the flow boiling heat transfer characteristics of R134a at saturation pressures of 1379-3608.3 kPa in a 10 mm internal diameter tube. They considered heat fluxes of 6 - 24 kW/m^2 and mass fluxes of 100-300 kg/(m^{2}s). They reported that, increasing saturation pressure did not produce any significant change in the heat transfer coefficient. However, with the trend of heat transfer coefficient versus vapor quality, it was observed that heat transfer coefficient increased with increasing vapor quality until dryout. Saitoh et al. [51] investigated the boiling heat transfer of R134a in a horizontal small diameter tube of 3 mm. Their study measured heat transfer coefficient and pressure drop for saturation pressures of 350 - 488 kPa, mass flux of 150 - 450 kg/(m^{2}s) and heat flux of 5-29 kW/m^2. Their results

concluded that saturation pressure had negligible effect on heat transfer coefficient for the conditions investigated. They reported an increasing trend of heat transfer coefficient with vapor quality over the entire vapor quality range until dryout is reached. It is interesting to observe that some experimental studies even reported a decreasing effect of saturation pressure on heat transfer coefficient. For example, Balachander and Raja [85] investigated the flow boiling heat transfer characteristics of R134a for saturation pressures of 164-293 kPa in a 7.49 mm internal diameter. Their study considered mass fluxes of 57-102 kg/(m^2 s) and heat flux of 7.5 and 8.3 kW/m^2. They reported that, increasing saturation pressure decreased heat transfer coefficient. Their results indicated a decreasing trend of heat transfer coefficient with vapor quality. They also reported that, nucleate boiling was the dominant mechanism controlling the heat transfer. With regards to saturation conditions, results from the literature above indicate that, increasing saturation pressure has a varying effect on heat transfer coefficient and different studies report different effects. Some studies reported an increasing effect of saturation pressure on heat transfer coefficient, some reported negligible effect of saturation pressure on heat transfer coefficient and others even reported a decreasing effect. It can be observed that there is no consensus on the effect of saturation conditions on heat transfer characteristics. The same can be said about the dominant mechanism controlling the heat transfer and trend evolution of heat transfer coefficient as a function of vapor quality for increasing saturation pressure which has been observed to vary without any agreed trend. Some studies report an increasing trend of heat transfer coefficient with vapor quality, some report a decreasing trend, some report a linear trend and others report a combination of these trends.

There are many correlations in literature for predicting flow boiling heat transfer in small diameter tubes; a fact that confirms that, the actual mechanism responsible for controlling the heat transfer is still not clear and agreed upon [86], [87]. These many correlations are designed based on different theories with many adjusting parameters [88]. Fang and Mahmoud et al. [87], [89] evaluated different correlations and concluded that various correlations poorly predicted the experimental data investigated during flow boiling for different interrelations of saturation conditions, mass fluxes, heat fluxes and vapor qualities. On the effect of saturation pressure on heat transfer coefficient during flow boiling in horizontal smooth tubes, Table 2.1 summarizes the experimental investigations reviewed above and the effect of saturation pressure on the heat transfer coefficient.

Table 2.1: Summary of experimental studies on flow boiling for R134a in horizontal smooth tubes

Author(s)	Fluid Type	Experimental Set up	P_{sat} kPa	G kg/(m² s)	q" kW/m²	Effect of Saturation Pressure on HTC
Greco and Vanoli	R134a	6 mm ID, horizontal smooth tube, 6 m length	300-1200	360	11-21	Increases
Celen and Dalkiliç	R134a	8.62 mm ID horizontal smooth tube	488.75-609.17	290-381	10-15	Increases
Eckel and Pate	R134a	8.0 mm ID, Horizontal smooth tube	350-490	125-400	9.1	Increases
Yu et al.	R134a	4.065 mm ID, Horizontal smooth tube	578-820	185-935	18-35.5	Increases
Grauso et al	R134a	6 mm ID, Horizontal smooth tube	264.11-445.59	146- 520	5-20.4	Negligible
Guo et al	R134a	10 mm ID, Horizontal smooth tube	1379-3608.3	100-300	6-24	Negligible
Saitoh et al	R134a	3.1 mm ID, Horizontal smooth tube	350-488	150-450	5-39	Negligible
Balachander and Raja	R134a	7.49 mm ID, Horizontal smooth tube	164-293	57-102	2-18	Decreases

Also as indicated earlier, there have been limited studies in literature that have considered heat transfer characteristics from subcooled liquid phase through two-phase to superheated vapor phase in a single experiment [47]. Many of these studies also focused on heat fluxes greater than 5 kW/m^2, vapor qualities of 0 – 1 and medium to high mass fluxes According to [90], applications that involve low heat and mass fluxes are being encountered in many fields recently including refrigerators and plate heat exchangers. Better understanding and accurate prediction of flow boiling heat transfer over wide range of vapor qualities from subcooled region to superheated region for low heat and mass fluxes is required for reliable design of systems that operate in such low conditions [7], [88], [91]. Several studies in literature have investigated the characteristics of this heat transfer coefficient over different ranges of vapor qualities. For example, Tibirica et al. [92] investigated flow boiling heat transfer of R134a and R245fa in a horizontal stainless-steel tube of 2.3

mm internal diameter. Their work evaluated mass fluxes from 50 - 700 kg/(m^2 s), heat flux of 5-55 kW/m^2, exit saturation temperature of 22, 31 and 41 °C. They considered vapor quality range of 0.05 to 0.99. They reported that, heat transfer coefficient increases with increasing heat flux, mass flux and saturation temperature. They also reported a distinctive heat transfer behaviour for increasing vapor quality below a threshold mass flux of 200 kg/(m^2 s). They indicated that, irrespective of the mass flux, an increased heat flux resulted in an increased heat transfer coefficient. Kanizawa et al. [93] also presented a flow boiling experimental study of R134a, R245fa and R600 refrigerant in small diameter tubes of 0.38 – 2.6 mm. The mass fluxes were varied from 49 to 2200 kg/(m^2 s) and heat fluxes of up to 185 kW/m^2. They investigated the effects of experimental conditions studied on heat transfer coefficient and dry-out quality identified. Their study reported that, heat transfer coefficient increased with increasing mass flux, heat flux and saturation temperature. They also reported a remarkable increase in heat transfer coefficient with heat fluxes below vapor quality of 0.4. They found negligible effect of saturation temperature at 5 kW/m^2 heat flux. However, at higher heat fluxes, the effect of heat fluxes on heat transfer coefficient was pronounced. They found that, mass flux has negligible effect on heat transfer coefficient at vapor qualities below 0.4. But beyond this vapor quality, increasing mass flux produced an increased heat transfer coefficient.

An interesting study by Lima et al. [50] of R134a flowing in a 13.84 mm internal diameter smooth horizontal copper tube on heat transfer coefficient was presented. Their study considered vapor qualities that ranges from 0.01 to 0.99, mass flux of 300 and 500 kg/(m^2 s), heat fluxes of 7.5 and 17.5 kW/m^2 and saturation temperatures of 5 °C, 15 °C, 20 °C. They observed that, heat transfer coefficient increased with mass flux. However, this increase was pronounced at higher vapor qualities. Heat transfer coefficient increased with higher heat fluxes at lower vapor qualities. This effect however decreased as vapor qualities increased until a local minimum was reached. The vapor quality at which this local minimum was observed was sensitive to both heat and mass fluxes. A complete evaluation of flow boiling phenomena and pressure drop in a smooth tube of 8.62 mm was presented by Celen et al. [53]. They evaluated the effect of mass flux, saturation temperature and heat flux on heat transfer coefficient and pressure drop for ranges of 290 – 381 kg/(m^2 s), 15 –22 °C and 10 – 15 kW/m^2 respectively. They reported that, heat transfer coefficient and pressure drop were affected by mass fluxes for all conditions investigated. They indicated that, at mass flux of 290 kg/(m^2 s), increasing heat flux lead to higher heat transfer coefficient. However, this effect decreased for mass flux of 381 kg/(m^2 s). Bandarra et al. [94] also performed an experimental study of flow boiling heat transfer and pressure drop on R134a in a horizontal smooth and microfin tube. The conditions studied were saturation temperature of 5 °C vapor quality range of 0.005 to 0.9,

mass flux range of 100 – 500 kg/(m^2 s) and heat flux of 5 kW/m^2. They reported that, heat transfer coefficient was negligibly affected by vapor qualities at lower mass fluxes of 150 kg/(m^2 s). However, at high mass flux, the heat transfer coefficient increases correspondingly.

An experimental investigation by Chiapero et al. [95] on the effect of mass flux and heat flux on heat transfer coefficient for a smooth stainless-steel tube with an inner diameter of 5 mm was performed using R134a at 34 °C. They concluded that, at lower vapor qualities, a higher heat flux produced a higher heat transfer coefficient. They also concluded that, the effect was more evidenced at lower mass fluxes in that, at low mass flux, the effect of vapor quality had no observable effect on the heat transfer coefficient. Balachander et al. [85] studied flow boiling heat transfer behaviour of R134a and R404A at low mass fluxes of 57 and 102 kg/(m^2 s). Heat fluxes for R134a were between 7.5 to 8.3 kW/m^2, saturation temperatures of -15 to 0 °C and vapor qualities between 0 and 1. The study was performed in a 7.9 mm tube. Their study revealed that, heat transfer coefficient was a strong function of heat flux and that, nucleate boiling was dominant. Heat transfer coefficient decreased with increasing vapor quality and increasing saturation temperature. They reported that, the flow pattern observed was stratified wavy. Another extensive flow boiling heat transfer study by Jabardo et al. [96] in a horizontal copper tube of 12.7 mm internal diameter. Their study considered mass flux range of 50 – 500 kg/(m^2 s), 5 – 20 kW/m^2, vapor quality between 0.005 to 1 and evaporating temperatures of 5 and 8 °C. They observed that, at low mass fluxes, the heat transfer coefficient did not have significant dependence on vapor quality. They report that, the heat transfer coefficient did not have significant dependence on vapor quality. They also report that, the heat transfer coefficient even decreased slightly with increasing vapor qualities. The heat fluxes have an effect on the heat transfer coefficient over the entire range of vapor qualities at low mass fluxes. At low qualities and even at higher mass fluxes, heat fluxes had an effect on the heat transfer coefficient. At mass fluxes greater than 200 kg/(m^2 s), heat transfer coefficient increased with increasing vapor quality until dry – out was reached.

It is interesting to observe that, there is a unanimous conclusion on how strongly, heat transfer coefficient depends on mass flux. However, with respect to heat fluxes, saturation conditions and vapor qualities in which cases most studies considered between 0 and 1, there is no agreement on their effect on heat transfer coefficient. For example, while [96] report that increasing vapor quality have a decreasing effect on heat transfer coefficient, Chiapero et al. [95] reports an ever-increasing effect of vapor quality on heat transfer coefficient. Also, there is less studies for low heat flux conditions below 5 kW/m^2 whose application is increasingly encountered in refrigerators and plate heat exchangers [11].

In order to bridge this gap in literature, an objective of this research was designed to focus on the heat transfer characteristics of R134a in a single horizontal circular stainless-steel smooth tube, from subcooled liquid region to superheated vapor region with small vapor quality increment for low heat flux and saturation pressure conditions.

In the case of convective boiling, several experimental studies have shown that within vapor quality of zero and one, heat transfer coefficient increases with mass flux and vapor quality with negligible effect of heat flux. For example, Lee et al. [97] investigated the characteristics of heat transfer coefficient of flow boiling in a horizontal rectangular channel having low aspect ratios. R113 was the refrigerant used. Their study covered a vapor quality range of 0.15-0.75. They observed that, heat transfer coefficient increases with mass flux and local vapor quality. They also observed a negligible effect of heat flux on the heat transfer coefficient. They indicated that, convective boiling was the dominant mechanism controlling heat transfer. The flow pattern observed was annular flow. Ong et al. [98] also studied flow boiling heat transfer of R134a, R236fa and R245fa in a single horizontal channel of different diameters over a range of experimental conditions. They observed a monotonic increase in heat transfer coefficient at higher vapor qualities corresponding to annular flow. Convective boiling was indicated as the dominant heat transfer mechanism. Paul et al. [99] recently investigated flow boiling heat transfer in a 5 mm smooth stainless steel using R134a as a refrigerant. Their study also observed that, heat transfer coefficient increases with mass flux and vapor quality with minor effect of heat flux. To contribute to understanding the characteristics of heat transfer during flow boiling, there is the need to experimentally study the heat transfer characteristics and from subcooled liquid region to superheated vapor region with small vapor quality increment. The wide range of vapor quality from single phase subcooled region through two-phase to superheated vapor region is scarcely reported in literature [15], [26].

Table 2 below summarizes the literature reviewed above.

Author(s)	Fluid Type	Experimental Set up	T_{sat} °C	G kg/(m² s)	q'' kW/m²	x (1)	Effect of parameters on heat transfer coefficient
Tibiricia & Ribatski	R134a, R245fa	Horizontal stainless steel, 2.3 mm ID	22-41	50-700	5-55	0.05-0.99	q'': ↑ G: ↑ T_{sat}: ↑
Kanizawa et al.	R134a, R245fa, R600	Smooth horizontal diameter, 0.38-2.6 mm ID	-	49-2200	185	0.05-0.90	q'': ↑ for x<0.4 G: ↑ for x>0.4 G: Negligible for x<0.4 T_{sat}: ↑
Lima et al.	R134a	Smooth horizontal copper tube 13.84 mm ID	5-20	300-500	7.5 & 17.5	0.01-0.99	G: ↑ q'': ↑ at low x T_{sat}: ↑ for low x T_{sat}: ↓ for higher x
Celen et al.	R134a	Smooth tube, 8.62 mm ID	15-22	290-381	10-15	0-1	G: ↑ T_{sat}: ↑ q'': ↑, Negligible at high G
Bandarra et al.	R134a	Smooth horizontal tube, 8.76 mm ID	5	100-500	5	0.02-1	G: ↑ q'': - x: ↑ for G>100 kg/(m² s)
Chaipero et al.	R134a	Smooth horizontal tube, 5 mm ID	34	300-500	10-20	0-1	G: ↑ q'': ↑ at low x x: ↑ for high G
Balachander et al.	R134a, R404A	7.9 mm ID, Horizontal smooth tube	-15 – 0	57-102	7.5-8.3	0-1	G: Negligible q'': ↑ at low x x: ↓ T_{sat}: ↓
Jabardo et al.	R134a, R404A, R22	12.7 mm ID, Horizontal smooth copper tube	5-8	50 - 500	5-20	0.05-1	G: ↑ q'': ↑ x: ↓ at G = 50 - 100 kg/m² s T_{sat}: ↑ only for q'' >20 kW/m²
Lee et al.	R113	Horizontal rectangular, smooth	-	50 - 200	15	0.15-0.7	G: ↑ q'': Negligible x: ↑

Ong et al.	R134a, R236fa, R245fa	Horizontal circu-lar,1.03 mm, 2.02 mm, 3.04 mm ID	31	200 - 1600	2.3-250	0-0.8	*G*: ↑ *q"*: Negligible *x*: ↑ for high *G* & ↓ for *q"*: - T_{sat}: -
Paul et al.	R134a,	Smooth horizontal circular 5 mm ID	18-27	300 - 800	8.5-9.0	0-1	*G*: ↑ *q"*: Negligible *x*: ↑ for high *G* & ↓ for *q"*: - T_{sat}: -

Table Key: increase (↑), decrease (↓), Internal Diameter (ID)

2.8 Chapter Conclusion

This chapter discussed the literature review related to the background of flow boiling heat transfer studies, flow patterns, flow pattern maps and flow visualization. Experimental investigations on flow boiling heat transfer of refrigerant were also presented focusing on the effect of flow parameters and trend evolution of heat transfer coefficient in relation to increasing or decreasing flow parameters. The state-of-the-art review guided in the identification of gaps for designing the objectives of this research. It was observed that, to properly understand two-phase flow boiling heat transfer and its practical application, there was a need to conduct a credible and systematic experimental investigation from single phase all liquid through saturation to single phase superheated vapor. Also, there is no unanimous conclusion on how flow parameters affect heat transfer with some studies reporting conflicting results for the same conditions of experimental investigation. From this review, a research plan was designed in order to address the gap and confusion presented in literature on flow boiling heat transfer in small diameter tubes.

Chapter 3

3 Description of Experimental Methods

3.1 Experimental Setup

A modified flow loop at the Two-Phase Flow Instability facility of the Department of Energy and Process Engineering in Norwegian University of Science and Technology (NTNU) was used to perform this experimental study. The facility was modified to regulate the working fluid characteristics such as mass flow rate, saturation conditions and inlet subcooling as the fluid enters the inlet of the heated test section. It is important to indicate that detailed design of the facility its description was obtained from [101], [102]. Figure 3.1 and Figure 3.2 show the schematics and picture of the experimental facility for this study. It is a closed loop facility made up of a heated section, a conditioner, a pump, a main tank and a visualization section. The working fluid used is R134a refrigerant whose inlet temperature is controlled with a shell and tube type heat exchanger. R134a was selected because it is easy to handle, it has low boiling point and low latent heat of vaporization. Table 3.1 below illustrates the thermophysical properties of R134a. The saturation conditions in the main tank are used to control the fluid pressure in the test section. The flow rates are measured by a Coriolis mass flow meter installed at the inlet of the test section. The test section is made of stainless-steel tube with a length of 2035 mm and internal diameter of 5 mm. It has an external diameter of 8 mm. The test section consists of 5 subsections of equal lengths which can be heated separately by Joule effect. A controller and a rectifier circuit are used to convert Alternate Current to Direct Current (AC-DC) power supply to the test section. The total electrical input power is calculated from measured voltage and current in the heated section. To reduce heat losses,

suitable insulation is used at the outer surface of the test section. Ten (10) thermocouples are installed at the outside bottom wall and seven (7) at the outside top wall for measuring the temperatures at different locations. At locations 1117 mm and 1917 mm from the inlet, thermocouples are installed on the top, bottom, and side walls along with in-flow internal thermocouples. Temperature, absolute pressures, pressure differences and mass flow rate are acquired at a frequency of 10 Hz. The experimental data are logged with LabVIEW National Instrument data acquisition system.

Table 3.1: Thermophysical properties of R134a (NBP: Normal Boiling Point, P_{crit}: Critical Pressure, T_{crit} : Critical Temperature, GWP: Global Warming Potential, MW: Molecular Weight, LHV: Latent Heat of Vaporization)

NBP (°C)	P_{crit} (kPa)	T_{crit} (°C)	GWP	MW (g/mol)	LHV
-26.1	4059	101.1	1430	102.03	217

Figure 3.1: Picture of the experimental facility

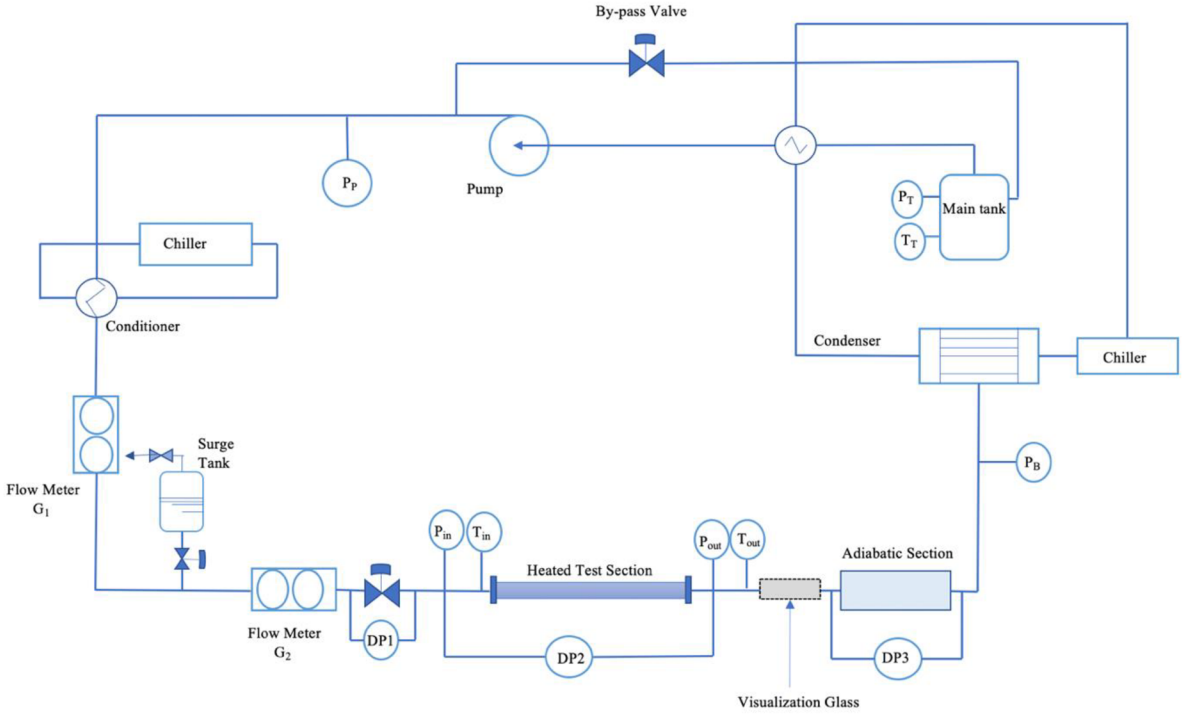

Figure 3.2: Simplified schematic of the experimental flow loop. Next, the main components mentioned above that make up the closed loop of the experimental facility is described.

3.1.1 Reservoir

The experimental loop has two operating modes for circulating working fluids from the reservoir through the loop. One is by the use of two tanks positioned at different pressures namely high-pressure tank and low-pressure tank. This mode is applicable for low flow rate application where the flow rate is created by establishing a difference in pressure between the high-pressure tank and the low-pressure tank. A constant pressure flow is thus maintained by a controlling valve. To maintain a constant saturation condition in the low-pressure tank, the pressure and temperature are kept constant by the conditions in the condenser. Nitrogen is used to pressurize the high-pressure tank. For applications that require high flow rate, a magnetic gear pump is used to control and pump the working fluid from the reservoir tank (low pressure-tank) through the loop. For this study, the pump mode of flow circulation was employed.

3.1.2 Pre-Conditioner

To set inlet conditions for the required experiment, a pre-conditioner (heat exchanger) is positioned before the test section to condition the working fluid to the required temperature before entering the test section.

3.1.3 Heat Source

The electrical heat source to the test section is divided into five (5) sections. This is to be able to provide both uniform and non-uniform heating to the test section and subsequently to the flowing working fluid.

3.1.4 Valves

There is an adjustable valve at the inlet to control the Inlet pressure. Flow restriction at the exit is provided by an orifice valve. Another adjustable valve is positioned in the by-pass region to regulate the constant pressure drop boundary conditions in the heated test section. At the inlet, the flow resistance coefficient (K_i) was maintained at $K_i \approx 2.63$. This was the case unless an experiment with flow restriction is performed where the valve is fully open. The flow restriction coefficients were determined during the single-phase calibration of the experimental rig given as:

$$K = \frac{\Delta P}{{}^{1}/_{2}\rho u^2} = \frac{2\Delta P \rho}{G^2} \quad . \qquad 3.1$$

3.1.5 Condenser

A condenser is positioned after the test section to condense the vapor exiting the test section. The condensed vapor flows to the low-pressure tank for storage.

3.1.6 Conditioner

A conditioner positioned before the magnetic gear pump is used to keep the fluid in a sub-cooled state (single phase) as it is being pumped. It is worth noting that, the pre-conditioner; conditioner and condenser are refrigerated by two secondary circuits.

3.1.7 Test Section

Figure 3.3 is the test section for the experimental study. It is a 5 mm internal diameter and 8 mm external diameter stainless steel tube. Seven (7) pressure taps are mounted on the test section for differential pressure drop measurements, twelve (12) external thermocouples for measuring wall temperature of the test section and two (2) internal thermocouples for measuring the internal fluid temperature for investigating the heat transfer characteristics. Six (6) electrodes are mounted on the test section to regulate the heat distribution. Joule's effect was the technique used to heat the test section. The total electrical energy input to the test section is determined from measurements of voltage and current in each heated sections of the test section. Two insulating materials are used to insulate the test section against heat transfer from and to the surroundings. A tube is

positioned parallel to the test section with the purpose of investigating pressure drop during the flow. This tube has a similar internal diameter as the test section (5 mm) and a length of 100 mm.

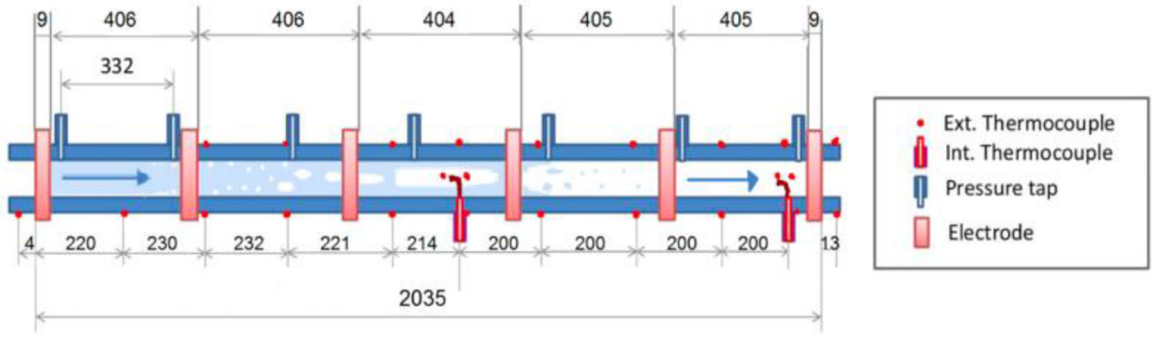

Figure 3.3: Schematic representation of the test section

3.1.8 Visualization Section

Figure 3.4: Visualization section

A visualization glass of 5 mm internal diameter, 8 mm external diameter and 200 mm long is mounted at the exit of the test section for visualizing flow patterns. It also serves as a dielectric and thermal insulator between the heated test section and the rest of the circuit. It is a borosilicate glass tube. Pressure test of up to 2500 kPa is performed on the visualization glass tube to ensure its ability to withstand pressure during maximum operation of about 1500 kPa. A photron FastCam SA3 high-speed camera is mounted on the visualization glass tube to investigate flow patterns. A

single white LED light source with a diffuser placed in front of it is mounted by the opposite side of the high-speed camera to enhance image and video capture. The high-speed camera is capable of recording at 1000 frames per second (FPS) with a shutter time of 1/20,000 to 1/40,000. A picture of the visualization section is shown in Figure 3.4 below.

3.1.9 Chillers and Heat exchangers

To facilitate the heat dissipation process from the heat exchangers and condenser, two secondary circuits are installed. The chillers responsible, namely K9 and K12 models, are sourced from the renowned company called Applied Thermal Control (ATC). For the pre-conditioning, a plate-fin heat exchanger (B8THx14 SWEP) is utilized, while a shell and tube heat exchanger (CFC-12 – Alfa Laval) serves as the condenser. The secondary refrigerant utilized comprises a mixture of glycol and water. To enable control and monitoring, the two chillers are connected to the computer via the RS485 serial protocol. This interface software grants the capability to adjust their reference temperature as required.

3.1.10 Pump

A magnetic gear micropump is employed in the setup to circulate the working fluid through the flow loop. The pump's velocity is regulated directly through the interface of the software, offering the advantage of controlling the flow rate to investigate the system's response to specific signals. To maintain a consistent flow rate, regardless of fluctuations in other system parameters, a PID controller is integrated into the system.

3.2 Measurements and Accuracy of Measurements

This section describes the measurement accuracy and calibration of the instruments making up the experimental set up. While the aim of the experimental measurement is to keep errors small, they cannot be reduced to null. In analyzing the uncertainty, for a measured variable say X, the uncertainty related to such measurement is given as δX_i. The variable together with the uncertainty is represented as:

$$X = X_{i(measured)} \pm \delta X_i \,. \qquad 3.2$$

For systematic uncertainty, in-house calibration or an uncertainty given by the instrument supplier is employed. Root sum square (RSS) is a method used to combine multiple uncertainties or errors from a measurement. When there are several sources of uncertainty or error that are independent

of each other, the root sum square method allows to calculate the combined or total uncertainty. The RSS method is based on the assumption that the individual uncertainties are statistically independent, meaning the errors from one source do not influence the errors from another source. In such cases, the combined uncertainty (RSS) is calculated by taking the square root of the sum of the squares of the individual uncertainties.

RSS method helps to obtain a single value that represents the total uncertainty associated with the measurement or analysis, taking into account the contributions from each independent source of uncertainty. This allows for a more comprehensive understanding of the overall reliability and accuracy of the measurement or result.

With the approach for uncertainty analysis, for a calculated results (R) from an experimental measurement which is a function of different variables say $X_{1,}X_{2,}X_{3,\dots}X_N$ is represented as:

$$R = R(X_{1,}X_{2,}X_{3,\dots}X_N) . \qquad 3.3$$

When the uncertainty on the calculated result is from a single independent measurement variable and this single variable is the only contributor of error, then the uncertainty is given as:

$$\delta R_{Xi} = \frac{\partial R}{\partial X_i}.\delta X_i . \qquad 3.4$$

When several independent variables are used in the function of R, the root sum square technique is employed and given as:

$$\delta R = \sqrt{\sum_1^N \left(\frac{\partial R}{\partial X_i}.\delta X_i\right)^2} . \qquad 3.5$$

Here, δX_i is the uncertainty from each single uncertainty term contributing to the total uncertainty δR from the results R.

3.3 Measurements

The goal of this study and consequently this set up is to investigate the heat transfer coefficient and pressure drop during flow boiling in a horizontal tube over a wide range but small increment of vapor quality. The heat transfer coefficient and vapor quality are therefore calculated from measured mass flow, heat flux, pressure and temperature recordings. Pressure drop measurement is taken directly with the pressure transducers mounted on the adiabatic test section purposed for pressure drop measurement. In this section, the measurement techniques for the variables recorded and the associated measurement uncertainties are presented.

3.3.1 Mass Flux

Bronkhorst Cori-Tech Coriolis flow meter with a capacity of measuring R134a flow at 3 litres per minute is positioned before the test section to measure the flow rate indicated in the scheme label as (*G*2). Further upstream to the flow meter (*G*2) is another flow meter with a label (*G*1) which is mounted near the pre-conditioner. The supplier assures an accuracy of 0.2 % based on the reading provided by these flow meters. From the measured flow rates, the mass flux is then calculated. To calculate the mass flux labelled (*G*), the volumetric flow rate data of the liquid refrigerant R134a is converted into mass flux using density values obtained from the NIST REFPROP database [103]. The mass flux is calculated as:

$$G = \frac{4\dot{m}}{\pi {d_i}^2}\,. \qquad 3.6$$

The uncertainty related to the calculated mass flux (G) is therefore determined by:

$$\delta G = \sqrt{\left(\frac{4}{\pi {d_i}^2}\delta\dot{m}\right)^2 + \left(\frac{-8\dot{m}}{\pi {d_i}^3}\delta d_i\right)^2}\,. \qquad 3.7$$

3.3.2 Temperature

The wall and fluid temperature for the experiment and calculation of the heat transfer coefficient were measured with a K-type thermocouple with a diameter of 0.5 mm. After conducting an in-house calibration, the thermocouple was found to have an accuracy of 0.1 K. Based on the equilibrium thermodynamical properties calculated using NIST REFPROP [103], the saturation temperature (T_{sat}) of the fluid is determined from the absolute pressure of the test section inlet. The inlet subcooling conditions are determined as the variance between the calculated saturation temperature and the measured fluid temperature.

3.3.3 Heat Flux

The experiment utilized a custom-built in-house power supply to provide input power. This power supply applies a voltage potential through a controller-rectifier circuit to six evenly distributed electrodes along the heated section. While a smooth direct current (DC) would have been ideal, capacitors were deliberately excluded from the power supply to reduce the transformers' load, resulting in a rectified sine wave. Given the considerable ripple in the signal, a digital oscilloscope was employed to analyze the voltage and current signals at each heated section. The data was recorded at a rate of 10 Hz (every 0.1 second), which was not directly compatible with the mains

frequency of 50 Hz, making direct sampling impractical. To address this sampling issue, the actual signal shape was numerically integrated to obtain average DC-equivalent values, which were then used as correction factors for the voltage and current measurements obtained through the acquisition card. The calibration process revealed that the accuracy of the input power measurement, including voltage and current, was below 10 %, assuming a power of 200 W, leading to a final accuracy of ±20 W. Since the heated section is well-insulated, nearly all the volumetric heat generated in the pipe wall effectively transfers to the fluid. However, thermal losses are still taken into account when determining the heat transfer to the fluid. Calibration was conducted using the test section inlet and two internal thermocouples, in conjunction with the principle of energy conservation. Throughout the experimental study, the heat losses were consistently below 8 %.

The input power supply to each section of the test section is determined from the equation:

$$P_{elect} = UI \tag{3.8}$$

From the input power supply, the heat flux is then calculated using the equation:

$$q'' = \frac{P_{elect}}{\pi D_i \Delta z}. \tag{3.9}$$

The corresponding uncertainty regarding the input power supply and the heat flux is calculated respectively as:

$$\delta P_{elect} = \sqrt{(U\ \delta I)^2 + (I\ \delta U)^2}, \tag{3.10}$$

$$\delta q'' = \sqrt{\left(\frac{1}{\pi d_i l}\delta P_{elect}\right)^2 + \left(\frac{P_{elect}}{\pi d_i^2 l}\delta d_i\right)^2 + \left(\frac{P_{elect}}{\pi d_i l^2}\delta l\right)^2}, \tag{3.11}$$

3.3.4 Pressure

At a position between the inlet valve and the heated test section, the absolute pressure of the system was recorded. GE-UNIK 5000 Premium pressure sensor was the pressure sensor used in the experiment. It has an overall accuracy of 0.04 % of its full scale (which is 1600 kPa). This accuracy represents approximately ± 0.1 kPa within the relevant experimental pressure range. To directly measure the two-phase pressure drop across the test section, a differential pressure transducer was employed. The test section is equipped with three differential pressure (D*P*) transducer, and the desired pressure taps for measurement are selected by adjusting several valves. Both the inlet valve and the exit, either an orifice plate or outlet section of the test section are fitted with differential pressure (D*P*) transducer as well. The inlet D*P*–transducer conveniently measures the

pressure difference across both the inlet restriction valve and the *G*2 flow meter. The brands for the differential pressure transmitters are Endress+Hauser brand, specifically the Deltabar S type which has a high reference accuracy of ± 0.075 %.

3.4 Measurement Accuracy

Accuracy of the measured parameters from the experimental facility is summarized in Table 3.2 below.

Table 3.2: Accuracy of the measured parameters from the experimental facility

Name	Instrument Type	Brand	Localization	Range	Measurement Accuracy	Maximum Statistical Error
D*P* 1	D*P*-transducer	Endress+ Hauser	Test Section	0-100 kPa	0.075 %	0.1 kPa
D*P* 2	D*P*-transducer	Endress+ Hauser	Orifice Valve	0-100 kPa	0.075 %	0.5 kPa
D*P* 2	D*P*-transducer	Endress+ Hauser	Outlet Section	0-100 kPa	0.075 %	0.2 kPa
D*P* 3	D*P*-transducer	Endress+ Hauser	Inlet Valve	0-100 kPa	0.075 %	0.2 kPa
T 1-20	K-Type Thermocouple	Standard	Whole Loop	-50-100 ℃	0.1 ℃	0.1 ℃
P 1-5	Absolute Pressure	GE-UNIK 5000	Whole Loop	1-1600 kPa	10 kPa	< 0.10 kPa
F 1-2	Flow-meter (Coriolis)	Bronkhorst Cori-Tech	Test Section	0-3 L/min	0.01 L/min	<0.01 L/min
Q 1-5	Power supply	In- house	Heated Sections	0-2500 W (5 sections)	20 W	20 W

3.4.1 Measurement Uncertainties

Uncertainties of the main operational parameters are summarized in Table 3.3 below

Table 3.3: Uncertainties of the main operational parameters

Parameter	Symbol	Uncertainties
Mass flux	G	$\pm$ 10 kg/(m^2 s)
Inlet Pressure	P_i	$\pm$ 10 kPa
Inlet temperature	T_i	$\pm$ 0.2 °C
Heat flux (all 5 zones)	q"	$\pm<$ 40 W

3.4.2 Experimental Conditions for the facility

The main features of the experimental facility for this study are summarized below.

Fluid – R134a

System pressure – P = 400 - 1200 kPa

Mass flow rate – G = 5 - 2000 kg/(m^2 s)

Inlet temperature (Subcooling) - T_{in} =-20 – 40 °C, ΔT_{sub}=0 – 50 °C

Maximum Power Input – Q = 1500 W

Test Section Orientation= Horizontal

Length of Test Section = 2.035 m

Internal Diameter = 5 mm

External Diameter = 8 mm

Inlet flow restriction coefficient= $K_i \approx 2.63$ (default unless the valve is fully open)

Exit flow restriction coefficient= $K_i \approx 2.70$ (default unless the valve is fully open)

3.4.3 User Interface of Software

The Laboratory Virtual Instrument Engineering Workbench (LabVIEW 2011), developed by National Instruments (NI), is a software system design platform and development environment based on visual programming. Its primary purpose in this study is to control the experimental parameters. The software interface serves multiple functions, including the regulation of pump speed and the management of heaters and chillers (specifically, the control of the inlet temperature from chiller 1 and the tank pressure from chiller 2). Furthermore, it enables monitoring by presenting readings from heaters, flow meters, absolute and differential pressure transducers, and thermocouples in a schematic flow diagram. Notably, the software allows real-time visualization of the inlet flow trace, providing valuable insights. For data logging during experiments, the LabVIEW

data acquisition tool is employed, which enables continuous online monitoring of experimental conditions in Matlab. The described software interface window is shown in Figure 3.5 below.

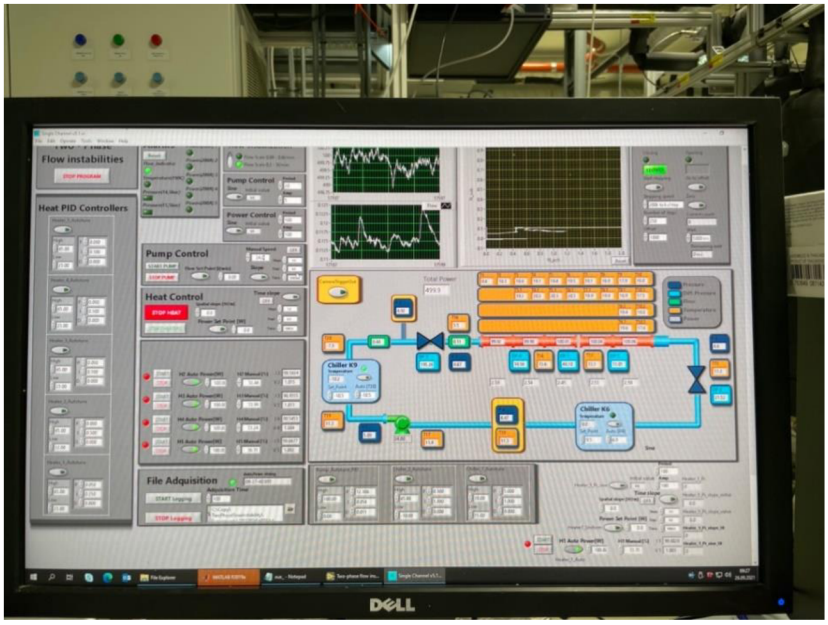

Figure 3.5a: LabVIEW software interface (Main control screen)

Figure 3.6: LabVIEW software interface (monitoring screen)

3.5 Experimental procedure and Data Reduction

This section describes the scientific methodology for collecting the experimental data and the analytical processes for analyzing the data in line with the objectives of the study.

3.5.1 Operational steps for the experimental facility

To run the test facility and set it ready for collecting experimental data, a set of systematic steps needed to be followed. First, the inlet and outlet valves are configured. The pump is then started. The chillers are turned on and the desired inlet subcooling and system pressure are set. Because tuning one parameter has an effect on other parameters, the condenser, conditioner and pump drive are continuously adjusted in order to obtain the desired subcooling, flow rate and pressure according to the experimental conditions are designed. After setting the initial desired conditions, a sizeable amount of time is given to reach a steady state. Steady-state conditions were confirmed when the time-averaged changes in the mass flux and pressure reached below ± 6 % as can be seen in Figure 3.8. The test section's inlet subcooling temperature was maintained at a minimum of 7 °C. The tuning and setting of parameters to reach a true steady state can take about one hour or more. When the true steady state is reached, the data logging begins.

3.5.2 Experimental Procedure

For each experiment, the pressure of the fluid at the test section's outlet was kept constant. Before recording the data, extra caution was taken to guarantee that steady-state conditions were met. As indicated above, the steady-state conditions were confirmed when the time-averaged changes in the mass flux and pressure reached below ± 6 %. The steady state conditions during the experiment are observed on a separate monitor as shown in Figure 3.7 below. The test section's inlet subcooling temperature was maintained at a minimum of 7 °C. This reduces the likelihood of subcooled boiling of the liquid before entering the test section. A valve at the inlet of the test section was adjusted to prevent the occurrence of two-phase flow instabilities [38, 39]. Each dataset was recorded for approximately 100 s, which was equivalent to about 1000 data points. The facility was heated up to the desired power level before the experiments. The data were then captured by lowering the power to a desired level. By doing so, the surge in wall temperature that occurs when nucleate boiling begins is prevented, as are changes in the flow pattern. This ensures that the experiments are repeatable. Furthermore, the experiments were carried out by gradually reducing the vapor quality from $x > 1$ to $x < 0$. This approach prevents the sudden

increase in wall temperature that happens, for example, when nucleate boiling begins or when the flow pattern changes [15, 41].

Figure 3.7: Picture of monitor for monitoring steady state condition to observe the time averaged changes in the experimental conditions

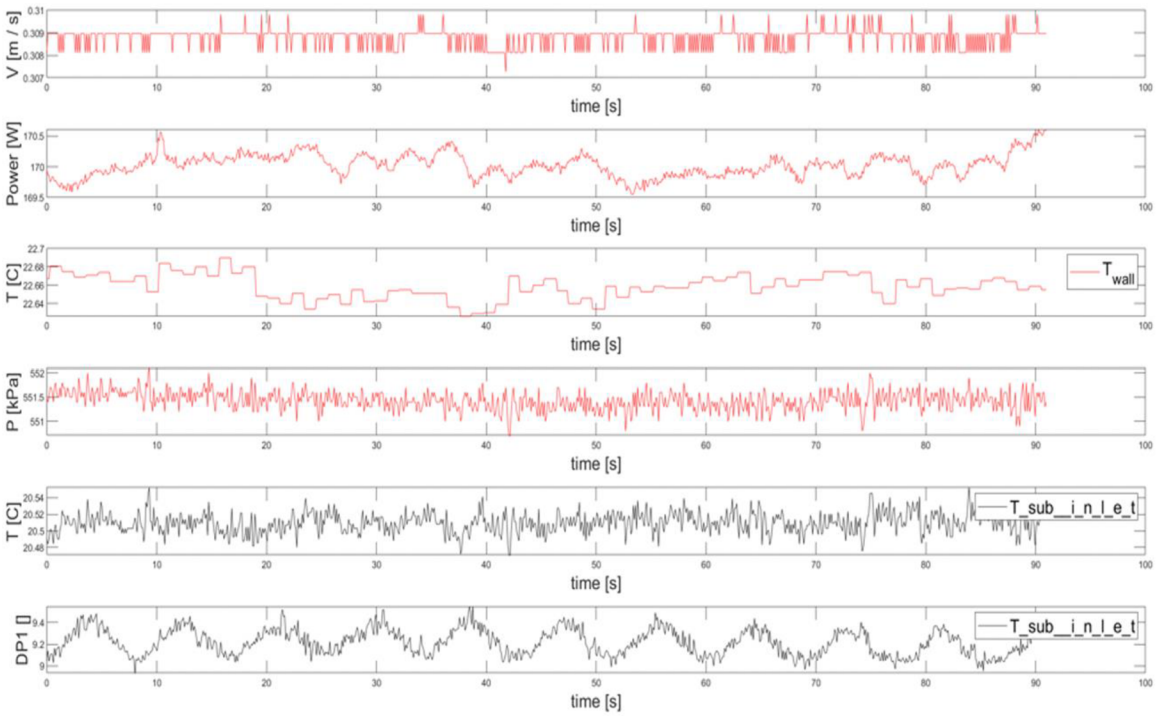

Figure 3.8: Picture of the steady state condition to observe the time averaged changes in the experimental conditions

3.5.3 Data Reduction

By performing data reduction, the huge numerical information from the experimental measurements are corrected, ordered and simplified. In this case, the experimental data is converted into suitable and convenient form that can be represented in figures and tables.

3.5.4 Heat transfer coefficient

The measurement of the heat transfer coefficient which is a paramount parameter in this research is presented. In this study, instead of global heat transfer coefficient, local heat transfer coefficient was employed and it was obtained at positions 1917 mm from the inlet of the test section. By employing Newton's cooling equation, it is calculated as:

$$h = \frac{q''}{T_{w,i} - T_f}. \qquad 3.12$$

The local heat transfer coefficient is represented by h, the fluid temperature T_f is recorded with the internal thermocouple, $T_{(w,i)}$ is the inner wall temperature; and q'' is the heat flux.

3.5.5 The inner wall temperature

Thermocouples for reading the wall temperatures are glued at the outer wall of the test section. However, the heat transfer coefficient is calculated with the inner wall temperature calculated from the outer wall temperature readings with the assumption that there is no heat loss and negligible heat flow in the axial direction. In order to compute the inner wall temperature $T_{(w,i)}$, one dimensional (1D) steady state heat conduction equation in the radial direction of the test section is solved by assuming a perfect insulation and taking into account thermal losses within the heat flux. The steady state heat conduction equation for the tube wall is given by:

$$\frac{1}{r}\frac{d}{dr}\left(r\frac{dT}{dr}\right) + \frac{q'''}{k_w} = 0, \qquad 3.13$$

where r (m) indicates the radial direction along the heated wall, q''' represents the volumetric heat rate obtained using Joule's effect to the pipe and k_w is the thermal conductivity of the wall.
The determined outer wall temperature, $T_{(w,o)}$, is regarded as a boundary condition as well as an assumption of no heat flux. This is the average temperature measured at four positions (top, bottom and two side walls) from the inlet of the test section. The equation for the inner wall temperature after integration is thus given as:

$$T_{(w,i)} = T_{(w,o)} + \frac{q'''}{4k_w}\left(R_o^2 - R_i^2\right) - \frac{q'''}{2k_w} R_o^2 \ln\left(\frac{R_o}{R_i}\right). \quad 3.14$$

Here, R_i (m) is the inner radius and R_o (m) is the outer radius of the tube. The volumetric heat generation rate which is assumed to be uniform is given as:

$$q''' = \frac{Pw_{elect}}{\pi\left(R_o^2 - R_i^2\right)\Delta z}, \quad 3.15$$

where the length of the heated section is denoted by Δz m. By combining equation 3.14 with equation 3.15, we obtain the final inner wall temperature as:

$$T_{(w,i)} = T_{(w,o)} + \frac{Pw_{elect}}{4\pi k_w \Delta z} - \frac{Pw_{elect}}{2\pi k_w \Delta z}\frac{R_o^2}{\left(R_o^2 - R_i^2\right)} \ln\left(\frac{R_o}{R_i}\right). \quad 3.16$$

The measurement difference between the thermocouple readings was less than 0.4 °C. At large heat fluxes, the mean measurement uncertainty of the heat transfer coefficients is around 10 %, but this can reach 30 % at low heat fluxes.

3.5.6 Vapor Quality

By performing heat balance along the test section, the vapor quality is obtained by:

$$x(z) = \frac{\int_{z_0}^{z} q'' \pi D_i dz - G\, A\, c_{pl} T_{sub}}{G\, A\, h_{lv}} \quad 3.17$$

The vapor quality at position $z\ (m)$ along the heated test section is represented by x. The mass flux is represented by G, The enthalpy of vaporization is represented by h_{lv}, and T_{sub} indicates the inlet subcooled temperature. The liquid-phase heat capacity of the fluid is represented by c_{pl}, while $A\ (m^2)$ is the pipe's cross-sectional area.

3.5.7 Heat Flux

As indicated above, the heat flux applied to flowing fluid through the tube was determined by the electrical Joule effect. A voltage potential was provided to the heated section through 6 electrodes spaced every 0.4 m on the heated test section. The power applied was provided by low-voltage together with high-current sine waves that have been rectified. The signal duty was used to regulate the quantity of power. $P_{electric}$ is the total amount of electrical power, which is calculated as:

$$P_{electric} = UI \quad . \quad 3.18$$

The tubes and heated portion are properly insulated, and because of this, practically all of the volumetric heat created in the pipe wall is forced to flow to the fluid. By neglecting heat losses, the total heat flux to the flowing fluid is given as:

$$q'' = \frac{P_{electric}}{\pi D_i \Delta z}, \qquad 3.19$$

where q'' is the heat flux supplied to the fluid, D_i is the heated section's inner diameter and Δz is the heated section's length where the electrical power is supplied. To account for heat losses, the supplied electrical power was compared to the thermal power provided by the balance using fluid thermocouples. The balance indicated that the heat loss never exceeded 8 %. After adjusting the electrical power with a logarithmic fitting, the ultimate accuracy reached was 3 %, which was judged to be inconsequential. This accuracy was thus transferred to the error in the quality and heat transfer coefficient measurements.

3.6 Concluding Remarks

The two-phase flow boiling experimental test facility modified at the Thermal Two-Phase Flow Lab in Norwegian University of Science and Technology (NTNU) to investigate flow boiling heat transfer of R134a refrigerant at varying conditions was extensively presented in this chapter. The facility was modified for heat transfer coefficient investigation, two phase flow pressure drop investigation and flow visualization. Measurement and uncertainty analysis were also presented together with data reduction procedures for the study. To validate the facility for two phase flow boiling heat transfer measurement and ensure accuracy of the experimental measurements, single phase flow validation was performed.

Chapter 4

4 Results and Discussion

This chapter presents the findings and discussions of this dissertation. To make this chapter presentable and readable, the results are presented in sections based on each objective spelt out to achieve the overall aim of this research that has been published [24], [104]–[107]. It is important to indicate that this chapter is presented based on contents from the listed publications of which I was the main author. The schematic plan for presenting the results and discussion is illustrated below:

- Experimental Validation
- Heat Transfer Coefficient from Subcooled Liquid through Saturation to Superheated Vapor
- Effect of Saturation Pressure on Heat Transfer
- Heat Transfer at Varying Heat Fluxes

Based on this plan, for experimental validation of the test rig, heat transfer validation of the test section, comparison of results with similar conditions from literature, test of repeatability and pressure drop validation was presented.

For heat transfer coefficient from subcooled liquid region through saturation to superheated vapor, the presentation of results and discussion were broken down into the sections of subcooled region, saturation region, dryout incipience (critical heat flux), superheated regions, flow patterns, temperature profiles and pressure drop.

For effect of saturation pressure on heat transfer coefficient, the results and discussion were presented in sections of flow boiling heat transfer coefficient, flow pattern and flow pattern maps, frictional pressure drop and comparison of experimental results with correlations. Finally, the heat transfer at varying heat fluxes was presented. The presentation of the results and the discussion was based on achieving the aims and objectives of this research.

4.1 Experimental Validation

Validation of the measurements from the work bench to ascertain the reliability of the experimental measurement is presented in this section. As indicated above, for the experimental validation, heat transfer validation of the test section, comparison of results with similar conditions from literature, test of repeatability and pressure drop validation are presented.

4.1.1 Heat Transfer Validation of the Test Section

To validate the experimental setup and the data reduction procedure for the heat transfer in the test section, the heat transfer coefficient for single-phase liquid and single-phase vapor are measured. The measured heat transfer coefficients are compared with the Dittus–Boelter equation [108] as seen in Figure 4.1, given as:

$$Nu = 0.023Re^{0.8}\,Pr^{0.4} \qquad 4.1$$

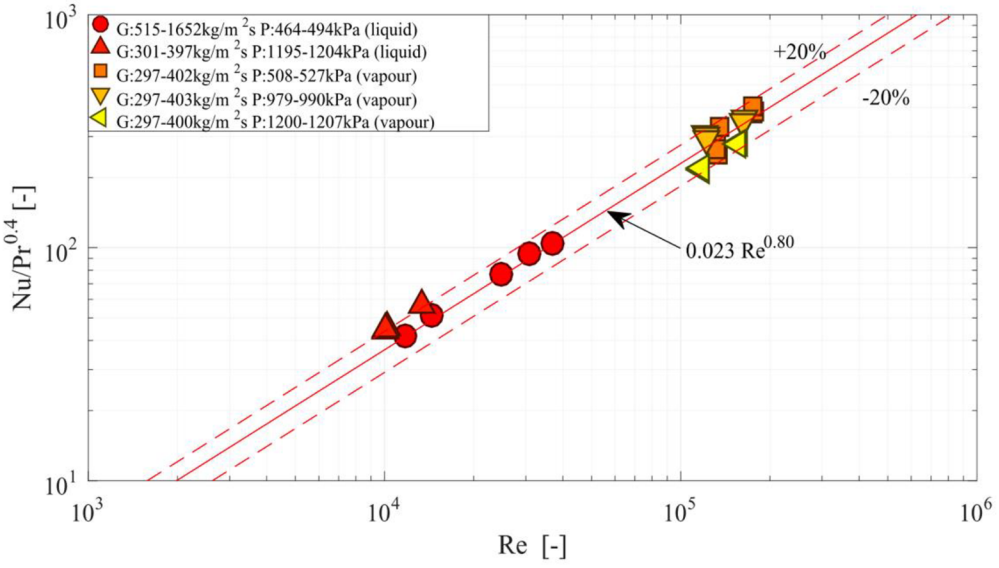

Figure 4.1: Comparison of single-phase liquid and vapor heat transfer coefficient results with prediction by Dittus–Boelter correlation

It can be observed that the measured single-phase data from the facility agrees with the Dittus–Boelter equation. Both the single-phase liquid and single-phase vapor measurement data fall within a confidence interval of 20 %. This validates the reliability of the heat transfer measurements from this experimental facility.

4.1.2 Comparison of Results with Similar Work from Literature

To further validate this experimental measurement, two-phase flow heat transfer coefficients for selected test conditions are compared with experimental data from the literature with similar working conditions, as can be seen in Figure 4.2 and Figure 4.3. It can be observed that, the heat transfer coefficient results and trend evolution with vapor quality for the selected conditions are almost similar. This further shows the trustworthiness of the experimental test facility.

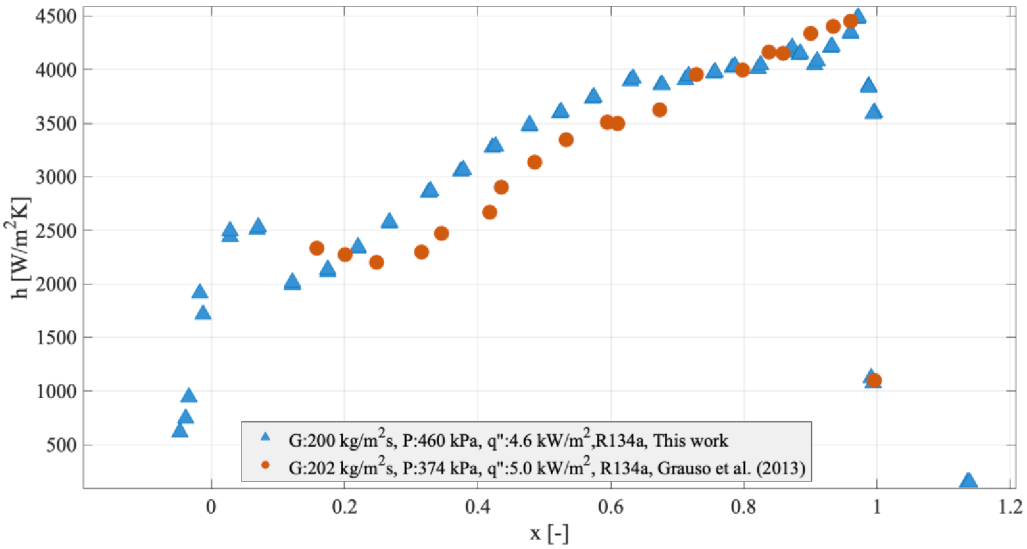

Figure 4.2: Comparison of two-phase flow heat transfer coefficient from this case with a similar case from the literature [84]

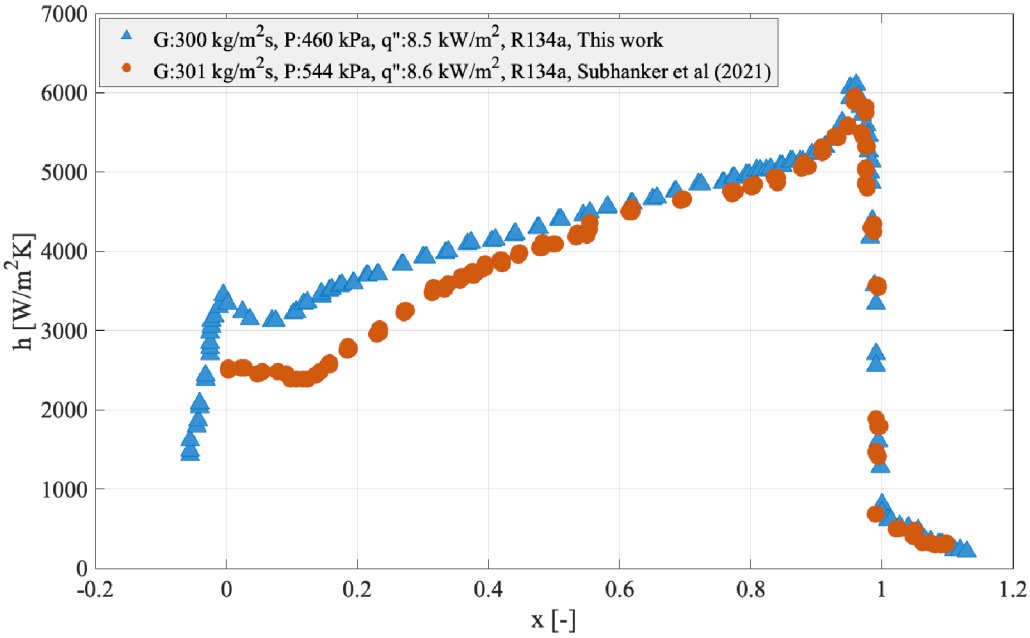

Figure 4.3: Comparison of the two-phase flow heat transfer coefficient from this case with a similar case from the literature [99]

4.1.3 Test of Repeatability

Heat transfer coefficient data of similar experimental conditions were performed at different times (3rd July 2017 and 4th November 2019) on the test facility. The results as shown in Figure 4.4 indicates how close the results are although the data were collected on different dates. This further validates the trustworthiness of experimental facility.

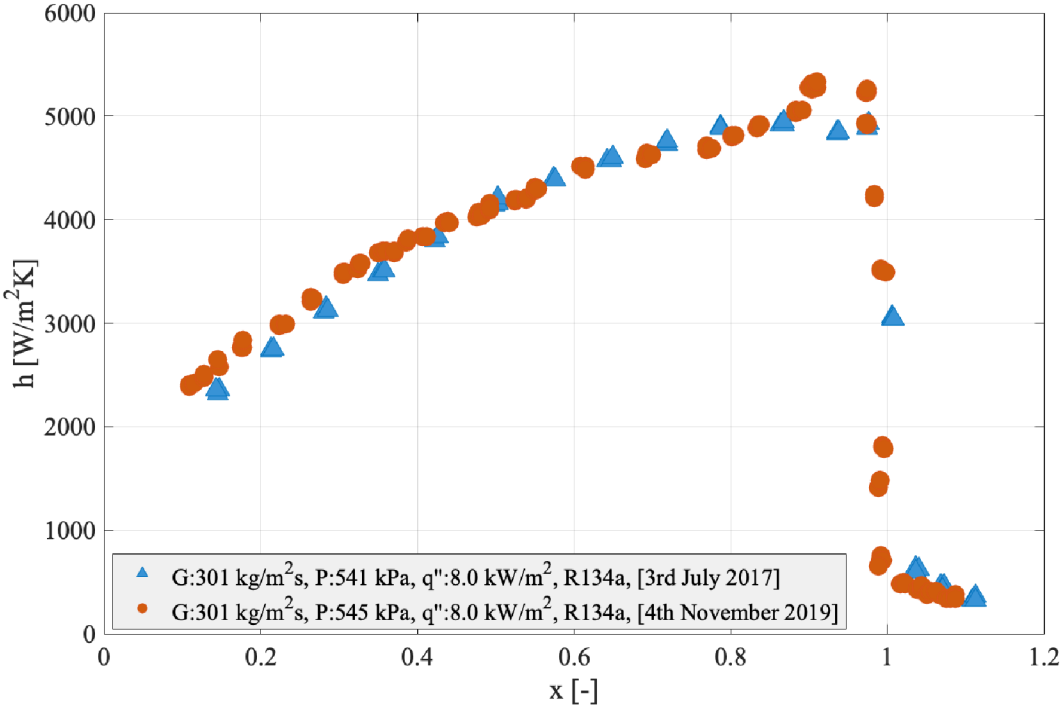

Figure 4.4: Test of repeatability for the heat transfer coefficient results

4.1.4 Pressure Drop Validation (Single phase)

Frictional pressure drop measurements were validated by comparing measured single-phase liquid friction factor *f* with well-known prediction methods from literature. The results were compared with correlations of Colebrook given as:

$$\frac{1}{\sqrt{f}} = -2\log\left(\frac{\epsilon/D_i}{37} + \frac{2.51}{Re\sqrt{f}}\right). \qquad 4.2$$

Here, *f* is the friction factor, D_i is the internal diameter of the tube, ϵ is the absolute pipe roughness and Re is the Reynolds number of the flow which is greater than 4000. Figure 4.5 represents the comparison of the Colebrook correlation and experimental data. The experimental results were within a confidence interval of 10 %. These validations indicate that the measurement uncertainty with the experimental facility is low and the results from this facility are trustworthy and reliable.

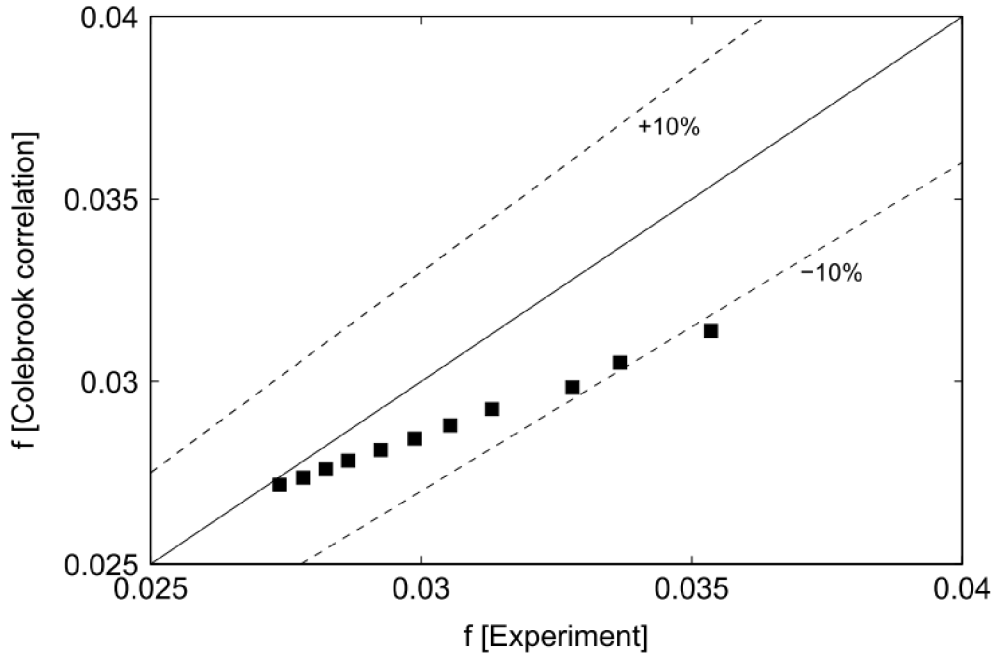

Figure 4.5: Validation of single-phase pressure drop

4.2 Heat Transfer Coefficient from Subcooled Liquid Region through Saturation Region to Superheated Vapor Region

Extensive and systematic experiments were performed over a wide range but small increment of vapor quality from a single-phase subcooled region through to two-phase to a superheated vapor region to investigate the effect of mass flux, heat flux and vapor quality on heat transfer coefficient and determine the dominant mechanism responsible for controlling heat transfer under the studied conditions. The flow patterns observed during this study were recorded using a high-speed camera at 2000 fps. The fluid, wall and saturation temperature profile associated with the heat transfer coefficient were also measured for the cases studied. The pressure drop for the cases studied was investigated.

4.2.1 Subcooled Region

Figure 4.6 and Figure 4.7 show how heat flux affects the heat transfer coefficient for a constant saturation pressure and a given mass flux of 200 kg/(m^{2}s) and 300 kg/(m^{2}s) in both figures. In the subcooled liquid region (SC) approaching a vapor quality of zero, it can be seen that the heat transfer coefficient rises linearly to a peak/maximum. This rise in peak is observed to be sensitive to heat flux in that the heat transfer coefficient peak increases to a higher peak with a higher heat flux for a given mass flux. This rise in heat transfer coefficient at the near zero vapor quality as a result of increasing heat flux could be attributed to poor bubble nucleation at the wall of the tube.

Due to this, the layer of fluid close to the wall gains heat and becomes superheated. With this superheated wall, once a bubble nucleates, it grows quickly and departs from the nucleation site, transferring the heat stored to the surrounding liquid and, thus, causing a sharp rise in heat transfer coefficient. Figure 4.8 and Figure 4.9 show how mass flux affects the heat transfer coefficient for a constant saturation pressure and a given heat flux in both figures. It can be seen that there is no obvious effect of mass flux on the heat transfer coefficient. The sensitivity of the heat transfer coefficient with heat flux and the insensitivity with mass flux indicate that the dominant mechanism responsible for heat transfer in the subcooled region is nucleate boiling. The flow pattern observed in this region, close to a vapor quality of one (1), is slug flow, which can be seen in Figure 4.10a. A similar trend was reported by [54], [60], [109].

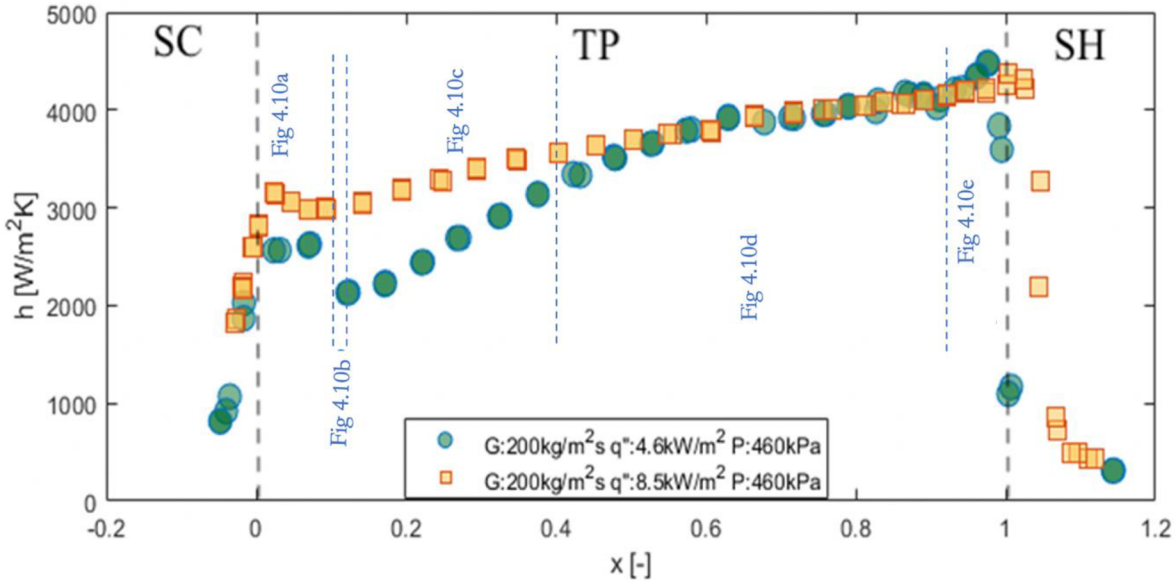

Figure 4.6: Variation in measured heat transfer coefficient for fixed mass flux of 200 kg/(m² s), constant pressure of 460 kPa and varying heat flux of 4.6 kW/m² and 8.5 kW/m² as a function of vapor quality. The ranges of the different boiling modes, as presented in Figure 4.10a-e, are indicated in the graph

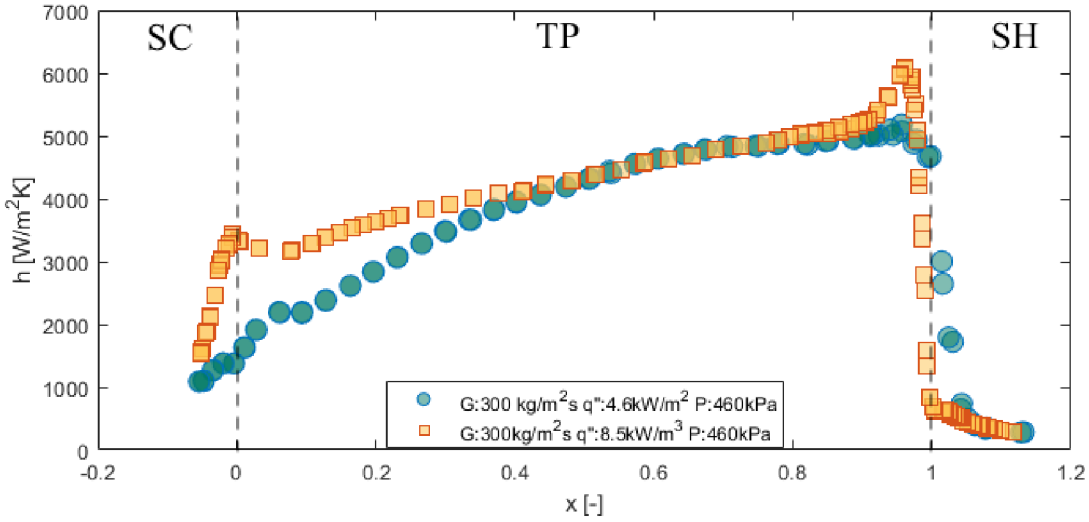

Figure 4.7: Variation in measured heat transfer coefficient for fixed mass flux of 300 kg/(m² s), constant pressure of 460 kPa and varying heat flux of 4.6 kW/m² and 8.5 kW/m² as a function of vapor quality.

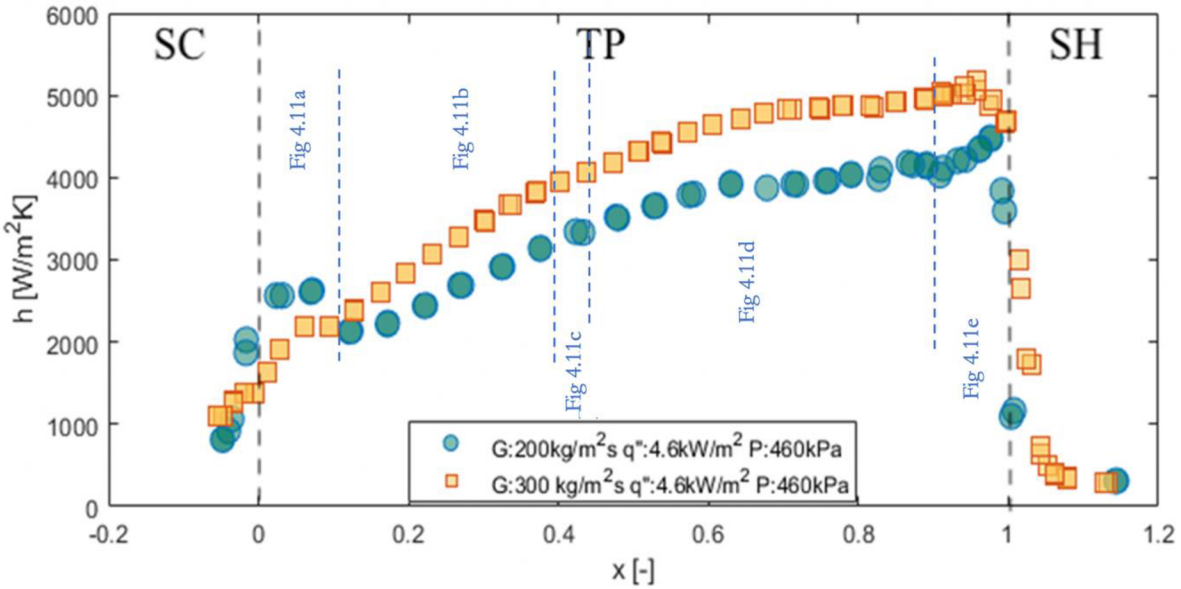

Figure 4.8: Variation in measured heat transfer coefficient for fixed heat flux of 4.6 kW/m², constant pressure of 460 kPa and varying mass flux of 200 kg/(m² s) and 300 kg/(m² s) as a function of vapor quality. The ranges of the different boiling modes, as presented in Figure 4.11a–e, are indicated in the graph

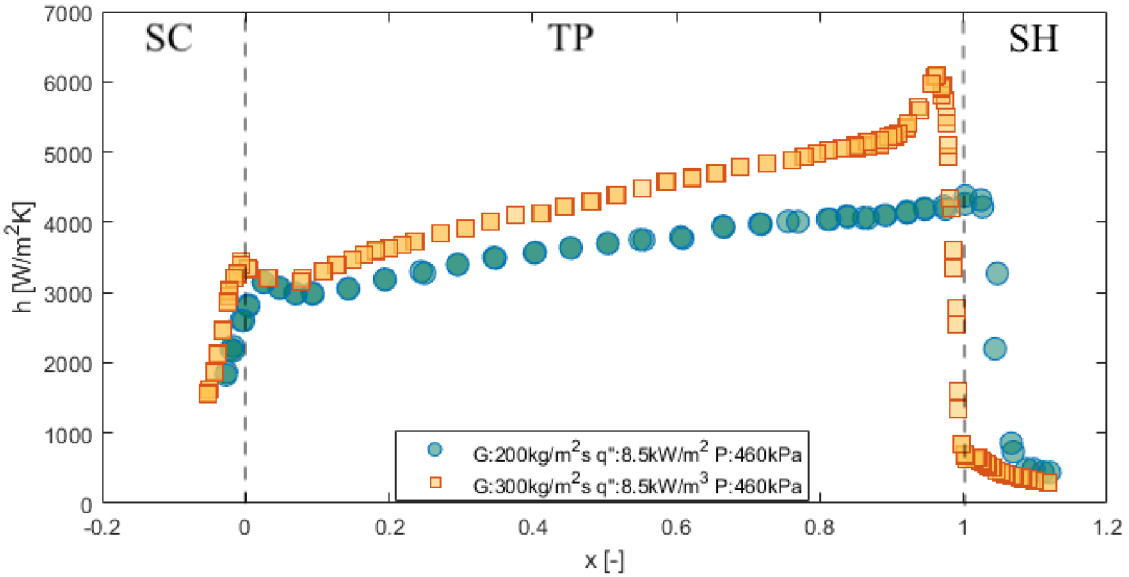

Figure 4.9:Variation in measured heat transfer coefficient for fixed heat flux of 8.5 kW/m², constant pressure of 460 kPa and varying mass flux of 200 kg/(m² s) and 300 kg/(m² s) as a function of vapor quality.

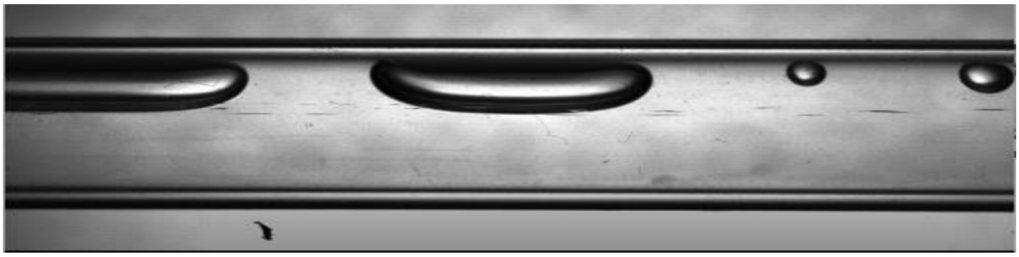

a) Slug flow pattern ($x < 0.1$)

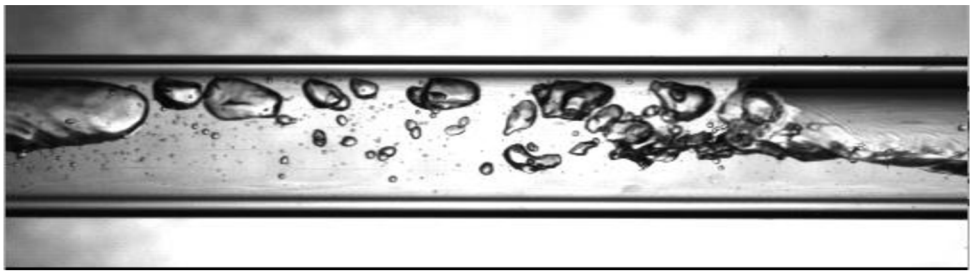

b) Slug intermittent flow pattern ($x \approx 0.1$)

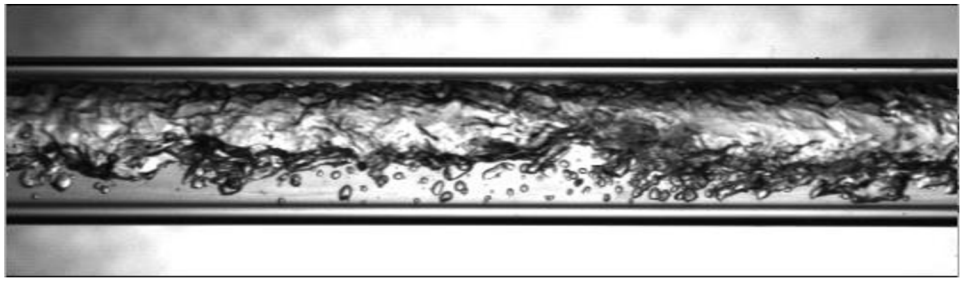

c) Intermittent flow pattern (x = 0.15 - 0.4)

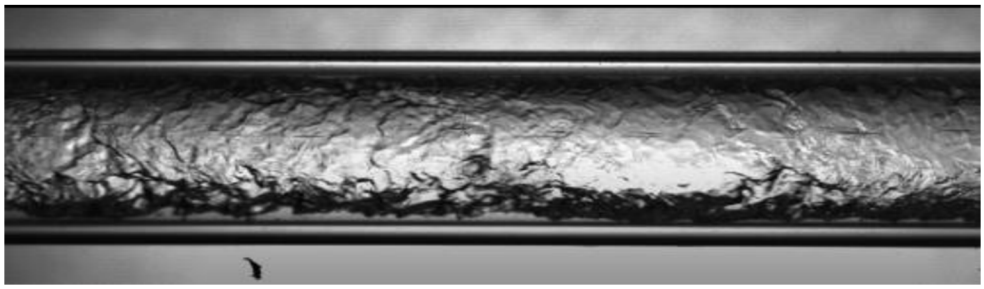

d) Annular flow pattern (x > 0.4)

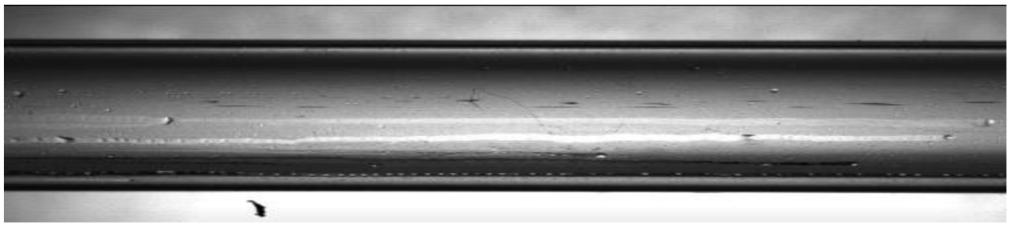

Dry-out–mist flow pattern (x > 0.9)

Figure 4.10: Slug flow pattern (x < 0.1); (**b**). Slug intermittent flow pattern ($x \approx 0.1$); (**c**). Intermittent flow pattern (x = 0.15-0.4); (**d**). Annular flow pattern (x > 0.4); (**e**). Dry-out–mist flow pattern (x > 0.9) of (G = 200 kg/(m² s), q" = 4.6 kW/m², P = 460 kPa), (G = 200 kg/(m² s), q" = 8.5 kW/m², P_{sat} = 460 kPa) and (G = 300 kg/(m² s), q" = 8.5 kW/m², P_{sat} = 460 kPa).

4.2.2 Two-Phase Region (Saturated Region)

In the saturated region, Figure 4.6 shows how heat flux affects the heat transfer coefficient at a low mass flux of 200 kg/(m² s). It can be seen that for a mass flux of 200 kg/(m² s), the heat transfer coefficient is higher for the higher heat flux. This heat transfer coefficient decreases slightly to its minimum over vapor quality, irrespective of the heat flux, before rising again as vapor quality increases. The decrease in heat transfer coefficient to a local minimum is observed at a lower vapor quality region below 0.1 (i.e., x < 0.1), which can be identified as the slug flow pattern. Figure 4.10a shows the flow pattern for slug flow below a vapor quality of 0.1. The local minimum is the region

of transition from slug to intermittent. This region of transition from slug to an intermittent flow pattern is presented in Figure 4.10b. According to Charnay [7] and Lima et al. [50], this region is a competition between nucleate boiling and convective boiling, in that the bubble nucleation and frequency of formation in the slug regime are suppressed as vapor quality increases, and this causes a decrease in heat transfer.

Figure 4.7 presents the effect of heat flux on the heat transfer coefficient at a mass flux of 300 kg/(m^2 s). With a mass flux of 300 kg/(m^2 s) but a lower heat flux (4.6 kW/m^2), the heat transfer coefficient increases steadily without any decrease in a similar vapor quality region. An increase in mass flux enhances convective boiling with a minimal effect from nucleate boiling when the heat flux is low. For this condition, the contribution of convective boiling increases with the vapor quality until dry-out is reached. This is as a result of high mass flux, causing the vapor phase to accelerate the liquid phase close to the wall of the tube, thereby enhancing the heat transfer coefficient. In this case, the flow patterns observed as vapor quality increases are slug, slug to intermittent, intermittent, intermittent to annular and annular, as presented in Figure 4.10. However, for a mass flux of 300 kg/(m^2 s) and heat flux of 8.5 kW/m^2, the heat transfer coefficient decreases slightly to a local minimum at low vapor quality before it increases as vapor quality increases. As the heat transfer coefficient decreases with vapor quality, it decreases to a local minimum before it begins to increase again. This deterioration in heat transfer coefficient to a local minimum at a low vapor quality is observed in all heat fluxes, except when the mass flux is higher. It can be assumed to be the transition from slug to intermittent, where bubble formation is suppressed in the process, leading to annular flow. The observance and position of this local minimum are highly dependent on the heat flux as compared to mass flux for the conditions studied. This is seen to occur in the slug regime and, thus, a dominant nucleate boiling region. The observed flow patterns for this case are presented in Figure 4.10. This trend of a local minimum has also been reported by [50].

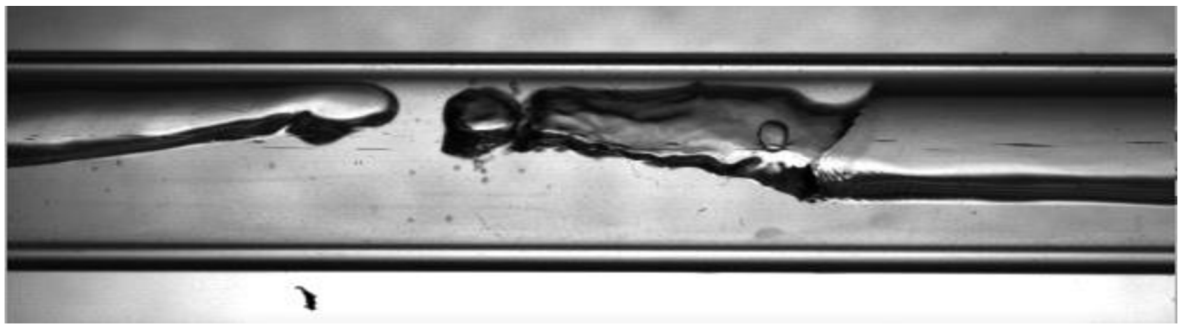

a) Slug flow pattern (x < 0.10)

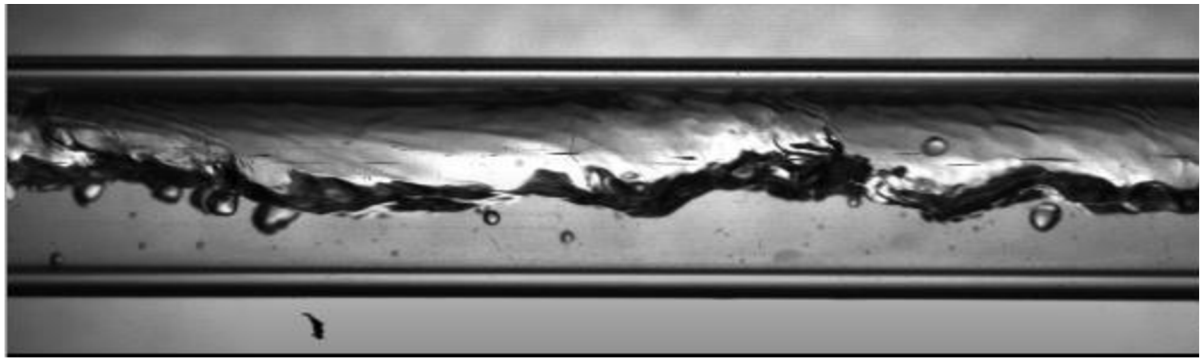

b) Intermittent flow pattern ($0.1 < x < 0.4$)

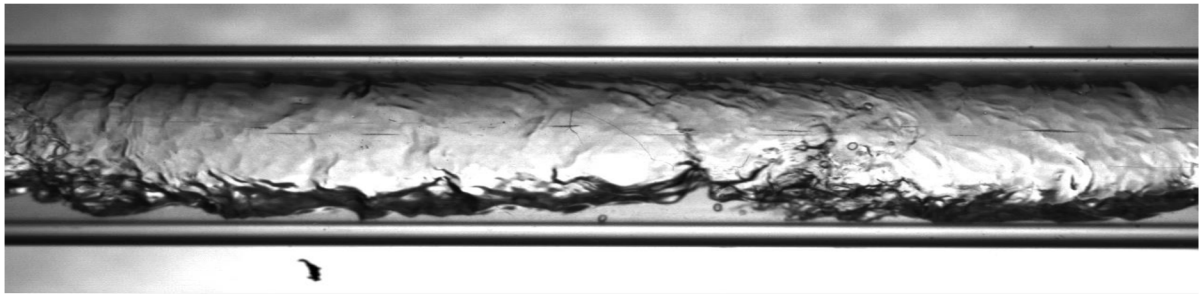

c) Intermittent–annular flow pattern ($x \approx 0.42$)

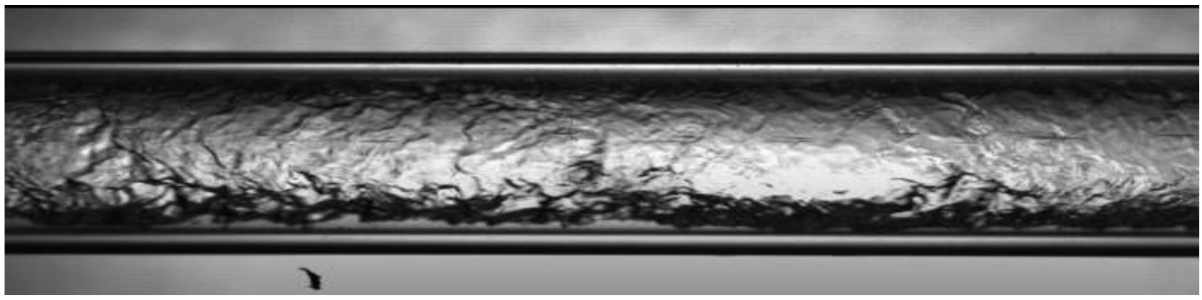

d) Annular flow pattern ($x > 0.4$)

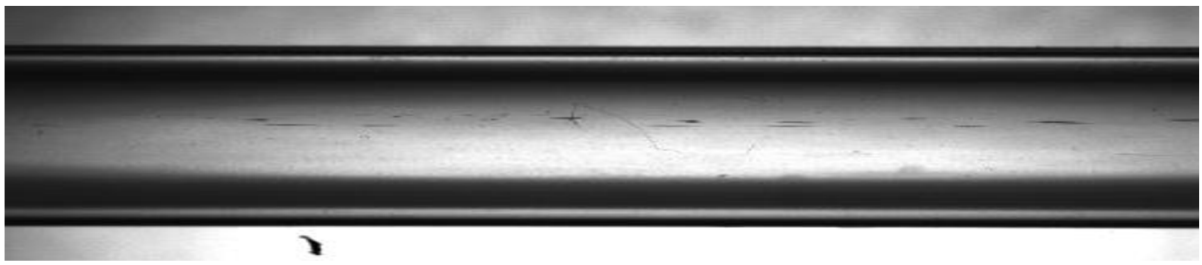

e) Dry-out–mist flow pattern ($x > 0.9$)

Figure 4.11: a) Slug flow pattern ($x < 0.10$); (b) Intermittent flow pattern ($0.1 < x < 0.4$); (c) Intermittent–annular flow pattern ($x \approx 0.42$); (d) Annular flow pattern ($x > 0.4$); (e) Dry-out–mist flow pattern ($x > 0.9$); Flow pattern for $G = 300$ kg/(m^2 s), $q" = 4.6$ kW/m^2, $P_{sat} = 460$ kPa.

In Figure 4.6 and Figure 4.7, for an increasing vapor quality (up to $x < 0.4$) for the same mass flux but varying heat flux, the heat transfer coefficient is sensitive to heat flux (increases with increasing heat flux). This regime is an intermittent to annular transition presented in Figure 4.11c, where the nucleate boiling effect is still observed and bubble formation is not completely suppressed. This effect of heat flux becomes negligible as vapor quality increases ($x > 0.4$), where the weakened effect of heat flux collapses the heat transfer coefficient into a single plot at high vapor qualities. This is because bubble nucleation is suppressed as vapor quality increases. This can be attributed to the role of vapor velocity due to mass flux and the reduction in liquid film thickness due to the increase in vapor quality. Therefore, at a higher vapor quality, the effect of heat flux on the heat transfer coefficient is suppressed. The flow regime is fully annular, as shown in Figure 4.10 and Figure 4.11d. The effect of heat flux is negligible in this regime.

In Figure 4.8 and Figure 4.9, at an increasing vapor quality, for the same heat flux but varying mass flux, the heat transfer coefficient increases with the increasing mass flux. Irrespective of the heat flux, a higher mass flux generates a higher heat transfer coefficient. However, this effect is less pronounced in a low-quality region ($x < 0.2$), where the effect of mass flux produces a less significant effect on the heat transfer coefficient. As vapor quality increases, the heat transfer coefficient becomes more sensitive to mass flux. This indicates that convective flow boiling dominates the flow, and this dominance is controlled by mass flux and vapor quality. The regime for this dominance is the annular flow regime, as shown in Figure 4.10 and Figure 4.11d. This observation can be attributed to the role of vapor velocity due to mass heat flux and the reduction in liquid film thickness as a result of the increase in vapor quality. A similar trend is reported by [50], [53], [84], [110].

4.2.3 Dry-Out Incipience and CHF

In the high annular flow regime with high vapor quality (x = 0.9 – 1.0), the heat transfer coefficient either increases sharply to a local maximum before a sudden drop or a monotonic drop without a sharp rise in local maximum of heat transfer coefficient, as can be observed in the two-phase (TP) region of Figure 4.6 to Figure 4.9. This region of high vapor quality just before the drop in heat transfer coefficient is known as dry-out incipience. This is where annular flow diminishes and makes way for dry-out as a result of the thinning and disappearance of the thin film. The steep rise in heat transfer coefficient is noticed in conditions of mass and heat flux (G = 300 kg/(m^{2}s)) and 8.5 kW/m^2. In other conditions of low mass flux, a steep rise in the heat transfer coefficient is observed. In low heat flux conditions, there is a monotonic drop in heat transfer without a sharp rise. At the dry-out incipience, the initiation of dry-out develops, where the flow quenches and rewets the wall surfaces, causing partial dry-out. A further increase in heat flux leads to a point where no liquid rewets the wall and critical heat flux occurs. This is where the liquid film completely dries out and transitions to the superheated region. It is observed in Figure 4.9 that the higher the mass flux, the lower the vapor quality at which drop out incipience commences. However, Deng et al. [55] observed in their study that the location and position of the dry-out incipience peak were almost the same for different mass fluxes. In contrast, a study by Lima et al. [55] reports that the higher the mass flux, the smaller the vapor quality for the occurrence of dry-out incipience. This region of the heat transfer coefficient is quite complicated because it is a transition from one flow pattern to another and that more data is required to understand the mechanism and tend responsible for this behavior. A possible explanation for varying observations could be that at high vapor qualities, vapor velocity is high and the thin film in this region is not stable until dry-out is reached; thus, the position and nature of the heat transfer coefficient cannot be easily predicted.

4.2.4 Superheated Region

A heat transfer coefficient beyond a vapor quality of one (1) is known to be in the superheated vapor region, indicated as SH in Figure 4.6 to Figure 4.9. In this region, the liquid film may have completely dried out and only vapor flows within the tube with little droplets entrained in it. This regime is known as the mist regime, which begins after dry-out ends. The heat transfer coefficient therefore drops to around zero (0) and becomes linear as vapor quality increases further. In this region, the gas phase is directly in contact with the wall surface and the heat transfer mechanism is different. It is also observed that both mass and heat flux have no significant effect on the heat transfer in this region. The mist flow pattern observed in this region is presented in Figure 4.10 and Figure 4.11e.

4.2.5 Temperature Profile

To further investigate the heat transfer coefficient from the subcooled region to the superheated region, the wall, fluid and calculated saturation temperature profile for the studied cases were measured. The typical flow boiling temperature profile from the subcooled region to the superheated region for the cases studied is depicted in Figure 4.12 to Figure 4.15. The heat transfer coefficient is usually defined as the difference between wall and bulk fluid temperature. This is given as:

$$h = \frac{q''}{T_w - T_f}, \qquad 4.3$$

where h denotes the heat transfer coefficient, q'' denotes the heat flux, T_w denotes the wall temperature and T_f is the temperature of the fluid.

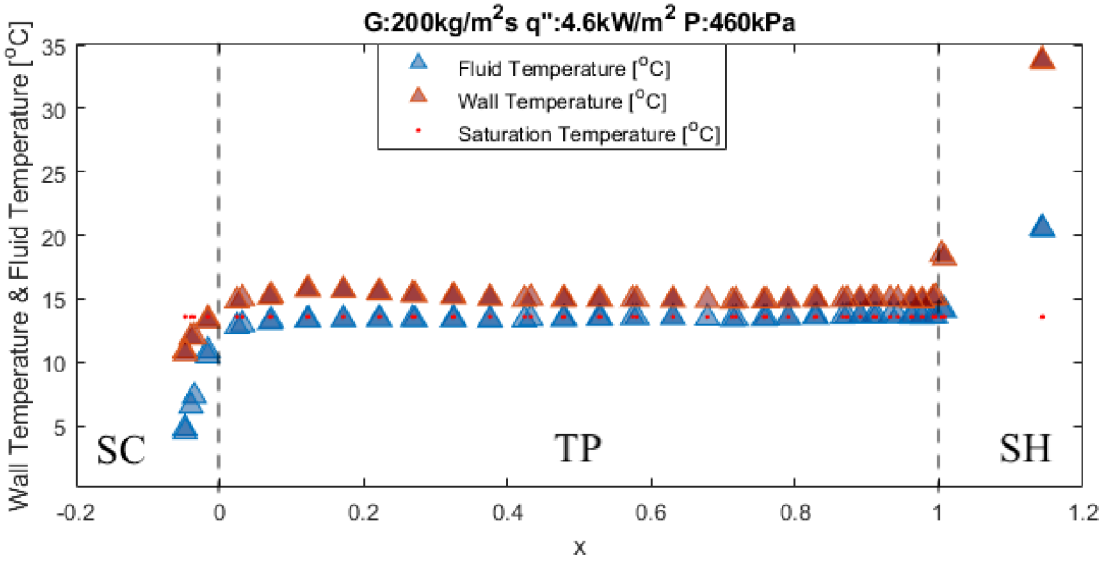

Figure 4.12: Variation in measured wall, fluid and calculated saturation temperatures as a function of vapor quality for G = 200 kg/(m² s) and q" = 4.6 kW/m² at a constant saturation pressure of 460 kPa.

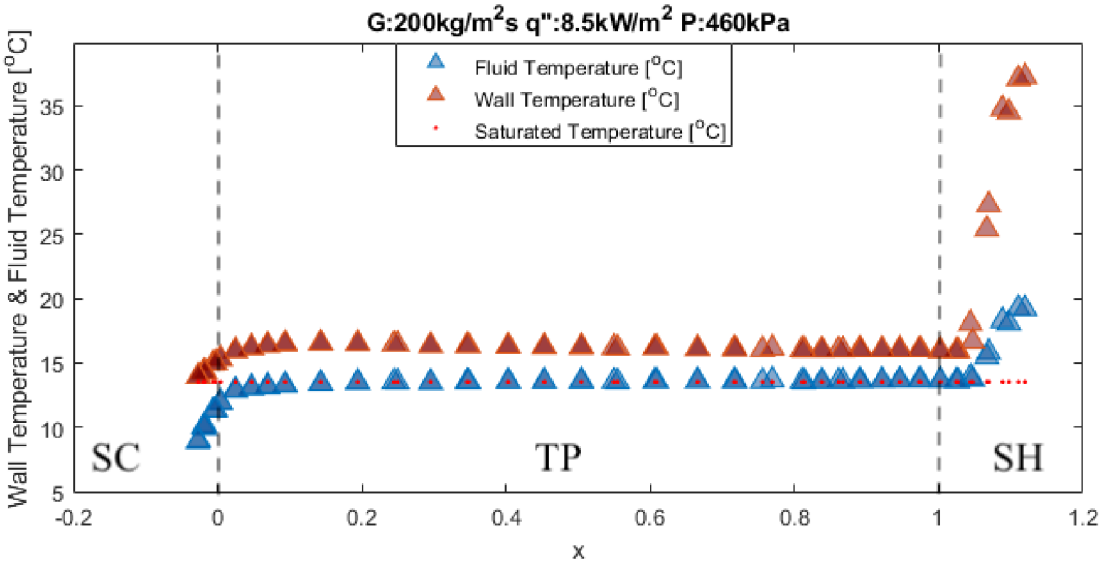

Figure 4.13: Variation in measured wall, fluid and calculated saturation temperatures as a function of vapor quality for G = 200 kg/(m² s) and q" = 8.5 kW/m² at a constant saturation pressure of 460 kPa.

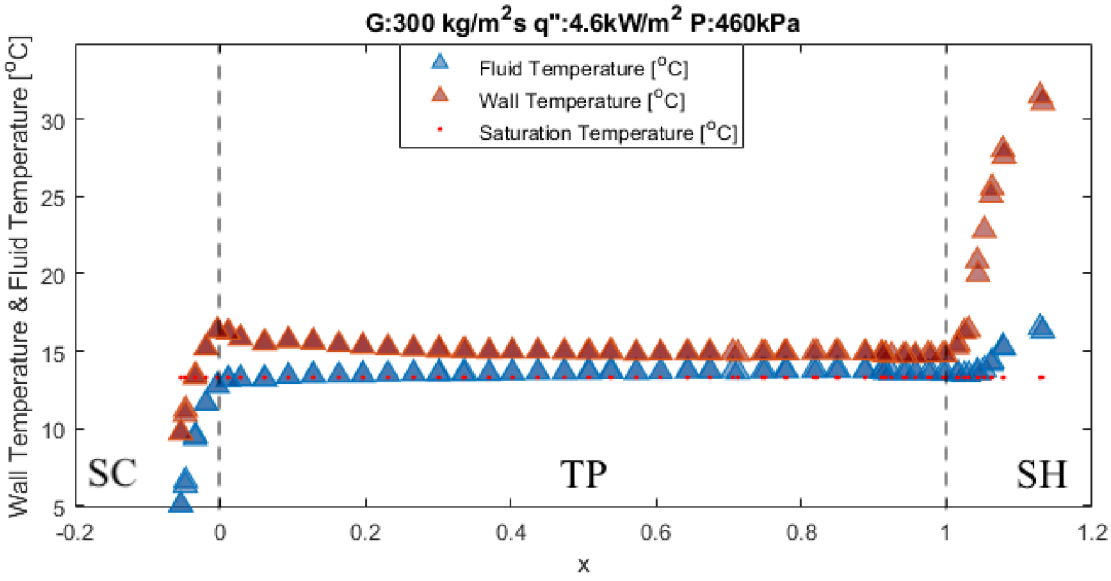

Figure 4.14: Variation in measured wall, fluid and calculated saturation temperatures as a function of vapor quality for G = 300 kg/(m² s) and q" = 4.6 kW/m² at a constant saturation pressure of 460 kPa.

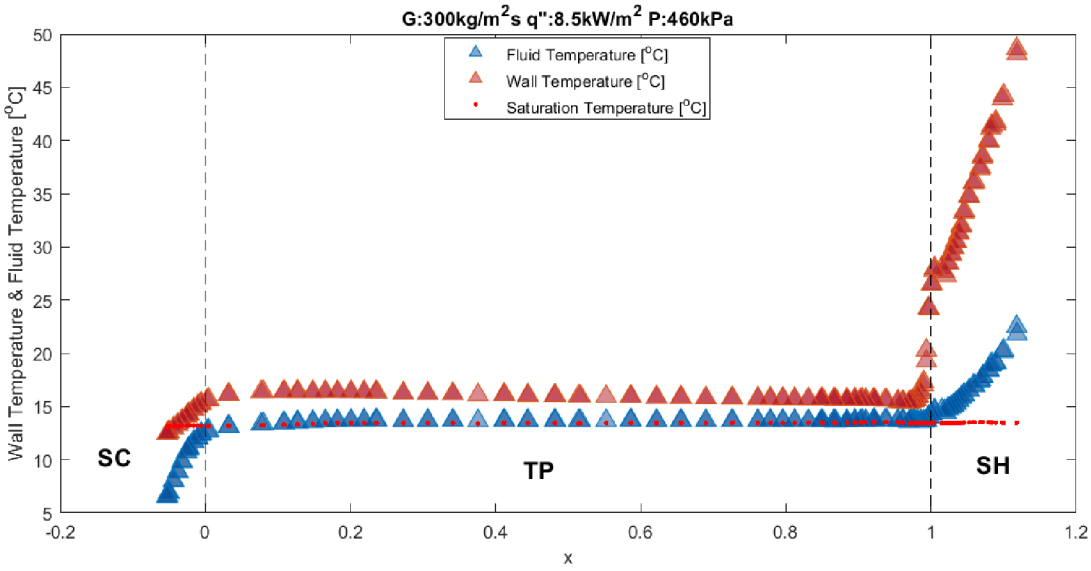

Figure 4.15: Variation in measured wall, fluid and calculated saturation temperatures as a function of vapor quality for G = 300 kg/(m² s) and q'' = 8.5 kW/m² at a constant saturation pressure of 460 kPa.

In the subcooled region, as the liquid heats up, the wall temperature rises correspondingly. The wall temperature rises to exceed the saturation temperature. In this case, the fluid temperature is less than the saturation temperature ($T_f < T_{sat}$) and the heat transfer coefficient in this region is given as:

$$h = \frac{q''}{\Delta T_{sat} + \Delta T_{sub}} . \qquad 4.4$$

This can be observed in section SC of Figure 4.12 to Figure 4.15, where the red triangles indicate wall temperature, blue triangles indicate fluid temperature and red dots indicate calculated saturated temperature from saturation pressure.

For the two-phase saturation region, as heating proceeds, a further increase in liquid temperature causes the bulk fluid to reach saturation. In this region, the flow boils through different flow boiling regimes. For the two-phase saturation region indicated as TP of Figure 4.12 to Figure 4.15, the fluid temperature is almost equal to saturation temperature ($T_f = T_{sat}$). The wall temperature increases above the fluid temperature. However, both the fluid and wall temperature are observed to be almost linearly constant with vapor quality, with a slight decrease in wall temperature at a higher vapor quality.

At high vapor quality close to one (1) or at one (1), the thin film in the annular region dries out and dry-out occurs. This is as a result of critical heat flux, which causes the wall temperature to rise abruptly to dissipate the supplied heat flux. This causes the fluid temperature to rise correspondingly. This is observed in the SH region of Figure 4.12 to Figure 4.15. The temperature profile

in the subcooled region for these conditions accurately represents the temperature profile proposed by Kandlikar [59].

4.2.6 Pressure Drop

The experimental adiabatic frictional pressure drop for the different mass fluxes and heat fluxes studied for the heat transfer coefficient results is presented in Figure 4.16 to Figure 4.19. The adiabatic frictional pressure drop is measured in the adiabatic test section, where the frictional pressure drop is equal to the pressure difference detected by the differential pressure transducer. In this experiment, gravity and acceleration are considered negligible.

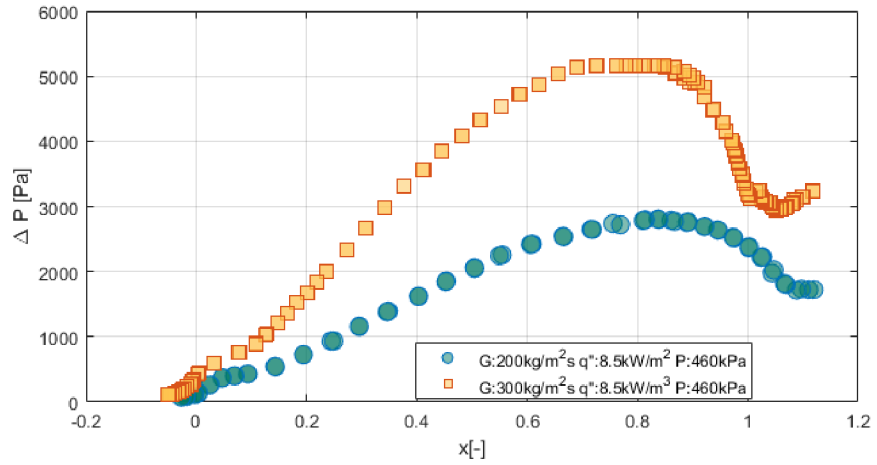

Figure 4.16: Variation in pressure drop as a function of vapor quality for a varied mass flux, fixed heat flux and constant saturation pressure.

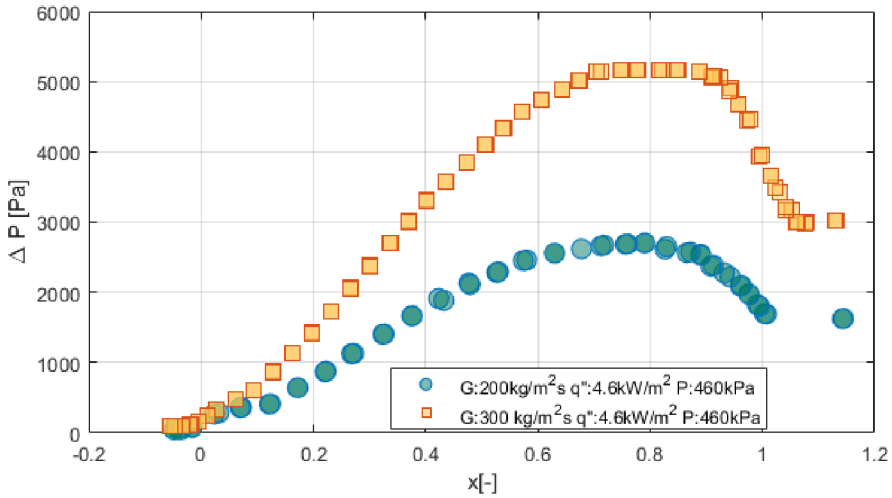

Figure 4.17: Variation in pressure drop as a function of vapor quality for a varied mass flux, fixed heat flux and constant saturation pressure.

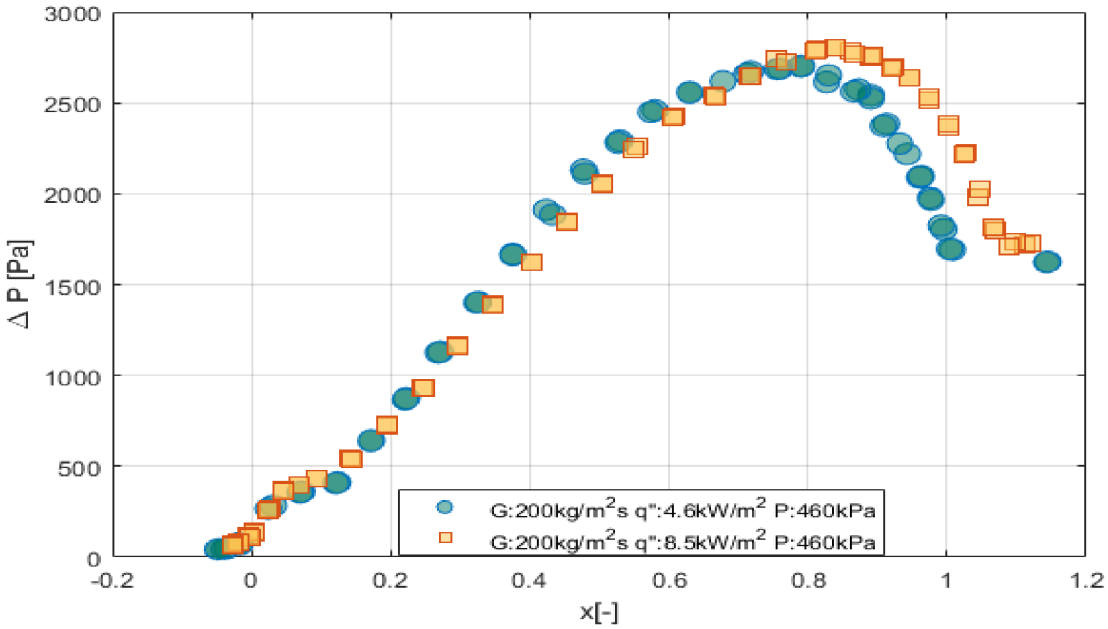

Figure 4.18: Variation in pressure drop as a function of vapor quality for a varied heat flux, fixed mass flux and constant saturation pressure.

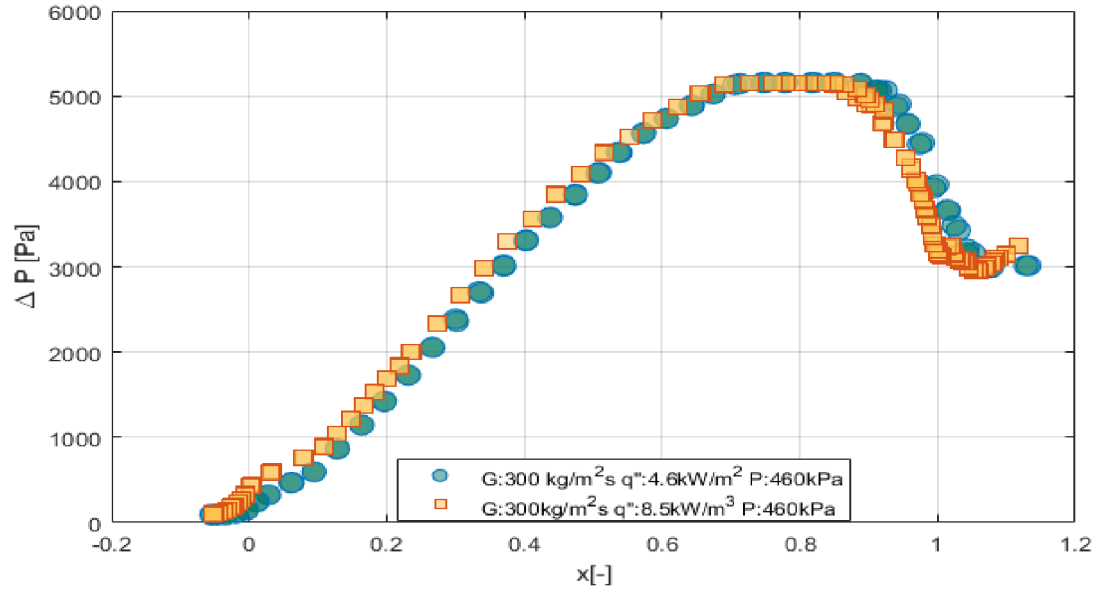

Figure 4.19: Variation in pressure drop as a function of vapor quality for a varied heat flux, fixed mass flux and constant saturation pressure.

The effect of mass flux at a fixed heat flux and constant saturation pressure on the frictional pressure drop is shown in Figure 4.16 to Figure 4.17. It can be observed that pressure drop increases with vapor quality from the subcooled region until a peak is reached. As the vapor quality increases further, the pressure drop begins to decline until it reaches the superheated region. From the superheated region, the pressure drop linearizes or increases slightly. As expected, the higher

the mass flux, the higher the pressure drop for the two-phase region. This is because of the increase in friction and drag force between the two phases in the two-phase region. This increase is not observed clearly in the subcooled region. This effect is observed because the higher the mass flux, the higher the vapor velocity and, thus, the higher pressure drop.

The effect of heat flux at fixed mass flux and constant saturation pressure on the frictional pressure drop is shown in Figure 4.18 - Figure 4.19. It can be observed that the pressure drop increases with vapor quality until it reaches a peak and then a further increase in quality causes a decrease in pressure drop until it reaches the superheated region, where the pressure drop linearizes or increases slightly. However, increasing heat flux does not produce any significant effect on the pressure drop except for low mass fluxes at high vapor qualities where the effect of heat flux is observed after the peak is reached.

4.3 Effect of Saturation Pressure on heat transfer

This section of the thesis presents an investigation the characteristics of the heat transfer coefficient at different saturation pressures. Flow patterns were predicted with a well-known flow pattern map from Wojtan et al. [111] for the experimental conditions studied. The experimental results were compared with some popular flow boiling correlations developed based on different theories.

4.3.1 Flow Boiling Heat Transfer Coefficient

Figure 4.20 shows the effect of saturation pressure on the heat transfer coefficient for a low mass flux of 150 kg/(m^2s) and a heat flux of 8.26 kW/m^2. From the results, it can be seen that the heat transfer coefficient increases with increasing saturation pressure. The effect of saturation pressure on the heat transfer coefficient is more pronounced in a low vapor quality region of around 0.4 and below. However, for the characteristics of the heat transfer coefficient with increasing vapor quality, the heat transfer coefficient decreases slightly in the low-vapor quality region up to around 0.3 before it increases steadily and almost collapses into a single plot in the high vapor quality region until dryout occurs. Before dryout incipience, the heat transfer coefficient rises sharply to a maximum before deteriorating in the dryout region. Because the heat transfer coefficient highly depends on saturation pressure in the low vapor quality region, nucleate boiling heat transfer thus dominates the heat transfer in this region. As vapor quality increases, the dominance of nucleate boiling is suppressed, leading to the reduced effect of saturation pressure. This characteristic of the heat transfer coefficient is observed because increasing saturation pressure decreases

surface tension. This then leads to an increase in the number of active sites for nucleation to occur. The frequency of bubble generation thus increases with many bubbles generated in smaller sizes on the heating walls of the tube. Additionally, increasing saturation pressure has an increasing effect on vapor density and a decreasing effect on liquid density which does not favor convective heat transfer. However, as vapor quality increases, these effects are suppressed, liquid film thickness reduces, and nucleate boiling dominance is suppressed.

Figure 4.21 shows the effect of saturation pressure on the heat transfer coefficient for a low mass flux of 150 kg/(m^2s) and an increased heat flux of 23.3 kW/m^2. With an increased heat flux, it can be seen that the heat transfer coefficient increases with increasing saturation pressure over a wide range of vapor quality until dryout is reached. The trend of the heat transfer coefficient is fairly constant with increasing vapor quality. At an increased heat flux, the heat transfer coefficient is affected by saturation pressure even at high vapor qualities with minimal suppression until dryout incipience is reached. Both saturation pressure and heat flux are good promoters of nucleate boiling due to their ability to enhance bubble nucleation, growth and distribution over the walls of the tube. The dependence of the heat transfer coefficient on saturation pressure and heat flux even over a wide range of vapor quality indicates that the dominant mechanism for heat transfer, in this case, is nucleate boiling. At a vapor quality of around 0.8, dryout begins to occur with a monotonic drop in the heat transfer coefficient without a sudden rise as in the case of Figure 4.20.

Figure 4.22 shows the effect of saturation pressure on the heat transfer coefficient for an increased mass flux of 300 kg/(m^2s) and a low heat flux condition of 8.26 kW/m^2. For this condition, it can be seen that the heat transfer coefficient is not significantly affected by the increasing saturation pressure except for low vapor quality ($x < 0.1$) where there is a slight effect. However, beyond this region ($x > 0.1$), the heat transfer coefficient increases with vapor quality until dryout is reached. In this case, the heat transfer is dominated by convective boiling except for low vapor quality ($x < 0.1$) where nucleate boiling dominates the heat transfer because of the independence of the heat transfer coefficient on vapor quality. For convective boiling, an increase in mass flux increases the flow velocity and by increasing the vapor quality, the vapor phase of the two-phase flow plays a significant role in accelerating the liquid flow close to the wall of the tube and a reduced effect of the liquid phase on the heat transfer coefficient. So, in as much as increasing saturation pressure increases the vapor density and decreases the liquid density which is promoters of nucleate boiling, an increased mass flux with an increasing vapor quality is sufficient to accelerate the flow velocity, decrease the liquid film thickness near the tube wall, and thus promote convective flow boiling over nucleation. According to [86], since this convective boiling mechanism is similar to the mechanism responsible for controlling the heat transfer during single-phase flow, the same

mechanism can be assumed to be controlling heat transfer during convective boiling. Contrary to many assumptions, the mechanism responsible for controlling heat transfer in a single phase is equivalent to the mechanism responsible for controlling heat transfer during convective boiling and the dominant thermal resistance is concentrated in the conductive sublayer layer.

Figure 4.23 shows the effect of saturation pressure on the heat transfer coefficient for a mass flux of 300 kg/(m^{2}s) and increased heat flux condition of 23.3 kW/m^2. It can be observed that for this condition, there is no significant effect of saturation pressure on the heat transfer coefficient except for saturation pressure of 660 kPa which shows a slight increase in the heat transfer coefficient compared to the rest. However, the trend of the heat transfer coefficient with respect to increasing vapor quality is fairly constant until dryout is reached. This indicates the dominance of nucleate boiling in controlling the heat transfer for this condition studied where bubble generation near the walls of the tube promotes the effect of nucleation.

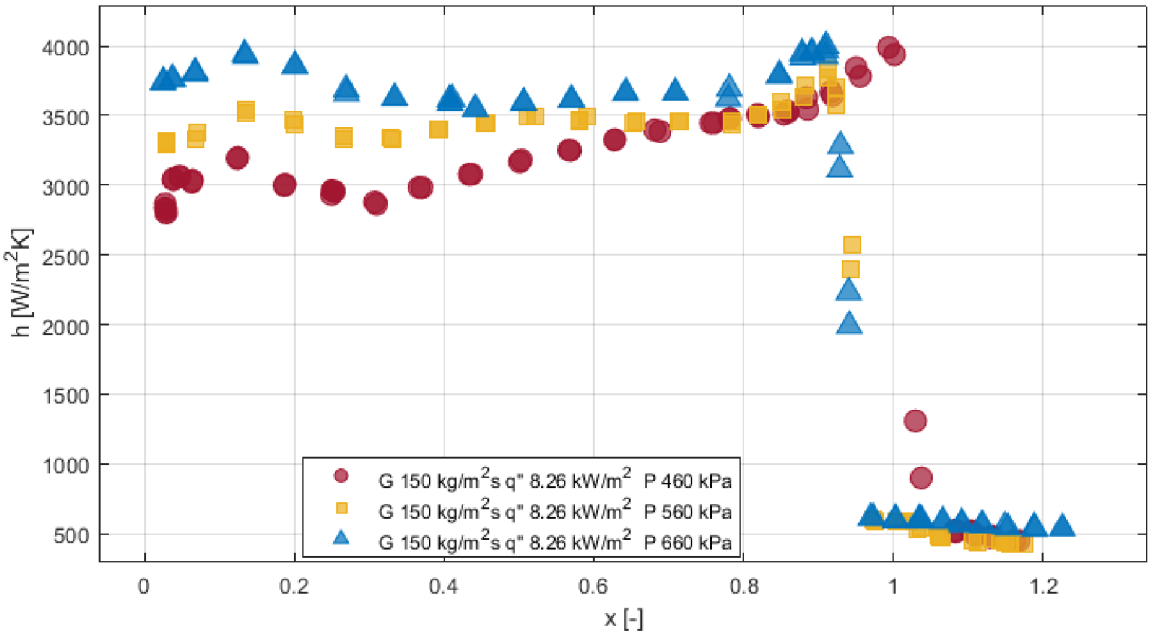

Figure 4.20: Effect of saturation pressure on heat transfer coefficient for mass flux 150 kg/(m^{2}s) and heat flux of 8.26 kW/m^2.

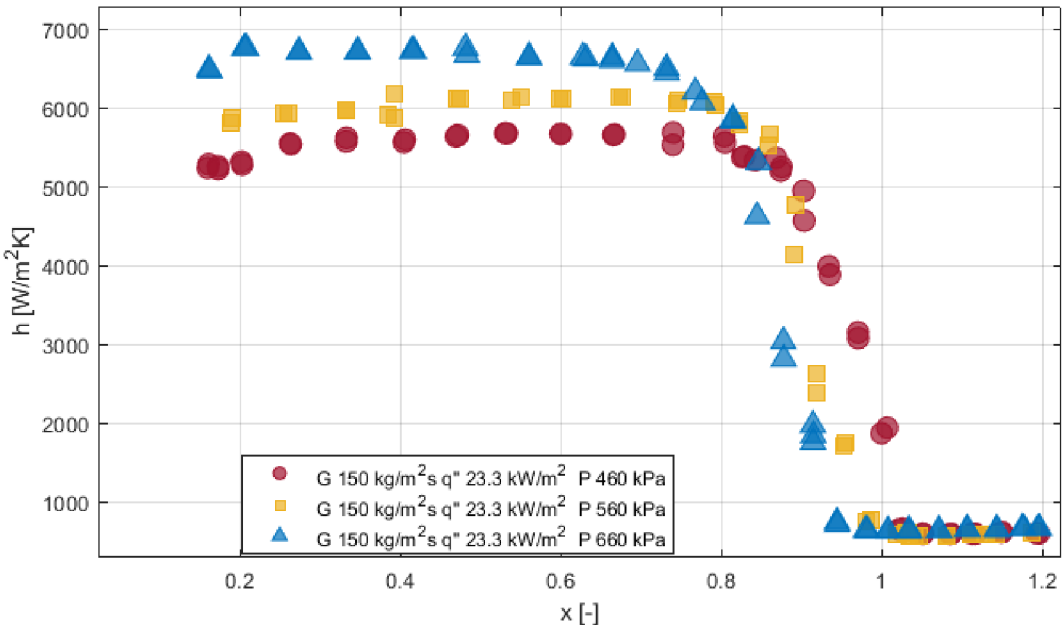

Figure 4.21: Effect of saturation pressure on heat transfer coefficient for mass flux of 150 kg/(m² s) and heat flux of 23.3 kW/m².

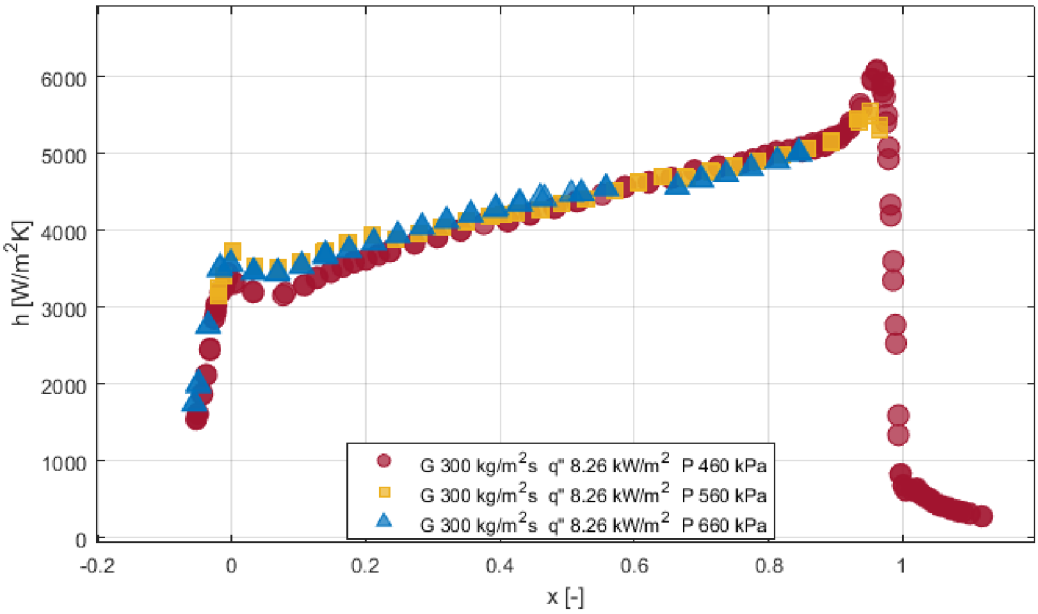

Figure 4.22: Effect of saturation pressure on heat transfer coefficient for mass flux of 300 kg/(m² s) and heat flux of 8.26 kW/m².

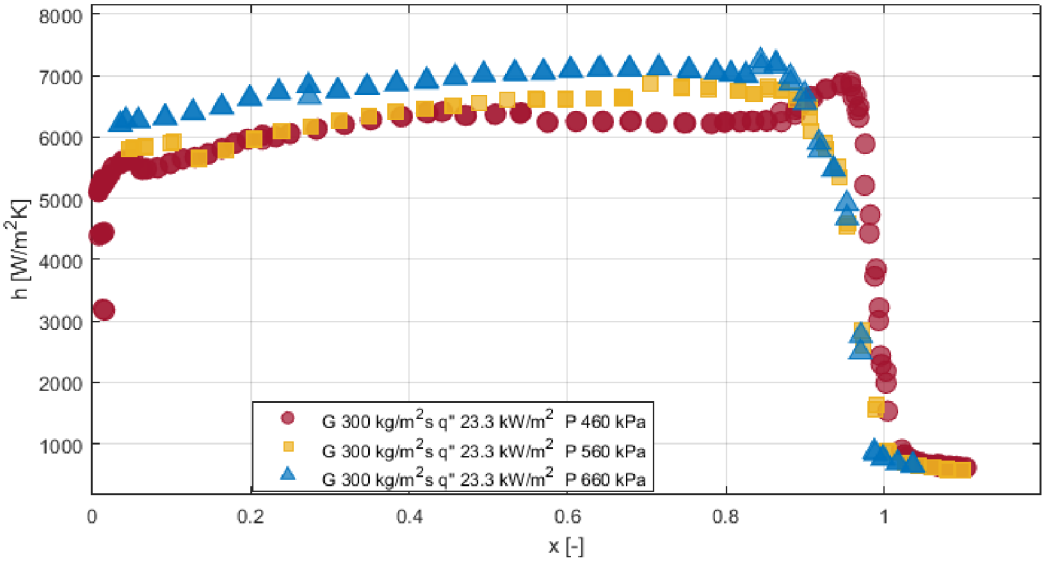

Figure 4.23: Effect of saturation pressure on heat transfer coefficient for mass flux of 300 kg/(m² s) and heat flux of 23.3 kW/m².

4.3.2 Flow Patterns

Next, Flow patterns for each experimental condition investigated were predicted with a well-known predictive flow pattern map from Wojtan et al. [111] shown in Figure 4.24a–l. Wojtan flow pattern map is an updated version of Kattan et al's flow pattern map with an inclusion of the effect of heat flux on the transition from dryout to mist flow.

Figure 4.24a–f shows the flow patterns for an increasing saturation pressure at G = 150 kg/(m² s), q"=8.26 kW/m² (Figure 4.24a–c), and q" =23.3 kW/m² (Figure 4.24d–f) as predicted by a well-known flow pattern map from Wojtan et al. The flow patterns predicted for these experimental conditions are a mixture of slug and stratified wavy, purely stratified wavy, and dryout. Increasing saturation pressure increases the vapor quality at which the flow patterns transition from mixed slug and stratified to purely stratified wavy. At saturation pressures of 460 kPa, 560 kPa, and 660 kPa, the transitions occur at vapor quality of 0.345, 0.370, and 0.395, respectively. These flow patterns may be predicted because of insufficient refrigerant flow rate for the low mass flux of 150 kg/(m² s).

Figure 4.24g–l shows the flow patterns for an increasing saturation pressure of 460 kPa, 560 kPa, and 660 kPa at an increased mass flux of 300 kg/(m² s), heat flux of 8.26 kW/m² (Figure 4.24e–g), and 23.3 kw/m² (Figure 4.24h–l) as predicted by the flow pattern map from Wojtan et al. For these conditions, the flow patterns predicted are slug, intermittent, annular, dryout, and mist flow. Increasing saturation pressure increases the vapor quality at which the flow pattern transitions

from intermittent flow to annular flow. In addition, at saturation pressures of 460 kPa, 560 kPa, and 660 kPa, the transitions occur at vapor qualities of 0.345, 0.370, and 0.395, respectively. These flow patterns are observed because of sufficient mass flux for increasing the flow rate during flow boiling.

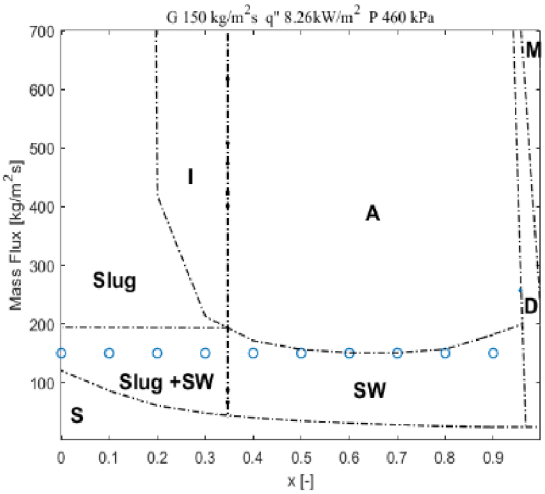

(a)

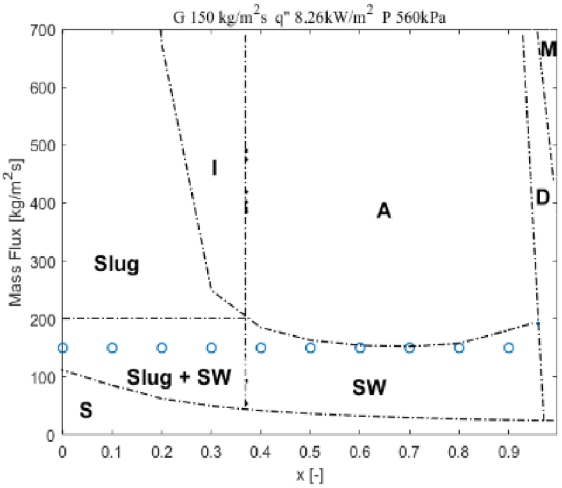

(b)

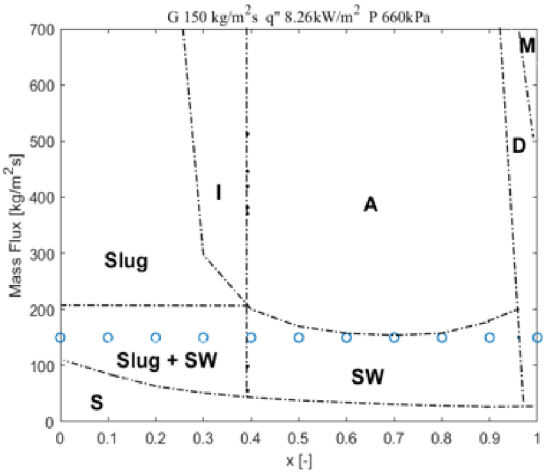

(c)

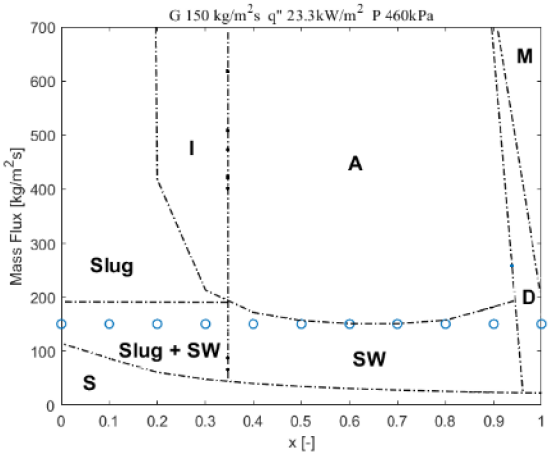

(d)

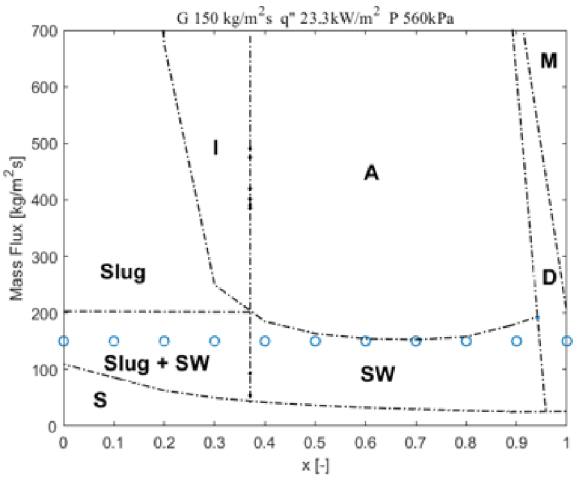
G 150 kg/m²s q" 23.3kW/m² P 560kPa
Mass Flux [kg/m²s]
x [-]
I
A
M
D
Slug
Slug + SW
SW
S

(e)

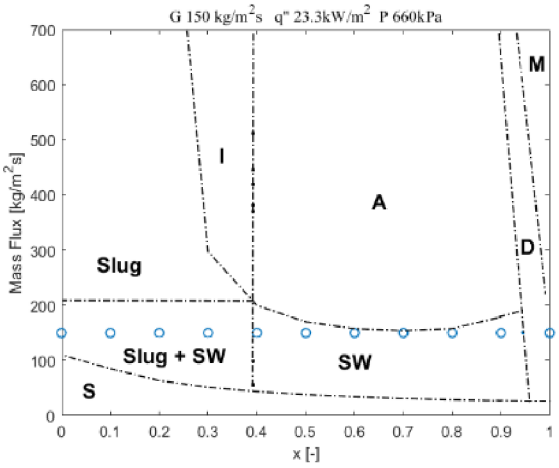
G 150 kg/m²s q" 23.3kW/m² P 660kPa
Mass Flux [kg/m²s]
x [-]
I
A
M
D
Slug
Slug + SW
SW
S

(f)

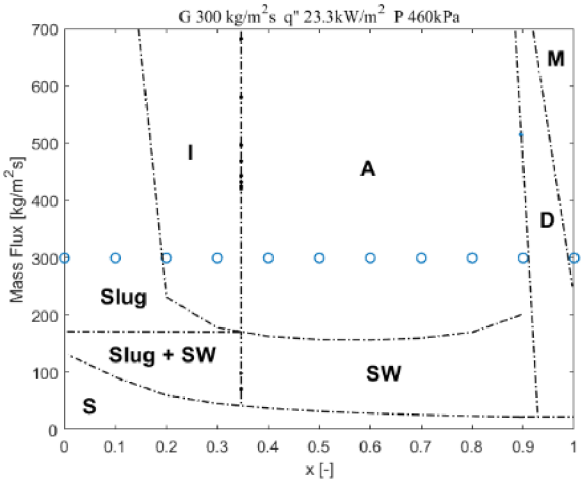
G 300 kg/m²s q" 23.3kW/m² P 460kPa
Mass Flux [kg/m²s]
x [-]
I
A
M
D
Slug
Slug + SW
SW
S

(g)

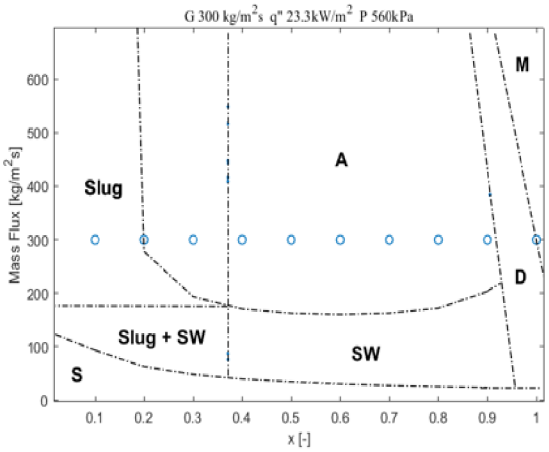
G 300 kg/m²s q" 23.3kW/m² P 560kPa
Mass Flux [kg/m²s]
x [-]
A
M
D
Slug
Slug + SW
SW
S

(h)

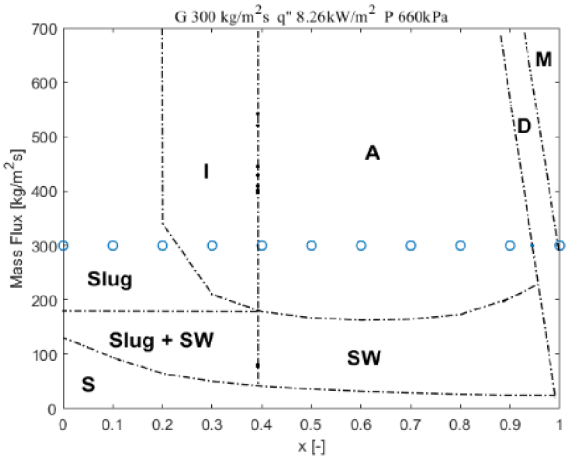
G 300 kg/m²s q" 8.26kW/m² P 660kPa
Mass Flux [kg/m²s]
x [-]
I
A
M
D
Slug
Slug + SW
SW
S

(i)

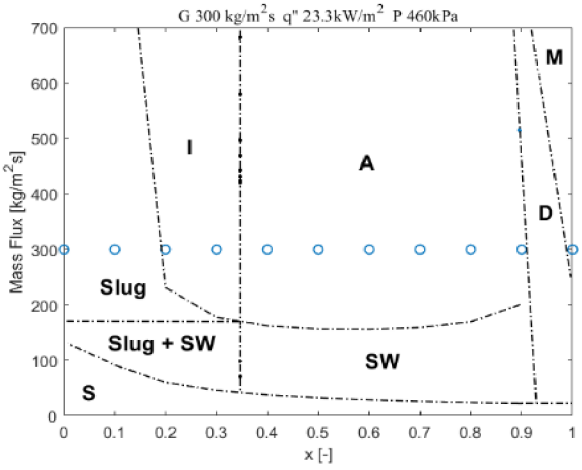
G 300 kg/m²s q" 23.3kW/m² P 460kPa
Mass Flux [kg/m²s]
x [-]
I
A
M
D
Slug
Slug + SW
SW
S

(j)

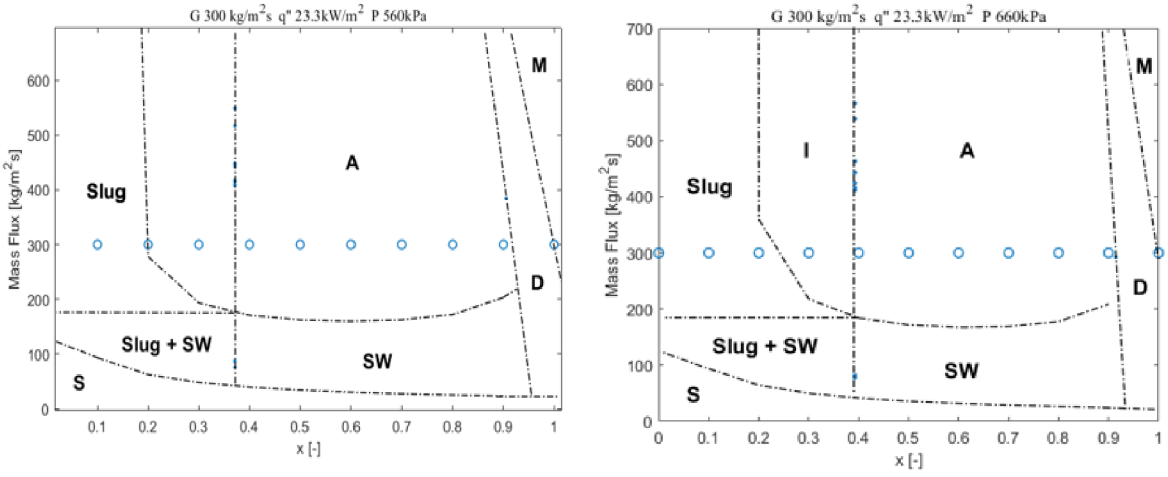

Figure 4.24: Flow pattern predictions by Wojtan et al. for increasing saturation pressures from 460 kPa to 660 kPa at G = 150 kg/(m² s), q" = 8.26 kW/m² **(a-c)**, G = 150 kg/(m² s), q" = 23.3 kW/m² **(d-f)**, G = 300 kg/(m² s), q" = 8.26 kW/m² **(g-i)** and G = 300 kg/(m² s), q" = 23.3 kW/m² **(j-l)**.

For the working conditions of mass fluxes G of 150 and 300 kg/(m² s) at heat flux q" of 8.26 kW/m² and saturation pressure $P_{sat}$of 560 kPa, flow patterns for increasing vapor quality (x) were recorded using a high-speed camera at 2000 fps. The goal was to compare these findings with flow patterns predicted by Wojtan et al. for similar conditions. For mass flux G of 150 kg/(m² s), heat flux q" = 8.26 kW/m² and saturation pressure P_{sat} = 560 kPa, the recorded flow patterns were stratified at vapor quality x of 0.15, stratified wavy at vapor quality x of 0.25, hybrid stratified wavy/annular at vapor quality x of 0.7 and dryout at vapor quality x of 0.9 as presented in Figure 4.25 below. For this working condition, the flow patterns predicted by Wojtan et al's flow pattern map were mixture of slug and stratified wavy, hybrid stratified wavy/annular and dryout. In the case of mass flux of 300 kg/(m² s) heat flux q" of 8.26 kW/m² and saturation pressure P_{sat} of 560 kPa, the observed flow patterns recorded were slug at vapor quality of 0.2 (x), intermittent at vapor quality x of 0.4, annular at vapor quality x of 0.7 and dryout at vapor quality x of 0.9 as presented in Figure 4.26. For this, Wojtan et al's flow pattern map predicted slug, intermittent, annular and dryout. Generally, based on the comparison, it is fair to conclude that Wojtan et al's flow pattern map is capable of predicting flow patterns for the conditions investigated.

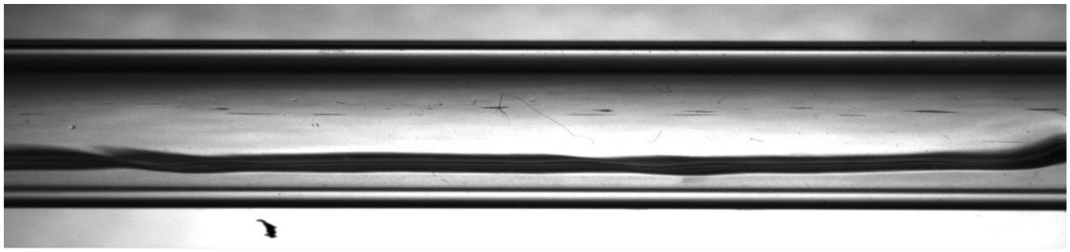

a) G = 150 kg/(m² s), q" = 8.26 kW/m², P_{sat} =560 kPa, x = 0.15 (Stratified)

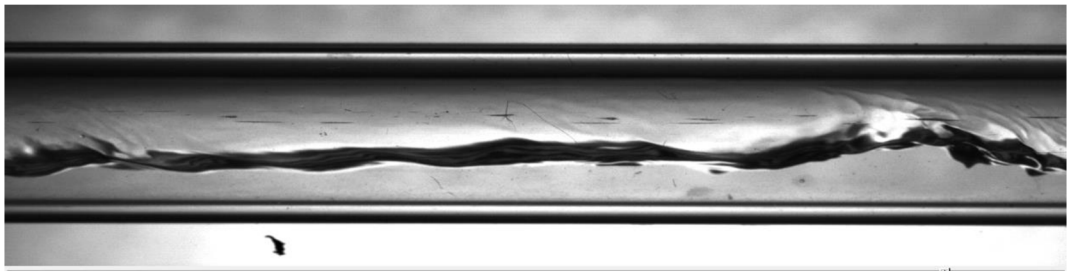

b) G = 150 kg/(m² s), q"=8.26 kW/m², P_{sat} =560 kPa, x = 0.25 (Stratified wavy)

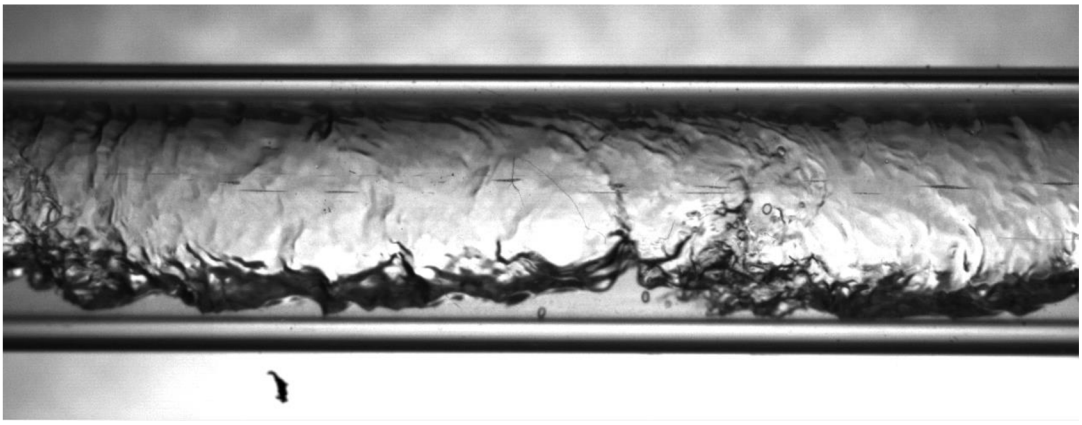

c) G = 150 kg/(m² s), q" = 8.26 kW/m², P_{sat} = 560 kPa, x = 0.7 (Hybrid stratified wavy/Annular)

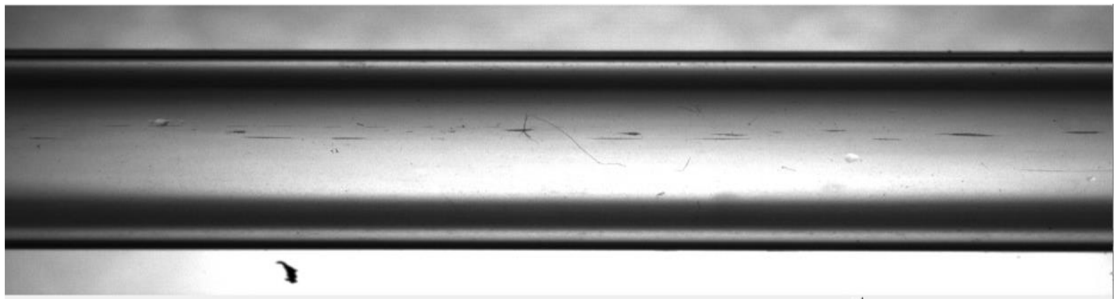

d) G = 150 kg/(m² s), q" = 8.26 kW/m², P_{sat} = 560 kPa, x = 0.9 (Dryout)

Figure 4.25: Flow pattern evolution with increasing vapor quality for G = 150 kg/(m² s), q" = 8.26 kW/m², P_{sat} = 560 kPa

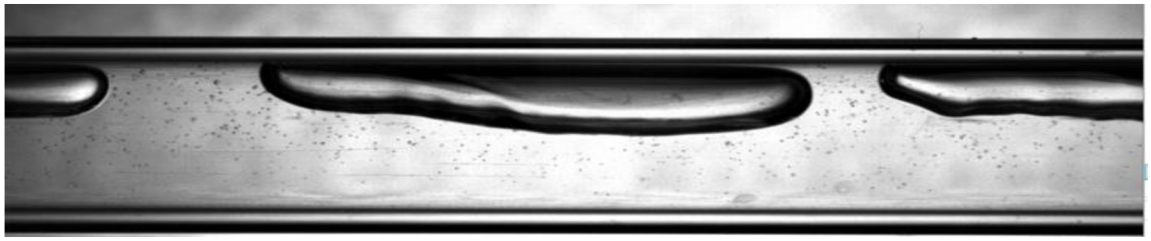

G = 300 kg/(m^2 s), q" = 8.26 kW/m^2, P_{sat} = 560 kPa, x = 0.2 (Slug)

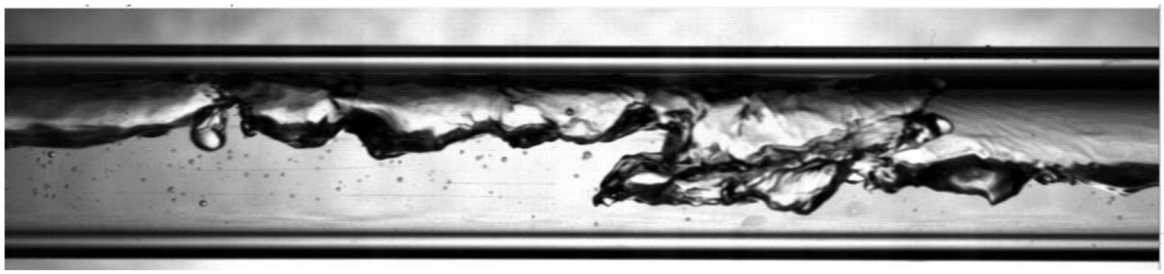

G = 300 kg/(m^2 s), q" = 8.26 kW/m^2, P_{sat} = 560 kPa, x = 0.4 (intermittent)

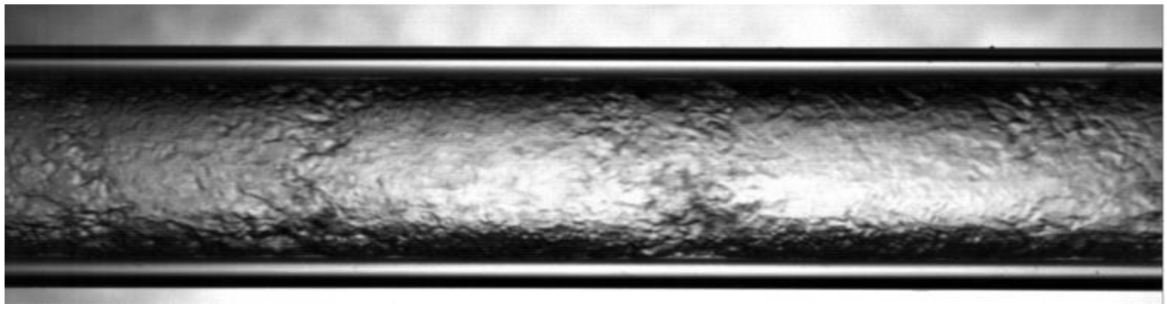

G = 300 kg/(m^2 s), q" = 8.26 kW/m^2, P_{sat} = 560 kPa, x = 0.7 (Annular)

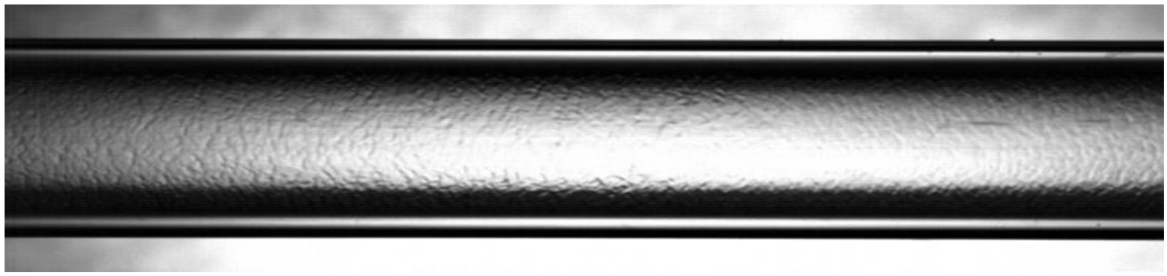

G = 300 kg/(m^2 s), q" = 8.26 kW/m^2, P_{sat} = 560 kPa, x = 0.15 (Dryout)

Figure 4.26: Flow pattern evolution with increasing vapor quality for G = 300 kg/(m^2 s), q" = 8.26kW/m^2, P_{sat} = 560 kPa

4.3.3 Frictional Pressure Drop

The total pressure drop of a fluid is as a result of changes in kinetic energy, potential energy, and friction effect. For this reason, the pressure drop (ΔP) is the summation of the static pressure drop ΔP_s due to elevation head, momentum pressure drop (ΔP_m) due to acceleration and frictional pressure drop (ΔP_f) due to the effect of frictional forces given as:

$$\Delta P = \Delta P_s + \Delta P_m + \Delta P_f \,. \qquad 4.5$$

Because the tube is horizontal and the flow has minimal flashing with little heat losses, the static and momentum pressure drop were assumed to be negligible. The total pressure drop is thus the adiabatic frictional pressure drop that was recorded in the adiabatic test section for the same operating conditions the heat transfer coefficient was recorded using a differential pressure transducer.

Figure 4.27a–d shows the effect of saturation pressure on adiabatic frictional pressure drop. It can be observed that, for a constant mass flux and heat flux condition, the frictional pressure drop increases with vapor quality until a maximum is reached and then it deteriorates up to a vapor quality of 1 where it tends to linearize or increase slightly. With respect to saturation pressure, frictional pressure drop decreases with increasing saturation pressure. This is because, when saturation pressure increases, vapor density increases. This then decreases the vapor velocity and thus results in the observed trend of decreasing pressure drop with increasing saturation pressure.

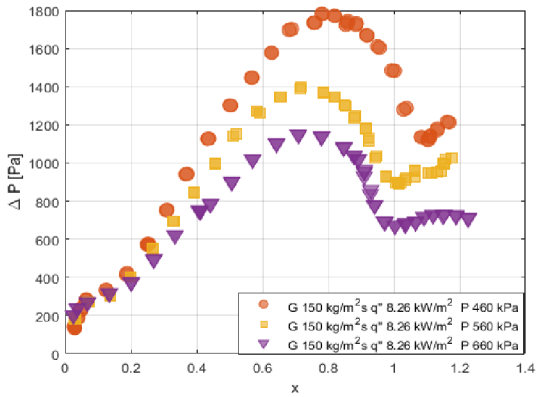

(**a**)

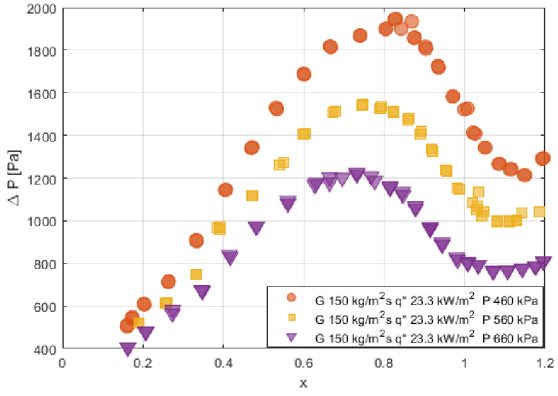

(**b**)

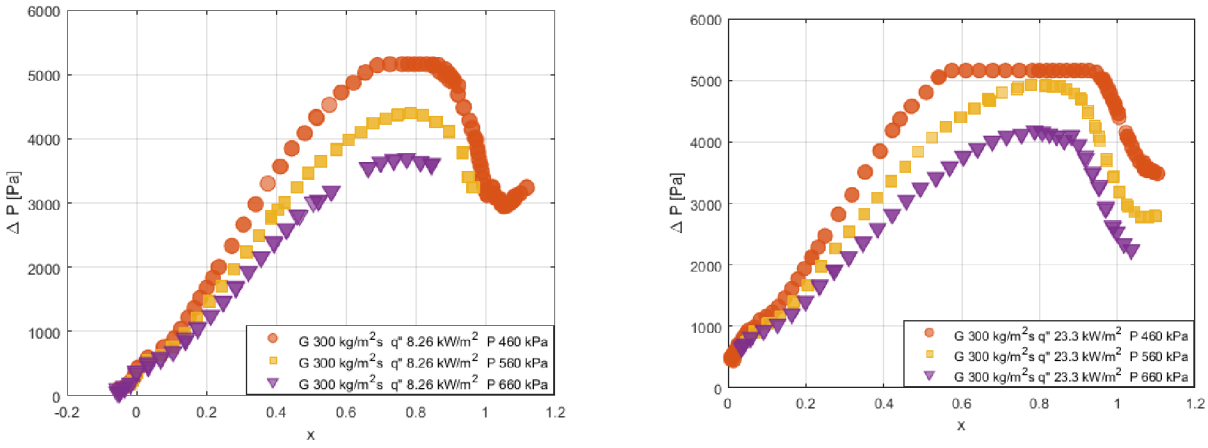

(**c**) (**d**)

Figure 4.27: Effect of saturation pressure on adiabatic frictional pressure drop at **(a)** G = 150 kg/(m² s), q" = 8.26 kW/m², **(b)** G = 150 kg/(m² s) q" = 23.3 kW/m², **(c)** G = 300 kg/(m² s), q" = 8.26 kW/m² and **(d)** G = 300 kg/(m² s), q" = 23.3 kW/m²

4.3.4 Comparison of Experimental Results with Correlations of Heat Transfer Coefficient Developed Based on Different Theories

Statistical analysis of the study on the effect of saturation pressure was performed by comparing experimental results obtained with different flow boiling heat transfer correlations and models developed based on different theories. Five different theoretical approaches upon which the selected models were formulated were considered for the statistical analysis. These are pool boiling type, superposition type, enhancement approach, asymptotic approach, and largest mechanism type. For pool boiling, we considered models by Cooper and Tran et al. [20], [112], for the superposition model, we considered Bertsch et al. [113], for the enhancement type of model, Warrier et al.'s model [114]was considered, for asymptotic, Wattelet et al.'s model [115] and the model of Liu and Winterton [116] were considered. Kandlikar's model [117] was considered for largest mechanism type of model.

The results from the comparison of the experimental data with the predicted models are summarized in Table 4.1 – 4.4 below where MRE is the mean relative error and MAE is the mean absolute error calculated by:

$$MRE = \frac{1}{N}\sum_{i=1}^{N}\left(\frac{h_{pred,i}-h_{exp,i}}{h_{exp,i}}\right) \quad 4.6$$

$$MAE = \frac{1}{N}\sum_{i=1}^{N}\left(\frac{|h_{pred,i}-h_{exp,i}|}{h_{exp,i}}\right) \quad 4.7$$

Here, h_{pred} and h_{exp} are the predicted and experimental heat transfer coefficient, respectively. N is the number of data points collected.

Figure 4.28a–l depicts the graphical representation of the comparison between each experimental result measured and the calculated heat transfer coefficient developed based on different theoretical assumptions at the different saturation conditions investigated in this study.

For saturation pressure of 460 kPa, the models that predicted the experimental data with an MAE of less than 30 % were Cooper [20], followed by Wattalet et al.[115] and Liu and Winterton [116] with MAE of 8.48 %, 9.0 %, and 16.75 %, respectively.

For saturation pressure of 560 kPa, the models of Wattelet et al. [115], Cooper [20] and Liu, and Winterton [20] best predicted the experimental data within a range of 30 % with a low MAE of 4.63 %, 5.25 %, and 24.85 %, respectively.

The models of Wattelet et al. [115] and Cooper [20] best predicted the experimental conditions at 660 kPa with a low MAE of 6.28 % and 9.85 %, respectively.

Overall, Cooper's model [20] and Wattelet et al.'s model [115] were the best predictors of the experimental data. Cooper's model [20] was developed based on pool boiling conditions where the effect of vapor quality was not considered and nucleate boiling dominated the heat transfer. This thus justifies why the dominant mechanism responsible for controlling heat transfer for most of the conditions was nucleate boiling. Wattelet et al.'s model [115] is also an asymptotic model that considers the summed effects of both nucleate boiling and convective boiling heat transfer. In most of these conditions, nucleate boiling dominated, and thus its ability to predict most of the data with low MAE.

Figure 4.29a–l shows the trend of how each predictive model is able to capture the experimental trend compared with experimental data over the entire range of vapor qualities. Generally, none of the models selected are able to satisfactorily trace the heat transfer coefficient over the entire range of vapor quality.

For cases where convective boiling dominated the heat transfer as discussed in Section 3 where the heat transfer coefficient increases with vapor quality, (such as in Figure 4.22), the models of Berstch et al. [32] and Wattelet et al. [115] are able to predict the trend of heat transfer coefficient over a wide range of vapor quality up to dryout.

For nucleate boiling-dominated heat transfer where the heat transfer coefficient did not respond significantly with vapor quality such as in

Figure 4.20, Figure 4.21 and Figure 4.23, models of Cooper [20], Wattelet et al. [115], Tran et al. [31], and Berstch et al. [32] are able to capture the trend of heat transfer over a wide range of vapor quality up to dryout. Although these models are able to capture the trend of the heat transfer coefficient with vapor quality until dryout is reached, they either over-predict or under-predict the experimental data except Cooper's model [20], which is able to both capture the trend of the heat transfer coefficient and accurately predict the experimental data for conditions of G = 150 kg/(m^{2}s), q" = 23.3 kW/m^2, P_{sat} = 460 kPa, and 560 kPa before dryout incipience.

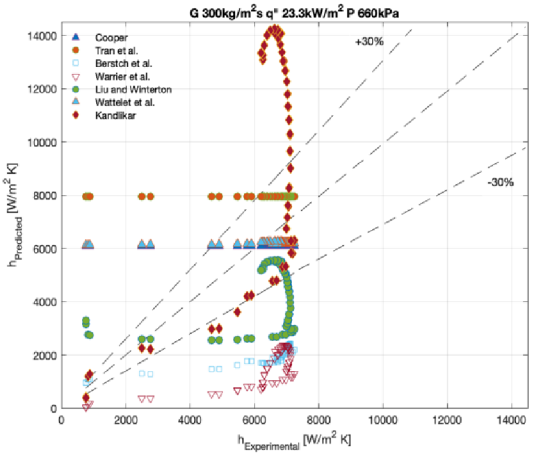

(**a**)

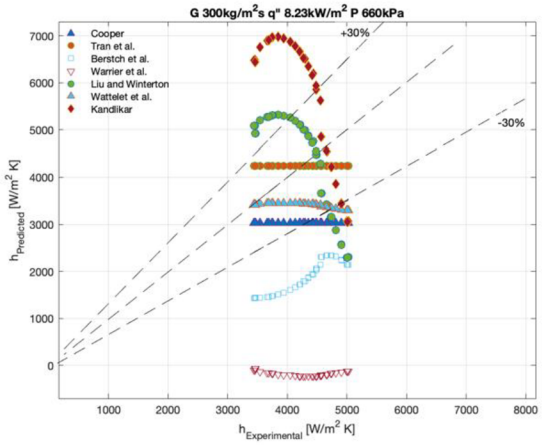

(**b**)

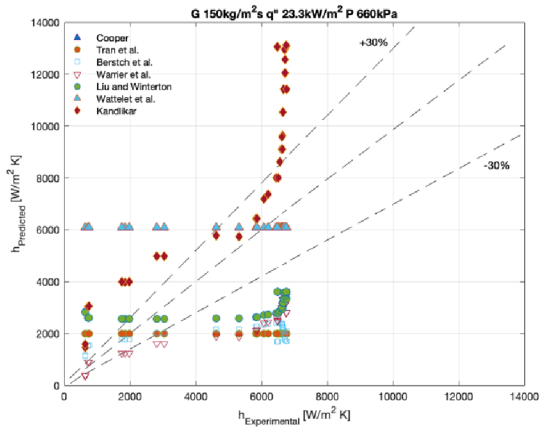

(**c**)

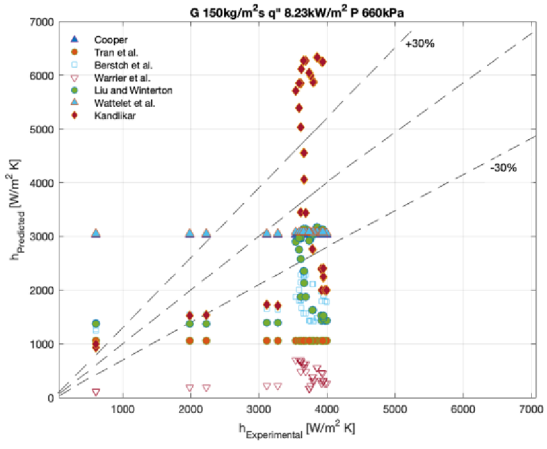

(**d**)

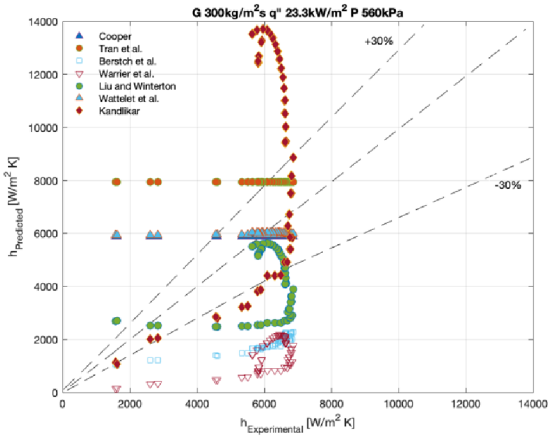
G 300kg/m²s q" 23.3kW/m² P 560kPa
Cooper
Tran et al.
Berstch et al.
Warrier et al.
Liu and Winterton
Wattelet et al.
Kandlikar
+30%
-30%
h_Predicted [W/m² K]
h_Experimental [W/m² K]

(e)

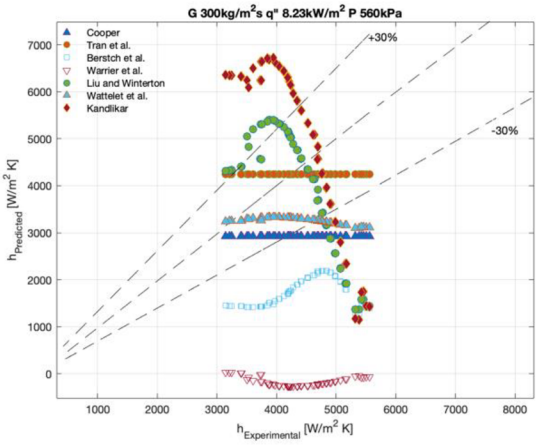
G 300kg/m²s q" 8.23kW/m² P 560kPa
Cooper
Tran et al.
Berstch et al.
Warrier et al.
Liu and Winterton
Wattelet et al.
Kandlikar
+30%
-30%
h_Predicted [W/m² K]
h_Experimental [W/m² K]

(f)

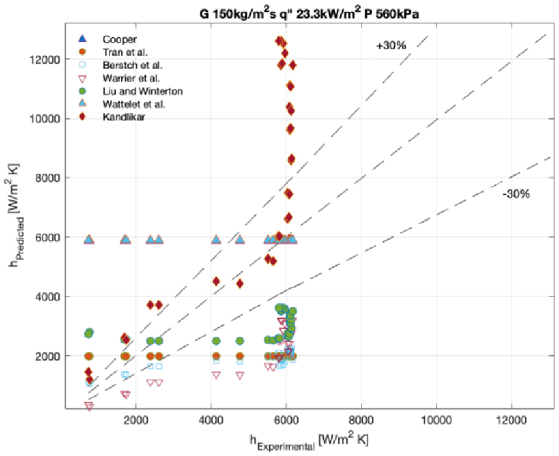
G 150kg/m²s q" 23.3kW/m² P 560kPa
Cooper
Tran et al.
Berstch et al.
Warrier et al.
Liu and Winterton
Wattelet et al.
Kandlikar
+30%
-30%
h_Predicted [W/m² K]
h_Experimental [W/m² K]

(g)

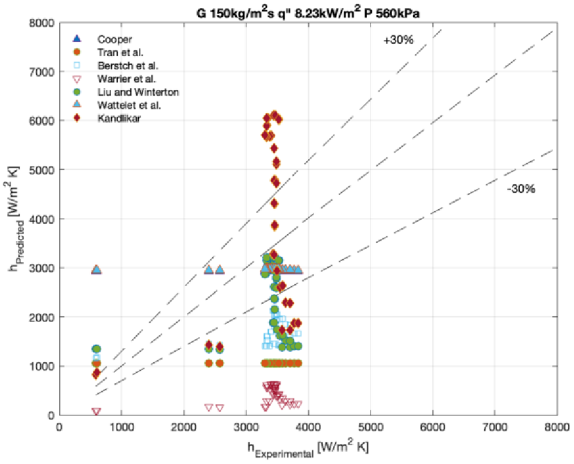
G 150kg/m²s q" 8.23kW/m² P 560kPa
Cooper
Tran et al.
Berstch et al.
Warrier et al.
Liu and Winterton
Wattelet et al.
Kandlikar
+30%
-30%
h_Predicted [W/m² K]
h_Experimental [W/m² K]

(h)

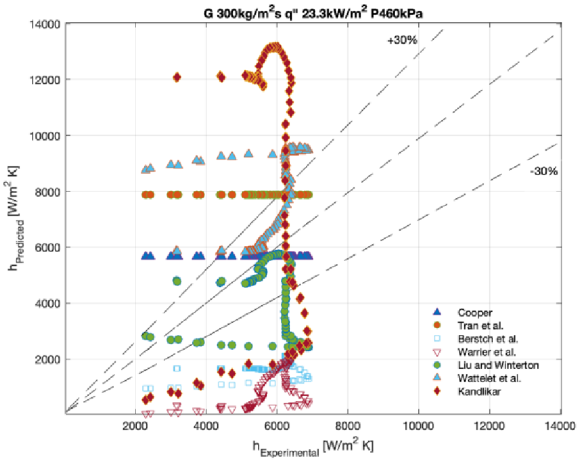
G 300kg/m²s q" 23.3kW/m² P460kPa
Cooper
Tran et al.
Berstch et al.
Warrier et al.
Liu and Winterton
Wattelet et al.
Kandlikar
+30%
-30%
h_Predicted [W/m² K]
h_Experimental [W/m² K]

(i)

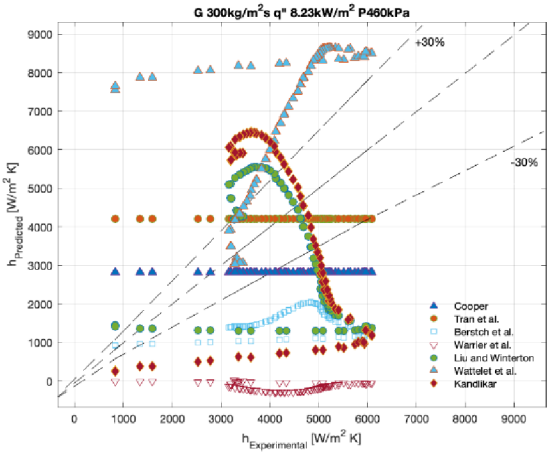
G 300kg/m²s q" 8.23kW/m² P460kPa
Cooper
Tran et al.
Berstch et al.
Warrier et al.
Liu and Winterton
Wattelet et al.
Kandlikar
+30%
-30%
h_Predicted [W/m² K]
h_Experimental [W/m² K]

(j)

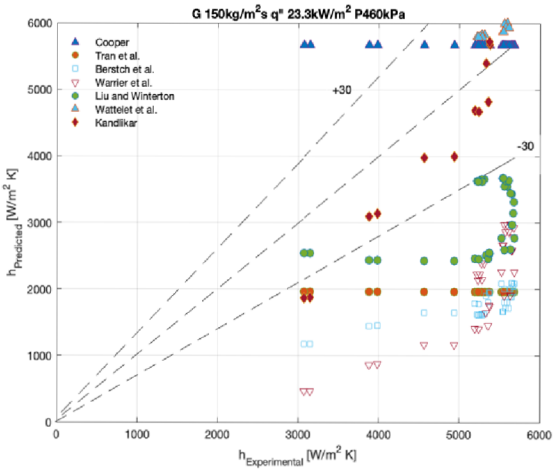

(**k**)

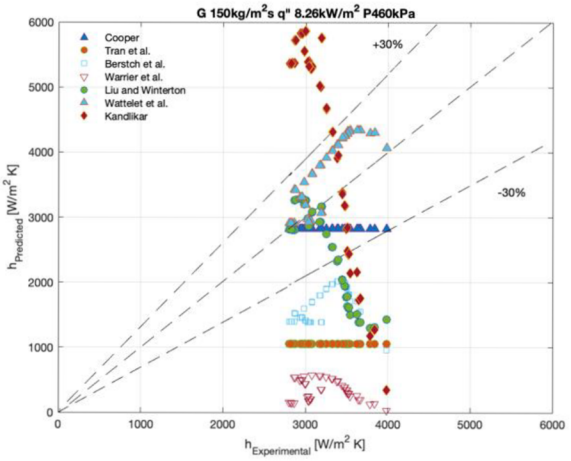

(**l**)

Figure 4.28: (a–l) Comparison between each experimental result measured at conditions of G = 150 - 300 kg/(m² s), q'' = 8.26 - 23.3 kW/m², P_{sat} = 460 - 660 kPa and the calculated heat transfer coefficient developed based on different theoretical assumptions by Cooper [20], Tran et al. [31], Berstch et al. [32], Warrier et al. [33], Wattelet et al. [115], Liu and Winterton [116] and Kandlikar [117]

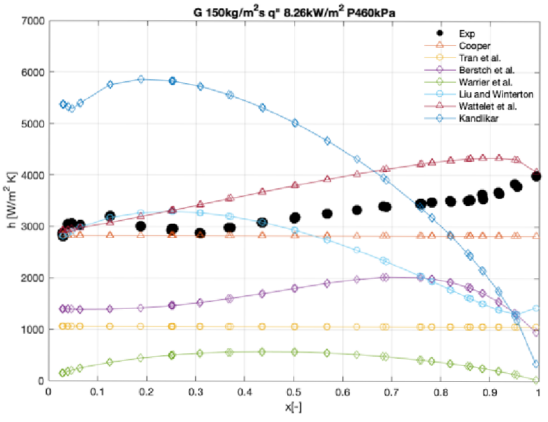

(**a**)

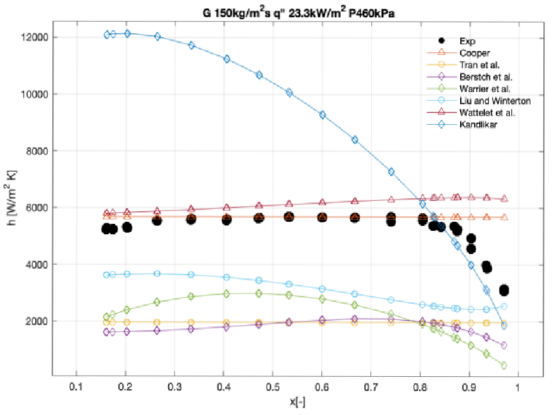

(**b**)

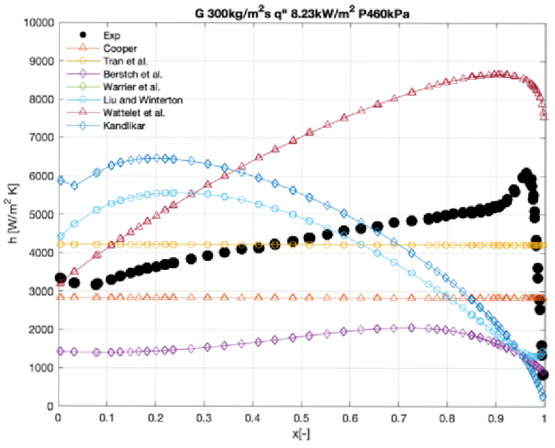

(**c**)

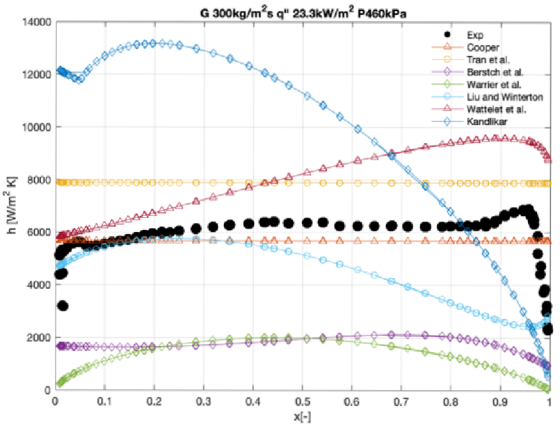

(**d**)

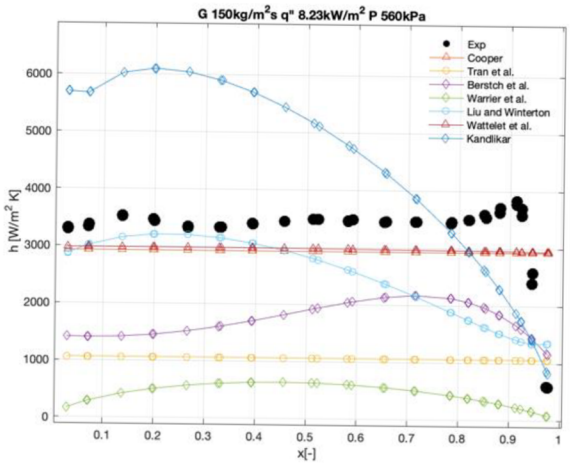
G 150kg/m²s q" 8.23kW/m² P 560kPa
Exp
Cooper
Tran et al.
Berstch et al.
Warrier et al.
Liu and Winterton
Wattelet et al.
Kandlikar
h [W/m² K]
x[-]

(e)

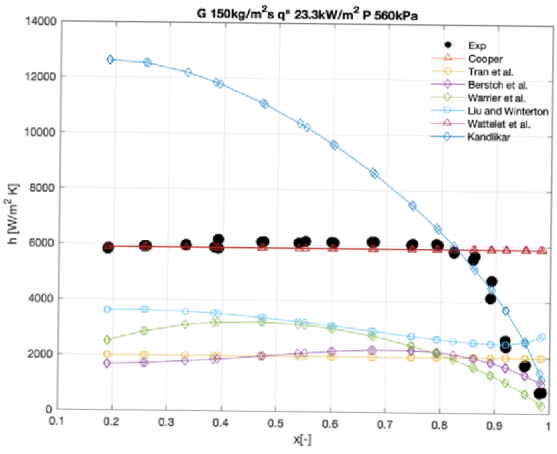
G 150kg/m²s q" 23.3kW/m² P 560kPa
Exp
Cooper
Tran et al.
Berstch et al.
Warrier et al.
Liu and Winterton
Wattelet et al.
Kandlikar
h [W/m² K]
x[-]

(f)

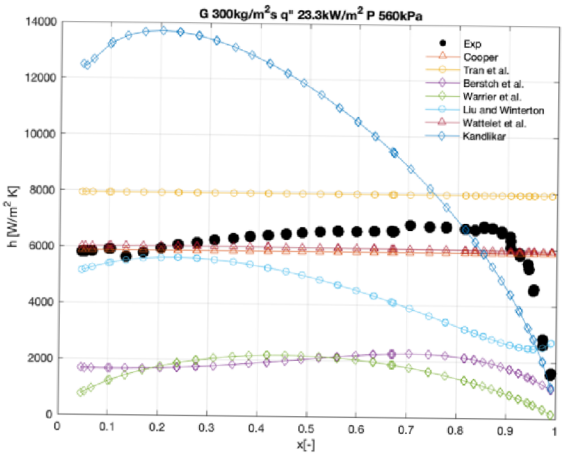
G 300kg/m²s q" 23.3kW/m² P 560kPa
Exp
Cooper
Tran et al.
Berstch et al.
Warrier et al.
Liu and Winterton
Wattelet et al.
Kandlikar
h [W/m² K]
x[-]

(g)

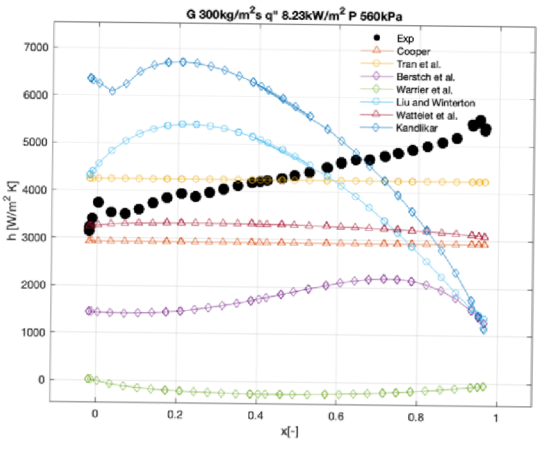
G 300kg/m²s q" 8.23kW/m² P 560kPa
Exp
Cooper
Tran et al.
Berstch et al.
Warrier et al.
Liu and Winterton
Wattelet et al.
Kandlikar
h [W/m² K]
x[-]

(h)

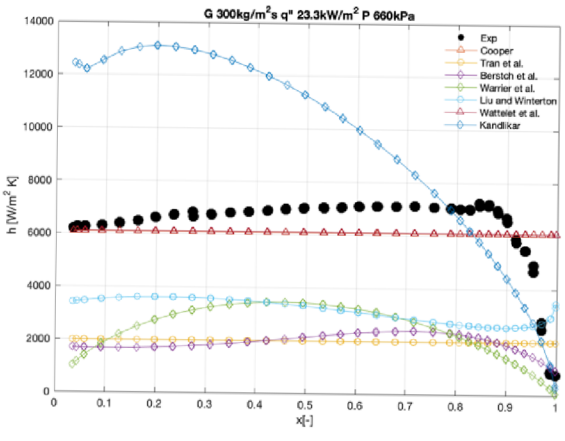
G 300kg/m²s q" 23.3kW/m² P 660kPa
Exp
Cooper
Tran et al.
Berstch et al.
Warrier et al.
Liu and Winterton
Wattelet et al.
Kandlikar
h [W/m² K]
x[-]

(i)

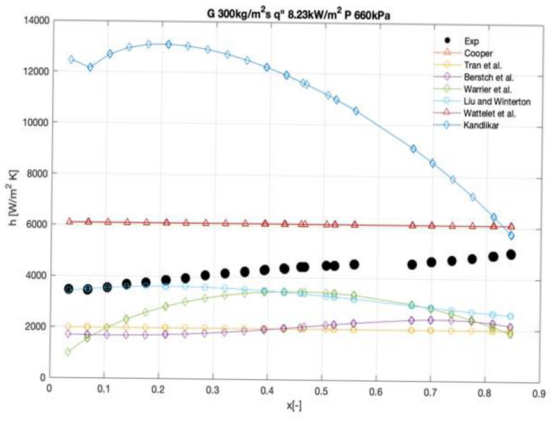
G 300kg/m²s q" 8.23kW/m² P 660kPa
Exp
Cooper
Tran et al.
Berstch et al.
Warrier et al.
Liu and Winterton
Wattelet et al.
Kandlikar
h [W/m² K]
x[-]

(j)

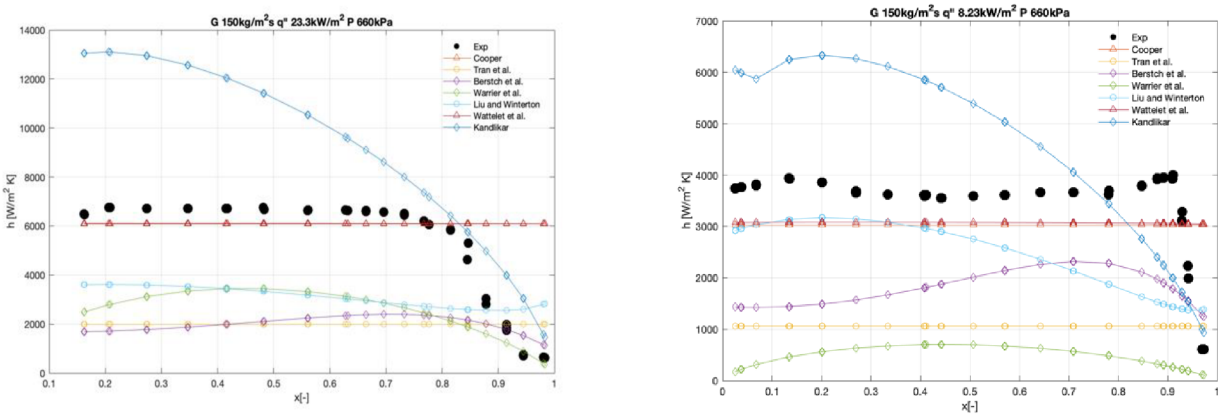

(k) (l)

Figure 4.29: (a–l) Comparison of how predictive models of Cooper [20], Tran et al. [31], Berstch et al. [32], Warrier et al. [33], Wattelet et al. [115], Liu and Winterton [116] and Kandlikar [117] are able to capture experimental trend over vapor quality for conditions of G = 150 - 300 kg/(m² s), q" = 8.26 - 23.3 kW/m², P_{sat} = 460 - 660 kPa.

Table 4.1: Statistical analysis of the comparison between experimental heat transfer coefficient and prediction models at saturation pressure of 460 kPa

Experimental Condition		**P_{sat} = 460 kPa G = 150 kg/(m² s) q" = 8.26 kW/m²**	**P_{sat} 460 kPa G = 150 kg/(m² s) q" = 23.3 kW/m²**	**P_{sat} = 460 kPa G = 300 kg/(m² s) q" = 8.26 kW/m²**	**P_{sat} =460 kPa G = 300 kg/(m² s) q" = 23.3 kW/m²**	**All Data at 460 kPa**
Cooper [20]	MRE %	−11.9	11.1	−27.7	3.5	−6.25
	MAE %	0.2	8.4	14.1	11.2	8.48
Tran et al.[31]	MRE %	−67.0	−61.4	8.0	43.7	−19.18
	MAE %	62.7	62.4	28.3	54.5	51.825
Bertsch et al. [32]	MRE %	−49.8	−65.8	−62.1	−70.0	−61.30
	MAE %	50.6	69.1	56.6	67.2	60.88
Warrier et al. [33]	MRE %	−88.7	−60.8	−103.5	−84.1	−84.28
	MAE %	94.7	59.0	99.4	95.6	87.18
Liu and Winterton [116]	MRE %	−19.2	−41.0	−15.4	−19.5	−23.78
	MAE %	0.39	30.9	28.1	7.6	16.75
Wattelet et al. [115]	MRE %	13.1	20.5	76.5	34.4	36.13
	MAE %	3.1	10.7	7.8	14.4	9.0
Kandlikar [117]	MRE %	38.6	52.8	−7.8	74.4	39.5
	MAE %	89.9	130.8	80.7	138.0	109.9

Table 4.2: Statistical analysis of the comparison between experimental heat transfer coefficient and prediction models at saturation pressure of 560 kPa.

Experimental Condition		**P_{sat} = 560 kPa G = 150 kg/(m² s) q'' = 8.26 kW/m²**	**P_{sat} = 560 kPa G = 150 kg/(m² s) q'' = 23.3 kW/m²**	**P_{sat} = 560 kPa G = 300 kg/(m² s) q'' = 8.26 kW/m²**	**P_{sat} = 560 kPa G = 300 kg/(m² s) q'' = 23.3 kW/m²**	**All Data at 560 kPa**
Cooper [20]	MRE %	5.2	64.7	−30.7	6.1	11.33
	MAE %	11.4	1.3	7.0	1.3	5.25
Tran et al. [31]	MRE %	−61.8	−44.4	0.6	43.3	−15.58
	MAE %	67.8	65.8	35.1	36.7	51.35
Bertsch et al. [32]	MRE %	−41.9	−55.0	−60.0	−68.5	−56.35
	MAE %	57.2	71.3	54.0	71.2	63.43
Warrier et al. [33]	MRE %	−87.4	−56.5	−103.9	−77.2	−81.25
	MAE %	94.9	56.8	99.2	86.9	84.45
Liu and Winterton [116]	MRE %	−22.0	−19.7	0.9	−27.2	−17.0
	MAE %	13.0	37.8	37.3	11.3	24.85
Wattelet et al. [115]	MRE %	6.6	65.1	−22.6	8.2	14.33
	MAE %	9.9	1.6	3.3	3.7	4.63
Kandlikar	MRE %	26.6	56.5	27.1	50.8	40.25
	MAE %	72.8	117.2	102.1	115.3	101.85

Table 4.3: Statistical analysis of the comparison between experimental heat transfer coefficient and prediction models at saturation pressure of 660 kPa.

Experimental Condition		**P_{sat} = 660 kPa G = 150 kg/(m² s) q'' = 8.26 kW/m²**	**P_{sat} = 660 kPa G = 150 kg/(m² s) q'' = 23.3 kW/m²**	**P_{sat} = 660 kPa G = 300 kg/(m² s) q'' = 8.26 kW/m²**	**P_{sat} = 660 kPa G = 300 kg/(m² s) q'' = 23.3 kW/m²**	**All Data at 660 kPa**
Cooper [20]	MRE %	2.8	110.4	−27.4	33.1	29.73
	MAE %	19.0	6.0	12.5	1.9	9.85
Tran et al. [31]	MRE %	−63.9	−31.4	1.9	73.7	−4.93
	MAE %	71.6	69.3	22.9	28.1	47.98

Bertsch et al. [32]	MRE %	−42.9	−41.5	−56.8	−64.4	−51.4
	MAE %	61.7	73.9	58.4	72.5	66.63
Warrier et al. [33]	MRE %	−87.0	−48.1	−104.1	−76.7	−78.98
	MAE %	95.5	61.4	101.9	88.7	86.88
Liu and Winterton [116]	MRE %	−26.8	−2.4	8.4	−16.9	−9.43
	MAE %	21.8	44.4	42.3	16.4	31.22
Wattelet et al. [115]	MRE %	4.2	110.9	−18.2	35.3	33.05
	MAE %	17.6	5.7	1.3	0.5	6.28
Kandlikar [117]	MRE %	24.1	80.6	42.0	48.9	48.90
	MAE %	61.9	101.7	86.2	115.1	91.23

Table 4.4: Statistical analysis of the comparison between experimental heat transfer coefficient and prediction models for all data at saturation pressures of 460–660 kPa.

Experimental Pressure	P_{sat} **= 460 kPa**		P_{sat} **= 560 kPa**		P_{sat} **= 660 kPa**	
	MRE %	MAE %	MRE %	MAE %	MRE %	MAE %
Cooper [20]	−6.25	8.48	11.33	5.25	29.73	9.85
Tran et al. [31]	−19.18	51.825	−15.58	51.35	−4.93	47.98
Bertsch et al. [32]	−61.30	60.88	−56.35	63.43	−51.4	66.63
Warrier et al. [33]	−84.28	87.18	−81.25	84.45	−78.98	86.88
Liu and Winterton [116]	−23.78	16.75	−17.0	24.85	−9.43	31.22
Wattelet et al. [115]	36.13	9.0	14.33	4.63	33.05	6.28
Kandlikar [117]	39.5	109.9	40.25	101.85	48.90	91.23

4.4 Flow boiling Heat Transfer Characteristics at Varying Heat Fluxes

This section discusses the effect of increasing heat flux on heat transfer characteristics during flow boiling at constant mass flux and saturation pressure. Figure 4.30 presents experimental results of heat transfer coefficient versus vapor quality for mass flux of 300 kg/(m^2 s), saturation pressure of 460 kPa for a varying heat flux from 7.2 – 14.3 kW/m^2. With respect to the heat transfer coefficient, it can be observed that, at these low heat flux conditions, heat transfer coefficient increases with vapor quality until dryout occurs. This trend is characterized with big steepness in slope of the heat transfer coefficient up to dryout. For this case, convective boiling is deemed to dominate the heat transfer as discussed in previous sections. Convective boiling dominates the heat transfer when heat transfer coefficient has a dependency on vapor quality and mass flux.

Increasing heat flux begins to decrease the slope toward zero as observed in Figure 4.31 for heat fluxes from 28.1 to 47.4 kW/m^2. The zero slope of the heat transfer coefficient at high heat flux indicates the dominance of nucleate boiling characteristics. Nucleate boiling is assumed to be highly favored by heat flux and saturation condition with minimal effect of mass flux and vapor quality as discussed earlier. It is worth mentioning that, for low heat flux conditions, there is an observance of a local minimum. This local minimum is a region of transition from one flow pattern (slug) to another (intermittent). The vapor quality at which the local minimum occur is highly influenced by heat flux. Also, for low heat flux conditions (7.2 and 14.3 kW/m^2) where convective boiling dominates the heat transfer, increasing heat flux only produces an observable increase in heat transfer coefficient in the low vapor quality region. However, at high vapor quality, the plots merge into a single plot without showing any effect of heat flux. This indicates the dominance of convective boiling at high vapor quality.

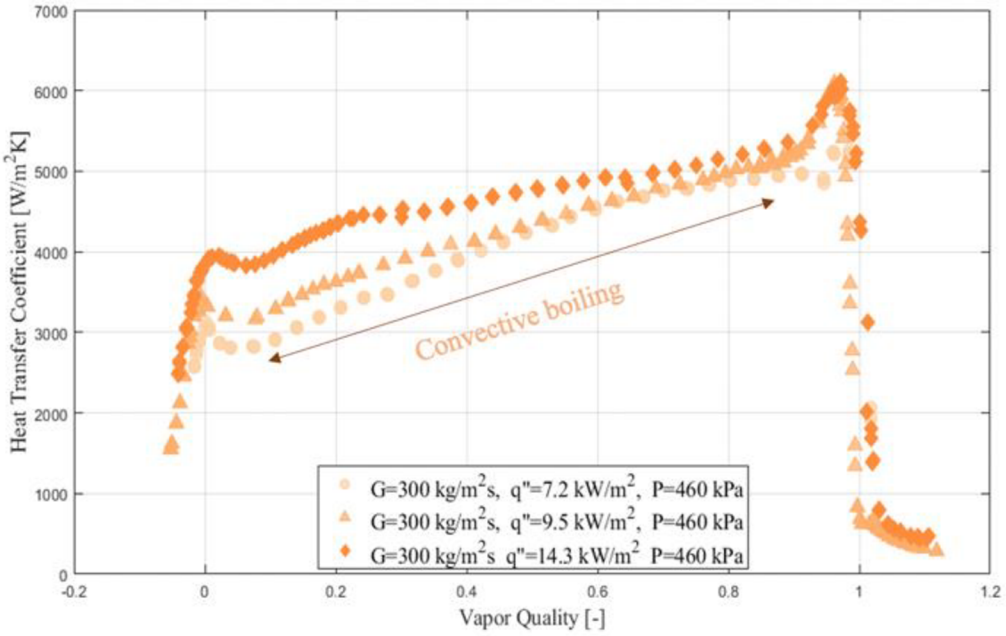

Figure 4.30: Heat transfer coefficient of R134a for mass flux of 300 kg/(m² s), saturation pressure of 460 kPa and heat fluxes from 7.2 to 14.3 kW/m² (convective boiling case)

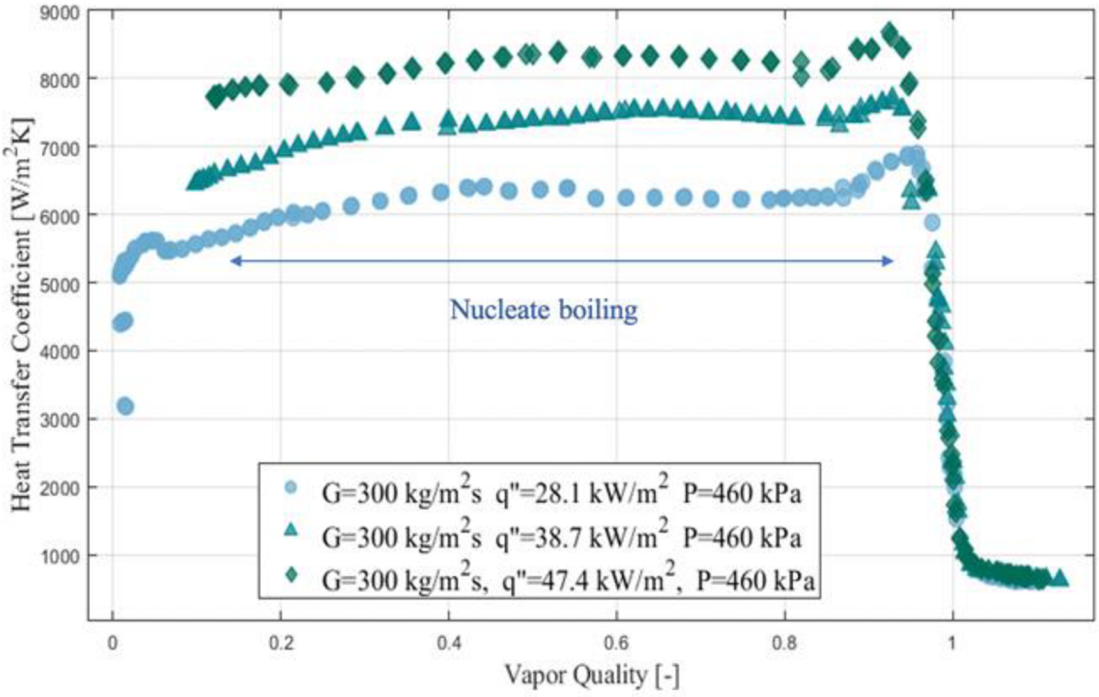

Figure 4.31: Heat transfer coefficient of R134a for mass flux of 300 kg/(m² s), saturation pressure of 460 kPa and heat fluxes from 28.1 to 47.4 kW/m² (Nucleate boiling case)

Figure 4.32a and b indicate plots of the wall, fluid, saturation temperature against vapor quality and their corresponding effect on heat transfer coefficient and flow patterns respectively. From these plots, for an imposed heat flux, the ratio of the applied heat flux to the difference between the heated wall temperature and the fluid temperature gives the local heat transfer coefficient. For the zone of saturated boiling, the heated wall temperature is higher than the bulk fluid temperature. The bulk fluid temperature is equal to the saturated temperature of the fluid ($T_{fluid} = T\_sat$) as observed in Figure 4.32a and b. At low heat flux conditions as observed in Figure 4.32a, with increasing vapor quality, bubbles begin to form, grow, detach from the heated walls and form slugs at low vapor quality. As vapor quality increases, annular flow develops where thin liquid films flow near the walls of the tube with vapor core at the center. Eventually, dry-out occurs where the liquid film dries out at higher vapor quality region where the wall temperature rises abruptly followed by the fluid temperature. This then leads to a sudden drop in the heat transfer coefficient. This is the case description for convective boiling heat transfer as described above. At high heat fluxes as observed in Figure 4.32b where nucleate boiling dominates the heat transfer, bubble formation predominantly controls the heat transfer coefficient. In this case, heat transfer coefficient is not appreciably affected with increasing vapor quality. At very high vapor quality, there is some effect of convective boiling as can be seen with the annular effects. Bubbles even nucleate in the thin liquid film in the annular region until dryout and mist flow occur where the liquid film dries out at higher vapor quality region and the wall temperature rises abruptly followed by the fluid temperature.

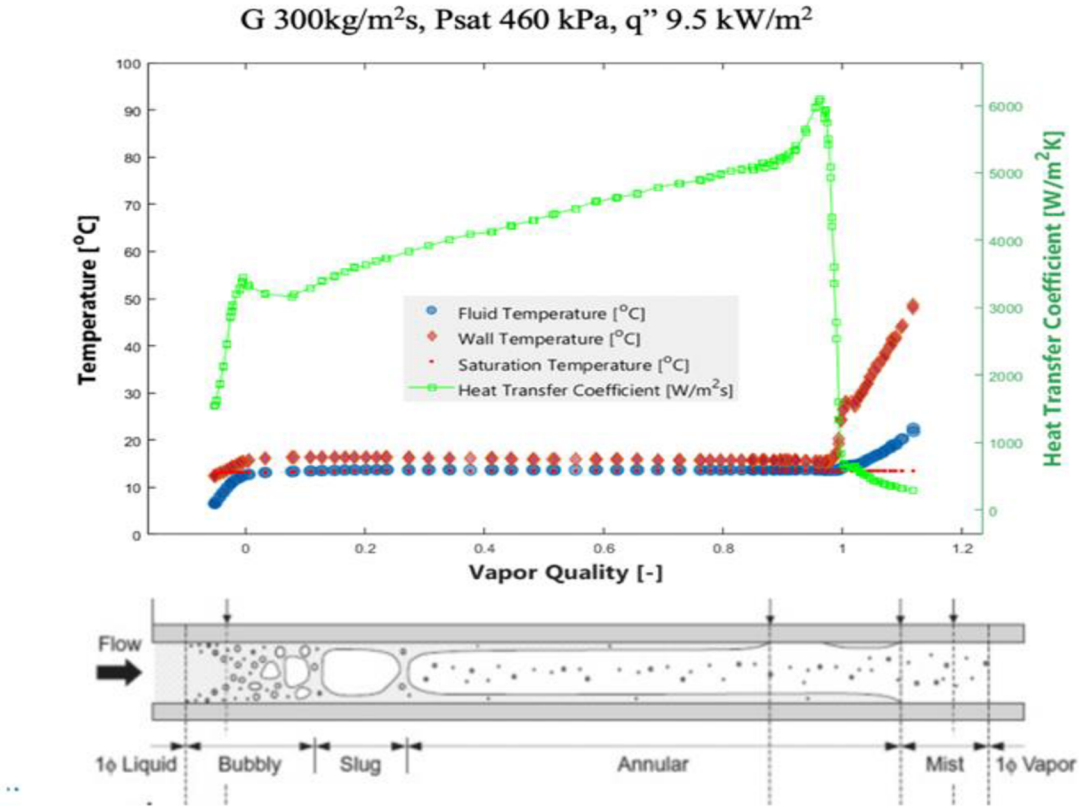

a. Convective boiling case

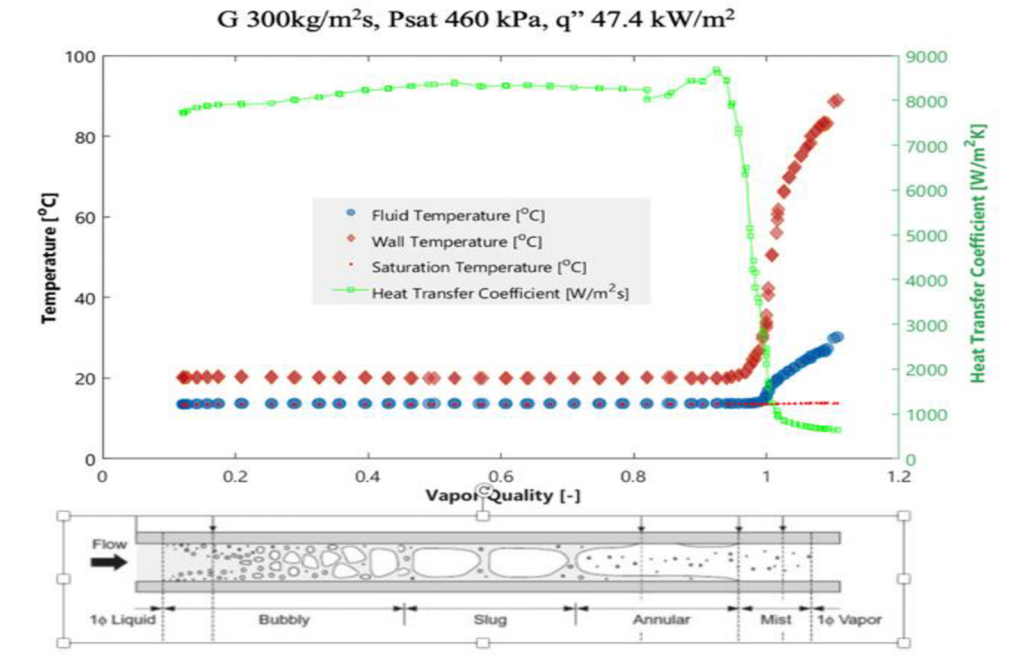

b. Nucleate boiling case

Figure 4.32a & b: Wall, fluid, saturation temperature, heat transfer coefficient and corresponding flow pattern evolution for both convective and nucleate boiling cases.

Chapter 5

5 Conclusion

This chapter summarizes the main findings of this PhD dissertation which was aimed at experimentally investigating flow boiling heat transfer characteristics in small diameter tubes. Recommendations to further this work in future are also presented here.

5.1 Recap

For this research, a state-of-the art experimental facility at the Thermal Two-Phase Lab of the Norwegian University of Science and Technology (NTNU) was modified to investigate flow boiling heat transfer characteristics over a wide range of experimental conditions which finds its application in air-conditioner, refrigeration system and other thermal management system. The study began with an introduction. This was aimed at introducing the motivation behind this work. Next, an extensive review from literature aiding in identifying the gaps and focus of this study was conducted. The experimental facility was described in details with the associated measurement accuracy, error analysis and data reduction. The findings were then presented in the results and discussion chapter. Unconventionally, the results and discussion chapter were presented in sections of objectives laid for each phase of this dissertation that was published in an impacted journal.

In achieving the aim of understanding the flow boiling process and the dominant mechanisms controlling the heat transfer, an extensive experimental investigation was conducted to investigate the effect of flow conditions over wide range but small increment of vapor quality from subcooled region through saturation phase to the superheated region. The findings conclude that:

- At the low saturation pressure and heat flux conditions, a maximum peak of the heat transfer coefficient near the vapor quality of zero (0) was observed. This peak was sensitive to heat flux and insensitive to mass flux.
- After the local maximum peak of the heat transfer coefficient reached near zero vapor quality, heat transfer coefficient deterioration is observed until a local minimum is reached. The decrease in heat transfer coefficient to a local minimum is observed at a low vapor quality region below 0.1 (i.e., $x < 0.1$).
- Heat flux had a considerable impact on the heat transfer coefficient in the low-vapor-quality region. However, this influence was reduced as vapor quality increased. The influence of mass flux in the low vapor quality region was mild, except at low heat fluxes. In high vapor quality region, the effect of mass flux on the heat transfer coefficient was highly pronounced. Generally, in the low vapor quality region, nucleate boiling heat transfer was the dominant mechanism controlling the heat transfer coefficient, whereas in the high vapor quality region, convective heat transfer was the dominant mechanism.
- The flow patterns observed were recorded with a high-speed camera to help analyze the results. The main flow patterns observed were slug, intermittent in the low-quality region, and annular and dry-out to mist in the high-quality region.
- Pressure drop varied as a function of vapor quality and mass flux in the two-phase region and superheated vapor region. There was no significant effect of heat flux on pressure drop.

Also, for the second phase of the study where the effect of saturation pressure on flow boiling heat transfer was investigated, the study concludes that:

- At low mass flux, increasing saturation pressure increased heat transfer coefficient. This effect was more pronounced in the low vapor quality region and the dominant mechanism was nucleate boiling.
- At high mass flux, increasing saturation pressure led to an insignificant increase in heat transfer coefficient. At high mass flux but low heat flux, heat transfer coefficient increased with vapor quality, indicating convective boiling dominance. But for high heat flux, heat transfer coefficient was linear over vapor quality, indicating nucleate boiling dominance.
- Pressure drop was observed to decrease with increasing saturation pressure.
- Increasing saturation pressure increased the vapor quality at which the flow pattern transitions from intermittent flow to annular flow. The flow patterns predicted by Wojtan's flow pattern map were mixture of slug and stratified wavy and purely stratified wavy for low

mass fluxes. For increased mass fluxes, the flow patterns predicted were slug, intermittent, annular and dryout. Generally, based on the comparison with flow pattern recordings with high speed camera, it is fair to conclude that Wojtan et al's flow pattern map is capable of predicting flow patterns for flow boiling heat transfer in small diameter tubes.

- Cooper's model was the best predictor of the experimental data and the trend of heat transfer followed by models of Wattalete et al. and Liu and Winterton.

With single phase experiment (validations), it can be concluded that correlations proposed in literature for single phase flow and heat transfer were capable of predicting single phase heat transfer of liquid and vapor phase refrigerant flowing through small diameter tubes. Generally, with the effect of flow parameters on heat transfer mechanism, this work concludes that, saturation pressure and heat flux favor nucleate boiling whiles mass flux and vapor quality favor convective boiling. However, their interrelation is significant.

With investigating the effect of heat flux on heat transfer coefficient at varying heat flux conditions, the work concludes that:

- At low heat flux, the heat transfer is predominantly controlled by convection boiling with a higher slope of heat transfer coefficient.
- As heat flux increases, nucleate boiling predominates the heat transfer. The predominance of nucleate boiling is strongly experienced at low vapor quality when the higher slope in convective boiling begins to disappear as nucleate boiling dominates.
- Dry-out vapor quality inception was not affected appreciably by heat flux contrary to what is generally reported in literature.

5.2 Final Remarks and recommendation

Although this study was broadly aimed at advancing the knowledge in flow boiling heat transfer and the mechanisms responsible for controlling the heat transfer, further research both experimental and numerical is highly recommended to broaden the database concerning flow boiling heat transfer. In furthering this work with the goal of improving heat transfer, investigating the impact of different surface coatings or nanostructured surfaces on flow boiling heat transfer in small diameter channels will be a recommended area to focus in future studies. This could involve studying how these coatings influence nucleation, bubble dynamics, and overall heat transfer performance. Another recommendation will be to evaluate and develop novel techniques for enhancing flow boiling heat transfer in small diameter channels.

Also, with the advance of machine learning, this study recommends the development and validation of advanced numerical models and simulations from a wide range of database that accurately predict flow boiling heat transfer in small diameter channels. These models can help provide insights into complex phenomena that are difficult to capture experimentally. With recent concerns about climate change and regulations regarding carbon emission, future studies in line with this work should consider natural refrigerants and other refrigerants with low carbon emission.

Publications of the author

Journal publications

- Bediako E. G., Dancova P., Vit T., (2023) *"Flow Boiling Heat Transfer of R134a at Varying Heat Fluxes"*, Journal of Fluid Flow, Heat and Mass Transfer (JFFHMT), Volume 10 - 2023 - Pages 43-50 https://doi.org/10.11159/jffhmt.2023.007

- Bediako E. G., Dancova P., Vit T., *"Flow Boiling Heat transfer of R134a in a horizontal smooth tube: Experimental results, flow patterns and assessment of correlations at three saturation pressures"* Energies 2022, 15, 7503. https://doi.org/10.3390/en15207503

- Bediako E. G., Dancova P., Vit T., (2022) *"Experimental Study of Flow Boiling Heat Transfer at Low Heat Fluxes"*, Journal of Fluid Flow, Heat and Mass Transfer (JFFHMT), Volume 9 - 2022 - Pages 148-156 DOI: 10.11159/jffhmt.2022.018

- Bediako E. G., Dancova P., Vit T., *"Experimental Study Of Horizontal Flow Boiling Heat Transfer Coefficient And Pressure Drop Of R134a From Sub-cooled Liquid Region To Superheated Vapor Region"* Energies 2022, 15(3), 681; https://doi.org/10.3390/en15030681

- Bediako E. G., Dancova P., Vit T., (2022) *"Effect of heat flux and Dryout Characteristics: Experimental Investigation"*, *submitted to* Journal of Fluid Flow, Heat and Mass Transfer (JFFHMT)

- Bediako E.G., Revillin R, Rulliere R., Marchetto D. and Petra Dancova, 2023, "*Flow boiling heat transfer of R1234ze in a horizontal Mini-channel at medium and high saturation temperatures*", *to be submitted to* Int. J. of Applied Thermal Engineering

Conference publications

- Bediako E. G., Dancova P., Vit T., (2022) *"Flow Boiling Heat Transfer Of R134a: Ef- fect Of Heat Flux And Dry-Out Characteristics"*, Proceedings of the 10th International Conference on Fluid Flow, Heat and Mass Transfer (FFHMT'23) Ottawa, Canada *DOI: 10.11159/ffhmt23.161*

- Bediako E. G., Dancova P., Vit T., (2022) *"Comparison Of Experimental Heat Transfer Coefficient With Qualitative Description Of Classical Heat Transfer Coefficient At Low Heat Flux Conditions"*, Proceedings of the 9th International Conference on Fluid Flow, Heat and Mass Transfer (FFHMT'22), Niagara Falls, Canada *DOI: 10.11159/ffhmt22.185*

- Bediako E. G., Dancova P., Vit T., (2022) *" Flow Boiling Heat Transferat Low Mass and Heat Fluxes: Heat Transfer Coefficient, Flow Pattern Analysis and Correlation Assessment"*, Proceedings of the 2022 International Conference on Fluid Flow, Heat and Mass Transfer (ICFFHMT 2022), International Journal of Aerospace and Mechanical Engineering, Vol:16, No:10, 2022

References

[1] Henley Jon, "World set to use more energy for cooling than heating | Climate crisis | The Guardian," Oct. 26, 2015. https://www.theguardian.com/environment/2015/oct/26/cold-economy-cop21-global-warming-carbon-emissions (accessed Aug. 04, 2023).

[2] Carroll Rory, "How America became addicted to air conditioning | Energy | The Guardian," Oct. 26, 2015. https://www.theguardian.com/environment/2015/oct/26/how-america-became-addicted-to-air-conditioning (accessed Aug. 04, 2023).

[3] "Lot Air Conditioning Compressor Old Town Singapore City Stock Photo by ©danilum 180044374." https://depositphotos.com/180044374/stock-photo-lot-air-conditioning-compressor-old.html (accessed Aug. 04, 2023).

[4] "COMMERCIAL & INDUSTRIAL REFRIGERATION EQUIPMENT MANUFACTURER: REFRIGERATORS, FREEZERS, COOLERS, CHILLERS - COOLPLUS CHINA." https://www.coolplusref.com/ (accessed Aug. 04, 2023).

[5] M. V. Sardeshpande and V. V. Ranade, "Two-phase flow boiling in small channels: A brief review," *Sadhana - Academy Proceedings in Engineering Sciences*, vol. 38, no. 6, pp. 1083–1126, 2013, doi: 10.1007/s12046-013-0192-7.

[6] M. Saad Kamel, F. Lezsovits, • Ahmed, and K. Hussein, "Experimental studies of flow boiling heat transfer by using nanofluids A critical recent review," *J Therm Anal Calorim*, vol. 138, doi: 10.1007/s10973-019-08333-2.

[7] R. Charnay, "Experimental study of flow boiling in horizontal minichannels at high saturation temperature," 2015.

[8] S. G. Kandlikar, "Heat transfer mechanisms during flow boiling in microchannels," *J Heat Transfer*, vol. 126, no. 1, pp. 8–16, Feb. 2004, doi: 10.1115/1.1643090.

[9] R. Ali, B. Palm, and M. H. Maqbool, "Flow boiling heat transfer characteristics of a mini-channel up to dryout conditiona," *J Heat Transfer*, vol. 133, no. 8, Aug. 2011, doi: 10.1115/1.4003669/467322.

[10] L. Wang, M. Chen, and M. Groll, "Flow Boiling Heat Transfer Characteristics of R134a in a Horizontal Mini Tube†," *J Chem Eng Data*, vol. 54, no. 9, pp. 2638–2645, Sep. 2009, doi: 10.1021/JE900140W.

[11] W. J. Van den Bergh, H. R. Moran, J. Dirker, C. N. Markides, and J. P. Meyer, "Effect of low heat and mass fluxes on the boiling heat transfer coefficient of R-245fa," *Int J Heat*

Mass Transf, vol. 180, p. 121743, Dec. 2021, doi: 10.1016/J.IJHEATMASSTRANSFER.2021.121743.

[12] G. Ribatski, "A critical overview on the recent literature concerning flow boiling and two-phase flows inside micro-scale channels," *Experimental Heat Transfer*, vol. 26, no. 2–3, pp. 198–246, 2013, doi: 10.1080/08916152.2012.737189.

[13] S. Nukiyama, "The maximum and minimum values of the heat Q transmitted from metal to boiling water under atmospheric pressure," *Int J Heat Mass Transf*, vol. 9, no. 12, pp. 1419–1433, Dec. 1966, doi: 10.1016/0017-9310(66)90138-4.

[14] S. M. Ghiaasiaan, *Two-Phase Flow, Boiling and Condensation in Conventional and Miniature Systems*. 2010. doi: 10.1017/cbo9780511619410.003.

[15] S. G. Kandlikar and J. N. Chung, *Multiphase Flow Handbook*. Taylor & Francis, 2006.

[16] S. Liaw and D. Dhir, "Effect of surface wettability on transition boiling heat transfer from a vertical surface," *International Heat Transfer Conference*, 1986, Accessed: Aug. 04, 2023. [Online]. Available: https://www.dl.begellhouse.com/download/article/2f5c5022713bcbc4/PB-07.pdf

[17] W. M. Rohsenow, "A Method of Correlating Heat-Transfer Data for Surface Boiling of Liquids," *J Fluids Eng*, vol. 74, no. 6, pp. 969–975, Aug. 1952, doi: 10.1115/1.4015984.

[18] V. K. Dhir, "Nucleate and transition boiling heat transfer under pool and external flow conditions," *Int J Heat Fluid Flow*, vol. 12, no. 4, pp. 290–314, Dec. 1991, doi: 10.1016/0142-727X(91)90018-Q.

[19] K. Stephan and M. Abdelsalam, "Heat-transfer correlations for natural convection boiling," *Int J Heat Mass Transf*, vol. 23, no. 1, pp. 73–87, Jan. 1980, doi: 10.1016/0017-9310(80)90140-4.

[20] M. G. Cooper, "Heat Flow Rates in Saturated Nucleate Pool Boiling-A Wide-Ranging Examination Using Reduced Properties," *Adv Heat Transf*, vol. 16, no. C, pp. 157–239, Jan. 1984, doi: 10.1016/S0065-2717(08)70205-3.

[21] F. T. Kanizawa and G. Ribatski, "Flow boiling and condensation in microscale channels," 2021, doi: 10.1007/978-3-030-68704-5.

[22] S. S. Kutateladze, "Boiling heat transfer," *Int J Heat Mass Transf*, vol. 4, no. C, pp. 31–45, Dec. 1961, doi: 10.1016/0017-9310(61)90059-X.

[23] J. C. Chen, "Correlation for boiling heat transfer to saturated fluids in convective flow," *Industrial and Engineering Chemistry Process Design and Development*, vol. 5, no. 3, pp. 322–329, Jul. 1966, doi: 10.1021/I260019A023/ASSET/I260019A023.FP.PNG_V03.

[24] E. G. Bediako, P. Dančová, and T. Vít, "Flow Boiling Heat Transfer of R134a in a Horizontal Smooth Tube: Experimental Results, Flow Patterns, and Assessment of Correlations," *Energies (Basel)*, vol. 15, no. 20, Oct. 2022, doi: 10.3390/EN15207503.

[25] R. Charnay, J. Bonjour, and R. Revellin, "International Journal of Heat and Fluid Flow Experimental investigation of R-245fa flow boiling in minichannels at high saturation temperatures : Flow patterns and flow pattern maps," *Int J Heat Fluid Flow*, vol. 46, pp. 1–16, 2014, doi: 10.1016/j.ijheatfluidflow.2013.12.002.

[26] L. Liebenberg and J. P. Meyer, "A review of flow pattern-based predictive correlations during refrigerant condensation in horizontally smooth and enhanced tubes," *Heat Transfer Engineering*, vol. 29, no. 1, pp. 3–19, 2008, doi: 10.1080/01457630701677049.

[27] É. Polytechnique, F. De Lausanne, and J. Moreno Quiben, "Experimental and analytical study of two-phase pressure drops during evaporation in horizontal tubes," 2005, doi: 10.5075/EPFL-THESIS-3337.

[28] Ovid. Baker, *"New pipelines techniques." Designing for Simultaneous Flow of Oil and Gas*. Full Report on Magnolia's Research on TWO-Phase Pipeline Design, 1954.

[29] G. Hewitt and D. Roberts, "Studies of two-phase flow patterns by simultaneous x-ray and flast photography," *Atomic Energy Research Establishment, Harwell, England (United Kingdom).*, 1969, Accessed: Aug. 10, 2023. [Online]. Available: https://www.osti.gov/biblio/4798091

[30] T. Sato, T. Minamiyama, M. Yanai, and T. Tokura, "Study of heat transfer in boiling two-phase channel flow. Part I. Flow patterns in a boiling channel.," *Heat Transfer - Jap. Res. 1: No. 4, 1-14(1972).*, Jan. 1972.

[31] J. M. Mandhane, G. A. Gregory, and K. Aziz, "A flow pattern map for gas—liquid flow in horizontal pipes," *International Journal of Multiphase Flow*, vol. 1, no. 4, pp. 537–553, Oct. 1974, doi: 10.1016/0301-9322(74)90006-8.

[32] M. Ishii, Ishii, and M., "Thermo-fluid dynamic theory of two-phase flow," *STIA*, vol. 75, p. 29657, 1975, Accessed: Aug. 10, 2023. [Online]. Available: https://ui.adsabs.harvard.edu/abs/1975STIA...7529657I/abstract

[33] Y. Taitel and A. E. Dukler, "A model for predicting flow regime transitions in horizontal and near horizontal gas-liquid flow," *AIChE Journal*, vol. 22, no. 1, pp. 47–55, Jan. 1976, doi: 10.1002/AIC.690220105.

[34] D. Steiner, *VDI-Wärmeatlas (VDI heat atlas)." Verein Deutscher Ingenieure, VDI-Gesellschaft Verfahrenstechnik und Chemieingenieurwesen (GCV*. 1993.

[35] N. Kattan, J. R. Thome, and D. Favrat, "Flow boiling in horizontal tubes: Part 1-development of a diabatic two-phase flow pattern map," *J Heat Transfer*, vol. 120, no. 1, pp. 140–147, 1998, doi: 10.1115/1.2830037.

[36] J. R. Thome, "On recent advances in modeling of Two-Phase flow and heat transfer," *Heat Transfer Engineering*, vol. 24, no. 6, pp. 46–59, 2003, doi: 10.1080/714044414.

[37] J. R. Thome and J. El Hajal, "Two-Phase Flow Pattern Map for Evaporation in Horizontal Tubes: Latest Version," *Heat Transfer Engineering*, vol. 24, no. 6, pp. 3–10, 2003, doi: 10.1080/714044410.

[38] O. Zürcher, D. Favrat, and J. R. Thome, "Development of a diabatic two-phase flow pattern map for horizontal flow boiling," *Int J Heat Mass Transf*, vol. 45, no. 2, pp. 291–301, Jan. 2002, doi: 10.1016/S0017-9310(01)00146-6.

[39] L. Wojtan, T. Ursenbacher, and J. R. Thome, "Investigation of flow boiling in horizontal tubes: Part I - A new diabatic two-phase flow pattern map," *Int J Heat Mass Transf*, vol. 48, no. 14, pp. 2955–2969, 2005, doi: 10.1016/j.ijheatmasstransfer.2004.12.012.

[40] P. E. L. Barbieri, J. M. S. Jabardo, and E. P. B. Filho, "FLOW PATTERNS IN CONVECTIVE BOILING OF REFRIGERANT R-134a IN SMOOTH TUBES OF SEVERAL DIAMETERS".

[41] L. Cheng, G. Ribatski, J. Moreno Quibén, and J. R. Thome, "New prediction methods for CO2 evaporation inside tubes: Part I – A two-phase flow pattern map and a flow pattern based phenomenological model for two-phase flow frictional pressure drops," *Int J Heat Mass Transf*, vol. 51, no. 1–2, pp. 111–124, Jan. 2008, doi: 10.1016/J.IJHEATMASSTRANSFER.2007.04.002.

[42] R. Mastrullo, A. W. Mauro, J. R. Thome, D. Toto, and G. P. Vanoli, "Flow pattern maps for convective boiling of CO2 and R410A in a horizontal smooth tube: Experiments and new correlations analyzing the effect of the reduced pressure," *Int J Heat Mass Transf*, vol. 55, no. 5–6, pp. 1519–1528, Feb. 2012, doi: 10.1016/J.IJHEATMASSTRANSFER.2011.11.003.

[43] J. B. Copetti, M. H. Macagnan, F. Zinani, and N. L. F. Kunsler, "Flow boiling heat transfer and pressure drop of R-134a in a mini tube: An experimental investigation," *Exp Therm Fluid Sci*, vol. 35, no. 4, pp. 636–644, 2011, doi: 10.1016/j.expthermflusci.2010.12.013.

[44] Y. Xu, X. Fang, G. Li, D. Li, and Y. Yuan, "An experimental study of flow boiling heat transfer of R134a and evaluation of existing correlations," *Int J Heat Mass Transf*, vol. 92, pp. 1143–1157, 2016, doi: 10.1016/j.ijheatmasstransfer.2015.09.044.

[45] D. Del Col, "Flow boiling of halogenated refrigerants at high saturation temperature in a horizontal smooth tube," *Exp Therm Fluid Sci*, vol. 34, no. 2, pp. 234–245, 2010, doi: 10.1016/j.expthermflusci.2009.10.035.

[46] S. G. Kandlikar, "Fundamental issues related to flow boiling in minichannels and microchannels," *Exp Therm Fluid Sci*, vol. 26, no. 2–4, pp. 389–407, 2002, doi: 10.1016/S0894-1777(02)00150-4.

[47] J. R. Simon and T. M. Bandhauer, "An experimentally validated evaporative phase change heat transfer model for low mass flux applications using R134a in plate heat exchangers," *International Journal of Refrigeration*, vol. 131, pp. 604–614, Nov. 2021, doi: 10.1016/J.IJREFRIG.2021.08.003.

[48] Z. Yang, M. Gong, G. Chen, X. Zou, and J. Shen, "Two-phase flow patterns, heat transfer and pressure drop characteristics of R600a during flow boiling inside a horizontal tube," *Appl Therm Eng*, vol. 120, no. October, pp. 654–671, 2017, doi: 10.1016/j.applthermaleng.2017.03.124.

[49] E. Manavela Chiapero, M. Fernandino, and C. A. Dorao, "Experimental results on boiling heat transfer coefficient, frictional pressure drop and flow patterns for R134a at a saturation temperature of 34°C," *International Journal of Refrigeration*, vol. 40, pp. 317–327, 2014, doi: 10.1016/j.ijrefrig.2013.11.026.

[50] R. J. da Silva Lima, J. M. Quibén, and J. R. Thome, "Flow boiling in horizontal smooth tubes: New heat transfer results for R-134a at three saturation temperatures," *Appl Therm Eng*, vol. 29, no. 7, pp. 1289–1298, 2009, doi: 10.1016/j.applthermaleng.2008.06.021.

[51] S. Saitoh, H. Daiguji, and E. Hihara, "Effect of tube diameter on boiling heat transfer of R-134a in horizontal small-diameter tubes," *Int J Heat Mass Transf*, vol. 48, no. 23–24, pp. 4973–4984, 2005, doi: 10.1016/j.ijheatmasstransfer.2005.03.035.

[52] R. Mastrullo, A. Mauro, A. Rosato, G. V. heat and mass transfer, and undefined 2009, "Carbon dioxide local heat transfer coefficients during flow boiling in a horizontal circular smooth tube," *Elsevier*, Accessed: Oct. 26, 2021. [Online]. Available: https://www.sciencedirect.com/science/article/pii/S0017931009002622

[53] A. Celen and A. S. Dalkılıç, "A complete evaluation method for the experimental data of flow boiling in smooth tubes," *International Communications in Heat and Mass Transfer*, vol. 89, no. November, pp. 108–121, 2017, doi: 10.1016/j.icheatmasstransfer.2017.09.024.

[54] J. R. Barbosa, "Two-phase non-equilibrium models: The challenge of improving phase change heat transfer prediction," *Journal of the Brazilian Society of Mechanical Sciences and Engineering*, vol. 27, no. 1, pp. 31–45, 2005, doi: 10.1590/s1678-58782005000100003.

[55] H. Deng, M. Fernandino, and C. A. Dorao, "Flow boiling in a horizontal tube at high vapor qualities," *ASME 2016 14th International Conference on Nanochannels, Microchannels, and Minichannels, ICNMM 2016, collocated with the ASME 2016 Heat Transfer Summer Conference and the ASME 2016 Fluids Engineering Division Summer Meeting*, no. c, pp. 1–9, 2016, doi: 10.1115/ICNMM2016-7978.

[56] C. A. Dorao, O. B. Fernandez, and M. Fernandino, "Experimental Study of Horizontal Flow Boiling Heat Transfer of R134a at a Saturation Temperature of 18.6 °c," *J Heat Transfer*, vol. 139, no. 11, pp. 1–11, 2017, doi: 10.1115/1.4037153.

[57] J. G. Collier, "Convective Boiling and Condensation ," *McGraw-Hill, Maidenhead, United Kingdom*, 1981.

[58] "Convective Boiling and Condensation - John G. Collier, John R. Thome - Google Books." https://books.google.cz/books?hl=en&lr=&id=B-1mFnS6UV4C&oi=fnd&pg=PR13&dq=collier++and+thome&ots=AU6EtH6Eph&sig=zCMLHL3SiwnnlGv1_cqv3TlnQSE&redir_esc=y#v=onepage&q=collier%20%20and%20thome&f=false (accessed Oct. 26, 2021).

[59] S. G. Kandlikar, "Development of a flow boiling map for subooled and saturated flow boiling of different fluids inside circular tubes," *J Heat Transfer*, vol. 113, no. 1, pp. 190–200, 1991, doi: 10.1115/1.2910524.

[60] K. Balasubramanian, P. S. Lee, C. J. Teo, and S. K. Chou, "Flow boiling heat transfer and pressure drop in stepped fin microchannels," *Int J Heat Mass Transf*, vol. 67, pp. 234–252, 2013, doi: 10.1016/j.ijheatmasstransfer.2013.08.023.

[61] G. Hewitt, "Challenges in boiling research," Keynote Lecture, Boiling, 2000. [Online]. Available: https://scholar.google.com/scholar?hl=en&as_sdt=0%2C5&q=Hewitt%2C+G.F.%2C+Challenges+in+Boiling+Research%2C+Keynote+Lecture%2C+Boiling+2000%3A+Phenomena+and+Emerging+Applications%2C+UEF%2C+April+30May+5%2C+Anchorage%2C+AK%2C+2000&btnG=

[62] S. Paul, S. Paul, M. Fernandino, and C. A. Dorao, "The overlooked role of pressure oscillations on heat transfer deterioration during self-sustained flow oscillations," *Appl Phys Lett*, vol. 117, no. 25, 2020, doi: 10.1063/5.0020361.

[63] Z. Malinowski, J. G. Lenard, and M. E. Davies, "A study of the heat-transfer coefficient as a function of temperature and pressure," *J Mater Process Technol*, vol. 41, no. 2, pp. 125–142, Feb. 1994, doi: 10.1016/0924-0136(94)90057-4.

[64] T. K.-Ph. D. Thesis, U. of L. (Imperial College), and undefined 1997, "Experimental investigation of forced convective boiling of hydrocarbon and hydrocarbon mixtures," *ci.nii.ac.jp*, Accessed: Oct. 26, 2021. [Online]. Available: https://ci.nii.ac.jp/naid/10010089538/

[65] N. Kattan, J. Thome, and D. Favrat, "R-502 and two near-azeotropic alternatives. Part 1: In-tube flow-boiling tests," 1995, Accessed: Oct. 26, 2021. [Online]. Available: https://www.osti.gov/biblio/87417

[66] "Flow boiling at low mass flux," *ihtcdigitallibrary.com*, Accessed: Oct. 26, 2021. [Online]. Available: http://www.ihtcdigitallibrary.com/jp/conferences/4eae15a77edee960,7dccb3ab77120b0d,7385d00257f4745d.html

[67] J. Thome, "Flow Boiling in Horizontal Tubes: A Critical Assessment of Current Methodologies.," 1995, Accessed: Oct. 26, 2021. [Online]. Available: https://infoscience.epfl.ch/record/53282

[68] S. M. Kim and I. Mudawar, "Review of databases and predictive methods for heat transfer in condensing and boiling mini/micro-channel flows," *Int J Heat Mass Transf*, vol. 77, pp. 627–652, 2014, doi: 10.1016/j.ijheatmasstransfer.2014.05.036.

[69] C. A. Dorao, O. B. Fernandez, and M. Fernandino, "Experimental Study of Horizontal Flow Boiling Heat Transfer of R134a at a Saturation Temperature of 18.6 °c," *J Heat Transfer*, vol. 139, no. 11, 2017, doi: 10.1115/1.4037153.

[70] C. A. Dorao, F. Morin, and M. Fernandino, "Experimental study of nucleate flow boiling to convective flow boiling transition in a horizontal heated pipe," *ASME 2018 16th International Conference on Nanochannels, Microchannels, and Minichannels, ICNMM 2018*, pp. 1–6, 2018, doi: 10.1115/icnmm2018-7682.

[71] A. Zhao, Y. Fan, Y. Suzuki, and K. Morimoto, "Dryout characteristics of low-GWP working fluids at low mass and heat fluxes in a vertical 4 mm diameter tube," *Int J Heat Mass Transf*, vol. 172, p. 121114, 2021, doi: 10.1016/j.ijheatmasstransfer.2021.121114.

[72] J. B. Copetti, M. H. Macagnan, F. Zinani, and N. L. F. Kunsler, "Flow boiling heat transfer and pressure drop of R-134a in a mini tube: An experimental investigation," *Exp Therm Fluid Sci*, vol. 35, no. 4, pp. 636–644, 2011, doi: 10.1016/j.expthermflusci.2010.12.013.

[73] S. Mortada, A. Zoughaib, C. Arzano-Daurelle, and D. Clodic, "Boiling heat transfer and pressure drop of R-134a and R-1234yf in minichannels for low mass fluxes," *International Journal of Refrigeration*, vol. 35, no. 4, pp. 962–973, 2012, doi: 10.1016/j.ijrefrig.2012.03.004.

[74] M. H. Oudah, M. K. Mejbel, and M. K. Allawi, "R134a flow boiling heat transfer (FBHT) characteristics in a refrigeration system," *Journal of Mechanical Engineering Research and Developments*, vol. 44, no. 4, pp. 69–83, 2021.

[75] R. Charnay, R. Revellin, and J. Bonjour, "Flow boiling characteristics of R-245fa in a minichannel at medium saturation temperatures," *Exp Therm Fluid Sci*, vol. 59, pp. 184–194, 2014, doi: 10.1016/j.expthermflusci.2014.01.011.

[76] S. Paul, M. Fernandino, and C. A. Dorao, "On the scaling of convective boiling heat transfer coefficient," *Int J Heat Mass Transf*, vol. 164, 2021, doi: 10.1016/j.ijheatmasstransfer.2020.120589.

[77] R. Charnay, R. Revellin, and J. Bonjour, "Flow boiling heat transfer in minichannels at high saturation temperatures: Part I - Experimental investigation and analysis of the heat transfer mechanisms," *Int J Heat Mass Transf*, vol. 87, pp. 636–652, 2015, doi: 10.1016/j.ijheatmasstransfer.2015.03.081.

[78] D. Hellenschmidt and P. Petagna, "Effects of saturation temperature on the boiling properties of carbon dioxide in small diameter pipes at low vapour quality: Heat transfer coefficient," *Int J Heat Mass Transf*, vol. 172, Jun. 2021, doi: 10.1016/J.IJHEATMASSTRANSFER.2021.121094.

[79] A. Greco and G. P. Vanoli, "Flow-boiling of R22, R134a, R507, R404A and R410A inside a smooth horizontal tube," *International Journal of Refrigeration*, vol. 28, no. 6, pp. 872–880, 2005, doi: 10.1016/j.ijrefrig.2005.01.008.

[80] A. Celen and A. S. Dalkılıç, "A complete evaluation method for the experimental data of flow boiling in smooth tubes," *International Communications in Heat and Mass Transfer*, vol. 89, no. November, pp. 108–121, 2017, doi: 10.1016/j.icheatmasstransfer.2017.09.024.

[81] S. J. Eckels and M. B. Pate, "An experimental comparison of evaporation and condensation heat transfer coefficients for HFC-134a and CFC-12," *International Journal of Refrigeration*, vol. 14, no. 2, pp. 70–77, 1991, doi: 10.1016/0140-7007(91)90078-U.

[82] Y. Xu, X. Fang, G. Li, D. Li, and Y. Yuan, "An experimental study of flow boiling heat transfer of R134a and evaluation of existing correlations," *Int J Heat Mass Transf*, vol. 92, pp. 1143–1157, Jan. 2016, doi: 10.1016/J.IJHEATMASSTRANSFER.2015.09.044.

[83] Q. Guo, M. Li, and X. Tian, "Experimental study on flow boiling heat transfer characteristics of R134a, R245fa and R134a/R245fa mixture at high saturation temperatures," *International Journal of Thermal Sciences*, vol. 150, p. 106195, Apr. 2020, doi: 10.1016/J.IJTHERMALSCI.2019.106195.

[84] S. Grauso, R. Mastrullo, A. W. Mauro, J. R. Thome, and G. P. Vanoli, "Flow pattern map, heat transfer and pressure drops during evaporation of R-1234ze(E) and R134a in a horizontal, circular smooth tube: Experiments and assessment of predictive methods," *International Journal of Refrigeration*, vol. 36, no. 2, pp. 478–491, 2013, doi: 10.1016/j.ijrefrig.2012.07.016.

[85] P. Balachander and B. Raja, "Investigation on the boiling heat transfer characteristics of R404A and R134a under stratified flow condition," *Heat and Mass Transfer/Waerme- und Stoffuebertragung*, vol. 51, no. 6, pp. 825–835, 2015, doi: 10.1007/s00231-014-1456-4.

[86] C. A. Dorao, S. Drewes, and M. Fernandino, "Can the heat transfer coefficients for single-phase flow and for convective flow boiling be equivalent?," *Appl Phys Lett*, vol. 112, no. 6, 2018, doi: 10.1063/1.5018659.

[87] M. M. Mahmoud and T. G. Karayiannis, "International Journal of Heat and Mass Transfer Heat transfer correlation for flow boiling in small to micro tubes," *Int J Heat Mass Transf*, vol. 66, pp. 553–574, 2013, doi: 10.1016/j.ijheatmasstransfer.2013.07.042.

[88] R. Charnay, R. Revellin, and J. Bonjour, "Flow boiling heat transfer in minichannels at high saturation temperatures: Part II - Assessment of predictive methods and impact of flow regimes," *Int J Heat Mass Transf*, vol. 87, pp. 653–672, 2015, doi: 10.1016/j.ijheatmasstransfer.2015.03.080.

[89] X. Fang, "A new correlation of flow boiling heat transfer coefficients based on R134a data," *Int J Heat Mass Transf*, vol. 66, pp. 279–283, 2013, doi: 10.1016/j.ijheatmasstransfer.2013.07.015.

[90] M. K. Smith, J. P. Wattelet, and T. A. Newell, "A Study of Evaporation Heat Transfer Coefficient Correlations at Low Heat and Mass Fluxes for Pure Refrigerants and Refrigerant Mixtures," 1993.

[91] R. Charnay, R. Revellin, and J. Bonjour, "Flow boiling characteristics of R-245fa in a minichannel at medium saturation temperatures," *Exp Therm Fluid Sci*, vol. 59, pp. 184–194, 2014, doi: 10.1016/j.expthermflusci.2014.01.011.

[92] C. B. Tibiriçá and G. Ribatski, "Flow boiling in micro-scale channels-Synthesized literature review," *International Journal of Refrigeration*, vol. 36, no. 2, pp. 301–324, 2013, doi: 10.1016/j.ijrefrig.2012.11.019.

[93] F. T. Kanizawa, C. B. Tibiriçá, and G. Ribatski, "Heat transfer during convective boiling inside microchannels," *Int J Heat Mass Transf*, vol. 93, pp. 566–583, 2016, doi: 10.1016/j.ijheatmasstransfer.2015.09.083.

[94] E. P. Bandarra Filho and P. E. L. Barbieri, "Flow boiling performance in horizontal microfinned copper tubes with the same geometric characteristics," *Exp Therm Fluid Sci*, vol. 35, no. 5, pp. 832–840, 2011, doi: 10.1016/j.expthermflusci.2010.06.012.

[95] E. Manavela Chiapero, M. Fernandino, and C. A. Dorao, "Experimental results on boiling heat transfer coefficient, frictional pressure drop and flow patterns for R134a at a saturation temperature of 34°C," *International Journal of Refrigeration*, vol. 40, pp. 317–327, 2014, doi: 10.1016/j.ijrefrig.2013.11.026.

[96] J. M. Saiz Jabardo and E. P. Bandarra Filho, "Convective boiling of halocarbon refrigerants flowing in a horizontal copper tube - an experimental study," *Exp Therm Fluid Sci*, vol. 23, no. 3–4, pp. 93–104, 2000, doi: 10.1016/S0894-1777(00)00040-6.

[97] H. Lee, S. L.-I. J. of M. Flow, and undefined 2001, "Heat transfer correlation for boiling flows in small rectangular horizontal channels with low aspect ratios," *Elsevier*, Accessed: Dec. 02, 2021. [Online]. Available: https://www.sciencedirect.com/science/article/pii/S0301932201000544

[98] C. Ong, J. T.-E. thermal and fluid science, and undefined 2011, "Macro-to-microchannel transition in two-phase flow: Part 2–Flow boiling heat transfer and critical heat flux," *Elsevier*, Accessed: Dec. 02, 2021. [Online]. Available: https://www.sciencedirect.com/science/article/pii/S0894177710002323

[99] S. Paul, M. Fernandino, and C. A. Dorao, "On the scaling of convective boiling heat transfer coefficient," *Int J Heat Mass Transf*, vol. 164, 2021, doi: 10.1016/j.ijheatmasstransfer.2020.120589.

[100] R. Charnay, R. Revellin, and J. Bonjour, "Flow boiling heat transfer in minichannels at high saturation temperatures: Part I - Experimental investigation and analysis of the heat transfer mechanisms," *Int J Heat Mass Transf*, vol. 87, pp. 636–652, 2015, doi: 10.1016/j.ijheatmasstransfer.2015.03.081.

[101] L. C. Ruspini, *Carlos Ruspini Experimental and numerical investigation on two-phase flow Undertittel på avhandlingen instabilities Fornavn Etternavn Leonardo Carlos Ruspini Tittel på avhandlingen Experimental and numerical investigation on Undertittel på avhandlingen fl.* 2013.

[102] M. Sorum, "Experimental investigation of the impact in the heat transfer coefficient and pressure drop during boiling flow instabilities," no. June, 2014.

[103] E. Lemmon, M. McLinden, and M. Huber, "NIST standard reference database 23-NIST thermodynamic and transport properties REFPROP, version 7.0," 2002, Accessed: Oct. 26, 2021. [Online]. Available: https://www.nist.gov/publications/nist-standard-reference-database-23-nist-thermodynamic-and-transport-properties-refprop

[104] E. G. Bediako, P. Dancova, A. F. A. Elbarghthi, and T. Vit, "Flow boiling heat transfer of R134a: Effect of heat flux and Dry-out characteristics," in *Proceedings of the 10th International Conference on Fluid Flow, Heat and Mass Transfer (FFHMT 2023)*, 2023. doi: 10.11159/ffhmt23.161.

[105] E. G. Bediako, P. Dancova, and T. Vit, "Experimental Study of Flow Boiling Heat Transfer at Low Heat Fluxes," *J Fluid Flow Heat Mass Transf*, vol. 9, 2022, doi: 10.11159/jffhmt.2022.018.

[106] E. G. Bediako, P. Dancova, and T. Vit, "Comparison of Experimental Heat Transfer Coefficient with Qualitative Description of Classical Heat Transfer Coefficient at Low Heat Flux Conditions," in *International Conference on Fluid Flow, Heat and Mass Transfer*, 2022. doi: 10.11159/ffhmt22.185.

[107] E. G. Bediako, P. Dančová, and T. Vít, "Experimental Study of Horizontal Flow Boiling Heat Transfer Coefficient and Pressure Drop of R134a from Subcooled Liquid Region to Superheated Vapor Region," *Energies (Basel)*, vol. 15, no. 3, Feb. 2022, doi: 10.3390/EN15030681.

[108] F. W. Dittus and L. M. K. Boelter, "Heat transfer in automobile radiators of the tubular type," *International communication in heat and mass transfer* , vol. 12.1, pp. 3–22, 1985, Accessed: Aug. 14, 2023. [Online]. Available: https://cir.nii.ac.jp/crid/1573668925661465984

[109] T. Kandlbinder, "EXPERIMENTAL INVESTIGATION OF FORCED AND BOILING OF HYDROCARBONS MIXTURES," no. November, 1997.

[110] P. Balachander, B. Raja, and D. M. Lal, "Evaporative heat transfer characteristics of R404A and R134a under varied heat flux conditions," *Experimental Heat Transfer*, vol. 25, no. 3, pp. 254–265, 2012, doi: 10.1080/08916152.2011.623820.

[111] L. Wojtan, T. Ursenbacher, and J. R. Thome, "Investigation of flow boiling in horizontal tubes: Part I - A new diabatic two-phase flow pattern map," *Int J Heat Mass Transf*, vol. 48, no. 14, pp. 2955–2969, 2005, doi: 10.1016/j.ijheatmasstransfer.2004.12.012.

[112] T. N. Tran, M. W. Wambsganss, and D. M. France, "Small circular- and rectangular-channel boiling with two refrigerants," *International Journal of Multiphase Flow*, vol. 22, no. 3, pp. 485–498, Jun. 1996, doi: 10.1016/0301-9322(96)00002-X.

[113] S. S. Bertsch, E. A. Groll, and S. v. Garimella, "Refrigerant flow boiling heat transfer in parallel microchannels as a function of local vapor quality," *Int J Heat Mass Transf*, vol. 51, no. 19–20, pp. 4775–4787, Sep. 2008, doi: 10.1016/J.IJHEATMASSTRANSFER.2008.01.026.

[114] G. R. Warrier, V. K. Dhir, and L. A. Momoda, "Heat transfer and pressure drop in narrow rectangular channels," *Exp Therm Fluid Sci*, vol. 26, no. 1, pp. 53–64, Apr. 2002, doi: 10.1016/S0894-1777(02)00107-3.

[115] J. P. Wattelet, J. C. Chato, A. L. Souza, and B. R. Christoffersen, "Evaporative characteristics of R-134a, MP-39, and R-12 at low mass fluxes," 1993, Accessed: Oct. 11, 2022. [Online]. Available: http://www.ideals.illinois.edu/handle/2142/9736

[116] Z. Liu and R. H. S. Winterton, "A general correlation for saturated and subcooled flow boiling in tubes and annuli, based on a nucleate pool boiling equation," *Int J Heat Mass Transf*, vol. 34, no. 11, pp. 2759–2766, Nov. 1991, doi: 10.1016/0017-9310(91)90234-6.

[117] S. G. Kandlikar, "A General Correlation for Saturated Two-Phase Flow Boiling Heat Transfer Inside Horizontal and Vertical Tubes," *J Heat Transfer*, vol. 112, no. 1, pp. 219–228, Feb. 1990, doi: 10.1115/1.2910348.